STUDIA

UNIVERSITATIS BABEŞ-BOLYAI

PHYSICA

2

1977

CLUJ-NAPOCA

ANUL XXII 1977

STUDIA
UNIVERSITATIS BABEŞ-BOLYAI

PHYSICA
2

Redacţia. 3400 CLUJ-NAPOCA, str. M. Kogălniceanu, 1 ● Telefon 1 34 50

SUMAR — CONTENTS — SOMMAIRE — INHALT

STUDIA UNIV BABEŞ—BOLYAI, PHYSICA, 2, 1977

DETERMINAREA VITEZELOR ŞI A SECŢIUNILOR EFICACE APARENTE DE DISOCIERE METASTABILĂ A IONILOR MOLECULARI (II)

Disocieri succesive în două trepte

I. MASTAN, A. TODEREAN şi V. MERCEA

1. **Introducere.** Prin disocieri metastabile succesive în două trepte înţelegem acele procese în care ionul fragment al primei trepte de disociere se disociază, la rîndul său, dînd naştere unui ion fragment stabil, deci procese de tipul

$$m_0^+ \xrightarrow{\lambda_1,\,\sigma_1} m^+ \xrightarrow{\lambda_2,\,\sigma_2} m_1^+ \qquad (1)$$

Problema disocierilor metastabile succesive ale ionilor moleculari a mai fost abordată în lucrările [1—3]. În lucrarea de faţă se încearcă dezvoltarea unei metode de determinare a valorilor aparente ale vitezelor de disociere spontană λ_1 şi λ_2 şi a secţiunilor eficace aparente de disociere indusă prin ciocnire σ_1 şi σ_2, în cazul unui proces de tipul (1). Ideea fundamentală a lucrării constă [4] în compararea rezultatelor experimentale cu expresii teoretice obţinute ca soluţii ale ecuaţiilor de bilanţ pentru curenţii ionici. Rezultatele experimentale se obţin tot cu un spectrometru de masă cu dublă focalizare şi geometrie inversată (vezi [4]). În consideraţiile teoretice care vor urma se presupune că procesul de tipul (1) este singura sursă de pierdere a ionilor m_0^+ respectiv m^+ şi că ionii m_0^+ nu pot trece direct în ionii m_1^+, ci doar prin intermediul ionilor m^+. În cele ce urmează se dau condiţiile de lucru pentru detectarea picurilor metastabile.

1.1. *Prima zonă fără cîmp.* Este porţiunea de traiectorie între ultima fantă a sursei de ioni, punctul 1, şi fanta de intrare în cîmpul magnetic, punctul 2. Pentru studiul disocierilor din această zonă se lucrează cu metoda defocalizării [5], intensitatea cîmpului electrostatic menţinîndu-se constantă, E_0. Fiecărui punct i, ($i = 0,1, \ldots, 6$), al traiectoriei îi ataşăm o distanţă x_i şi un timp de parcurgere a acestei distanţe t_i, menţionînd că $x_0 = 0$ şi $t_0 = 0$. Distanţele x_i rămîn fixe fiind parametrii instalaţiei cu care se lucrează. Timpii de zbor t_i variază în funcţie de potenţialul de accelerare aplicat ionilor. Astfel, pentru un potenţial de accelerare V timpii vor avea expresiile

$$t_i = \frac{x_1}{v_m} + \frac{\Delta x_i}{v}; \quad \Delta x_i = x_i - x_1; \qquad (i = 1, 2, \ldots 6) \qquad (2)$$

unde $v = 2v_m = \sqrt{2eV/m_0}$ este viteza ionilor din punctul 1 pînă la colector, iar v_m este viteza medie a ionilor pe porţiunea de accelerare [4]. Cînd procesul (1) este studiat în prima zonă fără cîmpuri pot apare următoarele situaţii:

a) Pentru detectarea ionilor părinți m_0^+, care au mai rămas în urma disocierilor, tensiunea de accelerare va fi $V = V_0$, viteza ionilor fiind deci $v = k_0 = \sqrt{2eV_0/m_0}$. Timpii se vor nota cu t_i.

b) Pentru detectarea ionilor fii m^+, care se produc în prima zonă fără cîmp, se lucrează cu tensiunea de accelerare $V = V_0(m_0/m)$. Viteza ionilor va fi $v = k = \sqrt{2eV_0/m}$ iar timpii îi vom nota cu t_i'. Expresiile lor se pot deduce din relațiile (2).

c) Pentru detectarea ionilor m_1^+, produși în prima zonă fără cîmp, se lucrează cu tensiunea de accelerare $V = V_0(m_0/m_1)$, viteza ionilor fiind $v = k' = \sqrt{2eV_0/m_1}$. Timpii se notează în acest caz cu t_i''.

1 2 *A doua zonă fără cîmp*. Este cuprinsă între ieșirea din analizorul magnetic, punctul 3, și intrarea în analizorul electrostatic, punctul 4. Disocierile care au loc în această zonă se studiază prin metoda DADI [5], potențialul de accelerare și intensitatea cîmpului magnetic rămînînd de data asta constante, V_0 respectiv H_0. Din punct de vedere al vitezelor și timpilor sîntem deci în cazul prezentat la punctul *a*. Baleajul spectrului metastabil se va face prin variația intensității cîmpului electrostatic. Pentru detectarea ionilor m^+, formați în cea de-a doua zonă fără cîmp, intensitatea cîmpului electrostatic va avea valoarea $E = E_0(m/m_0)$, iar pentru detectarea ionilor m_1^+ valoarea $E' = E_0(m_1/m_0)$ Desigur, în toate cazurile este vorba de ioni care au supraviețuit pînă în punctul 6, adică pînă la colector.

2 **Ecuațiile de bilanț.** În vederea scrierii ecuațiilor de bilanț se introduc următoarele notații $I_i(t_i)$ — curentul de ioni ai speciei m_0^+ în punctul i al traiectoriei, $(I(t_0 = 0) = I_0)$; $I_i'(t_i)$ — curentul de ioni ai speciei m^+ în punctul i al traiectoriei, $(I_0' = I_0'(t_0 = 0) = 0)$. Calculele de bilanț care se dezvoltă în paginile următoare se vor referi la ionii m^+, adică la specia intermediară procesului de disociere succesivă în două trepte (1).

2 1 *Prima zonă fără cîmp*. În conformitate cu schema (1) ionii m^+ se formează din ionii m_0^+ cu viteza λ_1 și secțiunea eficace σ_1 și se disociază în ionii m_1^+ cu viteza λ_2 și secțiunea eficace σ_2. Transcrierea matematică a acestui proces conduce [4, 6] la ecuația diferențială

$$\frac{dI'}{dt} = (\lambda_1 + \sigma_1 N v) I - (\lambda_2 + \sigma_2 N v) I' \tag{3}$$

Pentru porțiunea de traiectorie 0—1, viteza ionilor se ia $v = k_m$ iar timpul se marchează prin $t' \leqslant t_1'$. Rezolvarea ecuației diferențiale (3) duce în acest caz la soluția $I'_{t' \leqslant t_1'}$ a cărei expresie nu se dă aici Ea va putea fi dedusă din considerațiile dezvoltate în cele ce urmează. Pentru porțiunea de traiectorie 1—6, viteza ionilor va fi $v = k$ iar timpii se notează prin $t' \geqslant t_1'$. Soluția ecuației diferențiale (3) în acest caz va fi

$$I'_{t' \geqslant t_1'} = \frac{I_0(\lambda_1 + \sigma_1 N k) \cdot \exp\{-(\lambda_2 + \sigma_2 N k_m)(t' - t_1')\}}{(\lambda_2 + \sigma_2 N k_m) - (\lambda_1 + \sigma_1 N k_m)} \cdot \Big[\exp\{-(\lambda_1 + \sigma_1 N k_m) \cdot t_1'\} -$$

$$- \exp\{-(\lambda_2 + \sigma_2 N k_m) \cdot t_1'\}\Big] + \frac{I_0(\lambda_1 + \sigma_1 N k) \cdot \exp\{-(\lambda_1 + \sigma_1 N k_m) \cdot t_1'\}}{(\lambda_2 + \sigma_2 N k) - (\lambda_1 + \sigma_1 N k)} \cdot \tag{4}$$

$$\cdot [\exp\{-(\lambda_1 + \sigma_1 N k)(t' - t_1')\} - \exp\{-(\lambda_2 + \sigma_2 N k)(t' - t_1')\}]$$

La obținerea soluției (4) s-a ținut cont de faptul că în conformitate cu rezultatele obținute în [4] se poate scrie

$$I_{t'\geqslant t'_1} = I_0 \cdot \exp\{ - [\lambda_1 t' + \sigma_1 N k_m (2t' - t'_1)]\} \tag{5}$$

Prima parte a expresiei (4) se poate scrie sub forma

$$I'_1 \cdot \exp\{ - (\lambda_2 + \sigma_2 N k)(t' - t'_1)\} \tag{6}$$

„Pachetul" de ioni descris de (6) nu are o energie potrivită pentru a urma o traiectorie normală în spectrometrul de masă și ca urmare nu va ajunge la colector. Din această cauză în calculele ce urmează nu se va lua în considerare prima parte a expresiei (4).

„Stocul" de ioni m^+ cu care se ajunge în punctul 2 al traiectoriei se obține din (4) punînd $t' = t'_2$. Acest „stoc" de ioni m^+ nu se va mai îmbogăți dincolo de punctul 2 al traiectoriei, analizorul magnetic nepermițînd trecerea ionilor m_0^+, ci va descreşte datorită disocierilor de tipul $m^+ \xrightarrow{\lambda_1,\sigma_1} m_1^+$. Ținînd cont de legea conform căreia are loc o astfel de descreştere [4], expresia curentului I'_{6f} în punctul corespunzător lui $t' = t'_6$ va fi

$$I'_{6f} = \frac{I_0(\lambda_1 + \sigma_1 N k) \cdot \exp\{ -(\lambda_1 + \sigma_1 N k_m) \cdot t'_1\}}{(\lambda_2 + \sigma_2 N k) - (\lambda_1 + \sigma_1 N k)} \cdot [\exp\{ - [(\lambda_1 + \sigma_1 N k)(t'_2 - t'_1) +$$
$$+ (\lambda_2 + \sigma_2 N k)(t'_6 - t'_2)]\} - \exp\{ - (\lambda_2 + \sigma_2 N k)(t'_6 - t'_1)\}] \tag{7}$$

2.2. *A doua zonă fără cîmp.* Bilanțul curentului ionic al speciei m^+, pentru porțiunea de traiectorie 3—4, este descris de ecuația (3) în care $v = k_0$ iar $t \geqslant t_3$. Pentru acest caz, integrarea ecuației (3) duce la expresia

$$I'_{t\geqslant t_3} = \frac{I_0(\lambda_1 + \sigma_1 N k_0) \cdot \exp\{ - [\lambda_1 t_3 + k_{0m}\sigma_1 N(2t_3 - t_1)]\}}{(\lambda_2 + \sigma_2 N k_0) - (\lambda_1 + \sigma_1 N k_0)} \cdot$$
$$\cdot [\exp\{ - (\lambda_1 + \sigma_1 N k_0)(t - t_3)\} - \exp\{ - (\lambda_2 + \sigma_2 N k_0)(t - t_3)\}] \tag{8}$$

În cazul metodei DADI prin analizorul magnetic trec doar ionii m_0^+ avînd viteza k_0, deci în punctul 3 al traiectoriei numărul de ioni m^+ este nul. „Stocul" de ioni m^+ cu care se ajunge în punctul 4 al traiectoriei este I'_{4s}. Expresia lui I'_{4s} se obține din (8) în care se face substituția $t = t_4$. Acești ioni s-au format pe porțiunea de traiectorie 3—4. Dincolo de punctul 4 al traiectoriei va avea loc o descreştere a acestui „stoc" de ioni m^+ datorită disocierilor de tipul $m^+ \xrightarrow{\lambda_2,\sigma_2} m_1^+$. În consecință, în punctul 6 al traiectoriei vom avea

$$I'_{6s} = \frac{I_0(\lambda_1 + \sigma_1 N k_0) \cdot \exp\{ - [\lambda_1 t_3 + k_{0m}\sigma_1 N(2t_3 - t_1)]\}}{(\lambda_2 + \sigma_2 N k_0) - (\lambda_1 + \sigma_1 N k_0)} \cdot$$
$$\cdot [exp\{ - (\lambda_1 + \sigma_1 N k_0)(t_4 - t_3)\} \cdot \exp\{ - (\lambda_2 + \sigma_2 N k_0)(t_6 - t_4)\} - \tag{9}$$
$$- \exp\{ - (\lambda_2 + \sigma_2 N k_0)(t_6 - t_3)\}]$$

3. **Determinarea mărimilor** λ_1, λ_2, σ_1 **şi** σ_2. În scopul determinării valorilor aparente ale mărimilor λ_1, λ_2, σ_1 şi σ_2, mărimi care caracterizează procesele de disociere metastabilă succesivă în două trepte, de tipul (1), se introduc funcţiile

$$P[\lambda_1, \lambda_2, p(N)] = \frac{I'_{6f}}{I_6} = \frac{(\lambda_1 + \sigma_1 Nk) \cdot \exp\{-(\lambda_1 + \sigma_1 Nk_m) \cdot t'_1\}}{(\lambda_2 + \sigma_2 Nk) - (\lambda_1 + \sigma_1 Nk)}$$
$$\cdot \exp\{\lambda_1 t_6 + k_{om}\ \sigma_1 N(2t_6 - t_1)\} \cdot [\exp\{-[(\lambda_1 + \sigma_1 Nk)(t'_2 - t'_1) + \quad (10)$$
$$+ (\lambda_2 + \sigma_2 Nk)(t'_6 - t'_2)]\} - \exp\{-(\lambda_2 + \sigma_2 Nk)(t'_6 - t'_1)\}]$$

$$R[\lambda_1, \lambda_2, p(N)] = \frac{I'_{6s}}{I_6} = \frac{(\lambda_1 + \sigma_1 Nk_0) \cdot exp\{-[\lambda_1 t_3 + k_{0m}\sigma_1 N(2t_3 - t_1)]\}}{(\lambda_2 + \sigma_2 Nk_0) - (\lambda_1 + \sigma_1 Nk_0)} \cdot$$
$$\cdot \exp\{\lambda_1 t_6 + k_{0m}\sigma_1 N(2t_6 - t_1)\} \cdot [\exp\{-(\lambda_1 + \sigma_1 Nk_0)(t_4 - t_3)\} \cdot \quad (11)$$
$$\cdot \exp\{-(\lambda_2 + \sigma_2 Nk_0)(t_6 - t_4)\} - \exp\{-(\lambda_2 + \sigma_2 Nk_0)(t_6 - t_3)\}]$$

unde I_6 este curentul de ioni m_0^+ la colector. Dacă setul de curenţi ionici I'_{6f}, I'_{6s} şi I_6 se măsoară experimental pentru un şir de valori ale presiunii $p(N)$ din tubul de zbor, atunci se pot găsi corespondentele experimentale ale funcţiilor definite mai sus.

3.1. *Determinarea mărimilor* λ_1, λ_2. Pentru determinarea lui λ_1 şi λ_2 se pleacă de la extrapolatele liniare ale funcţiilor $P[\lambda_1, \lambda_2, p(N)]$ şi $R[\lambda_1, \lambda_2, p(N)]$, pentru $p(N) \to 0$, expresii care formează un sistem de două ecuaţii transcendente cu necunoscutele λ_1 şi λ_2 Celelalte mărimi care intervin în ecuaţii se pot calcula din parametrii de lucru şi din datele constructive ale aparatului. Extrapolatele $P[\lambda_1, \lambda_2, 0]$ şi $R[\lambda_1, \lambda_2, 0]$ se înlocuiesc cu valorile experimentale corespunzătoare. În vederea uşurării rezolvării sistemului de ecuaţii se face substituţia $\lambda_2 = \lambda_1 + \alpha$. Din expresia lui $R[\lambda_1, \lambda_2(\alpha), 0]$ se calculează λ_1 în funcţie de α iar din compararea expresiilor lui $P[\lambda_1, \lambda_2(\alpha), 0]$ şi $R[\lambda_1, \lambda_2(\alpha), 0]$ rezultă următoarea ecuaţie transcendentă

$$P[\lambda_1, \lambda_2(\alpha), 0] = \frac{R[\lambda_1, \lambda_2(\alpha), 0]}{\exp\{-\alpha(t_6 - t_4)\} - exp\{-\alpha(t_6 - t_3)\}} \cdot [\exp\{-\alpha(t'_6 - t'_2)\} - \quad (12)$$
$$- \exp\{-\alpha(t'_6 - t'_1)\}] \cdot \exp\left\{-\frac{\alpha \cdot R[\lambda_1, \lambda_2(\alpha), 0]}{\exp\{-\alpha(t_6 - t_4)\} - \exp\{-\alpha(t_6 - t_3)\}} \cdot (t'_6 - t_6)\right\}$$

unde singura necunoscută este α Cu α cunoscut se pot calcula λ_1 şi λ_2 pe calea substituţiilor inverse.

3.2 *Determinarea mărimilor* σ_1 *şi* σ_2 În acest caz se pleacă de la sistemul de ecuaţii format cu expresiile (10) şi (11) în care λ_1 şi λ_2 se consideră deja cunoscute. $P[\lambda_1, \lambda_2, p(N)]$ şi $R[\lambda_1, \lambda_2, p(N)]$ se înlocuiesc cu valorile experimentale corespunzătoare. Celelalte mărimi se pot deduce din condiţiile de lucru În vederea uşurării rezolvării sistemului de ecuaţii transcendente, (10) şi (11) se introduce substituţia $\sigma_2 = \sigma_1 + \beta$. Astfel, din expresia lui $R[\lambda_1, \lambda_2(\alpha), p'(N)]$ se deduce σ_1 în funcţie de β iar din compararea

expresiilor lui $R[\lambda_1, \lambda_2(\alpha), p'(N)]$ şi $P[\lambda_1, \lambda_2(\alpha), p'(N)]$ se obţine ecuaţia transcendentă

$$(\alpha + Nk\beta) \cdot P[\lambda_1, \lambda_2(\alpha), p'(N)] = [CD \cdot \exp\{-\beta N(x_6 - x_2)\} - CE \cdot \tag{13}$$

$$\cdot \exp\{-\beta N(x_6 - x_1)\}] \cdot \left[\lambda_1 + \frac{k}{k_0}\left[\frac{(\alpha + Nk_0\beta) \cdot R[\lambda_1, \lambda_2(\alpha), p'(N)]}{A \cdot \exp\{-\beta N(x_6 - x_4)\} - B \cdot \exp\{-\beta N(x_6 - x_3)\}} - \lambda_1\right]\right]$$

în care singura necunoscută este β.

4. **Studiul condiţiilor de extrapolare liniară.** Deoarece la determinarea mărimilor λ_1 şi λ_2 se porneşte de la extrapolatele, pentru $p(N) \to 0$, ale funcţiilor $P[\lambda_1, \lambda_2, p(N)]$ şi $R[\lambda_1, \lambda_2, p(N)]$, trebuiesc studiate condiţiile în care se pot efectua aceste extrapolări liniare. În acest scop se fac schimbările de variabilă $\sigma_1 N = a_1 = a$ şi $\sigma_2 N = a_2 = n\,a$. Acestea atrag după sine trecerea de la funcţiile $P[\lambda_1, \lambda_2, p(N)]$ şi $R[\lambda_1, \lambda_2, p(N)]$ respectiv la funcţiile $P^*[\lambda_1, \lambda_2, n, a]$ şi $R^*[\lambda_1, \lambda_2, n, a]$. Considerînd mărimile λ_1, λ_2 şi n constante, în cazul unui proces de disociere metastabilă succesivă bine determinat, definim condiţiile de extrapolare liniară a funcţiilor $P^*[\lambda_1, \lambda_2, n, a]$ şi $R^*[\lambda_1, \lambda_2, n, a]$ analog modului de definire dat în lucrarea [4]. Studiul cantitativ va fi abordat pentru cazul particular

$$m_0^+ (50 \text{ uam}) \xrightarrow{\lambda_1,\ \sigma_1} m^+ (40 \text{ uam}) \xrightarrow{\lambda_2,\ \sigma_2} m_1^+ (35 \text{ uam}) \tag{14}$$

şi pentru următorii parametrii experimentali: $V_0 = 3\,000$ volţi, $x_1 = 2$ cm, $x_2 = 27$ cm, $x_3 = 60{,}6$ cm, $x_4 = 80{,}6$ cm, $x_5 = 110{,}3$ cm şi $x_6 = 120{,}3$ cm. Calculele cantitative s-au efectuat pentru o serie de combinaţii ale mărimilor λ_1, λ_2, n şi a Rezultatele unei părţi a acestor calcule sînt reprezentate grafic în figurile 1—4. Curbele din figuri au fost trasate pentru valorile numerice ale lui λ_1 şi λ_2 încadrate în chenar.

Calculele numerice au fost efectuate însă şi pentru valorile lui λ_2 transcrise sub chenar. Curbele corespunzătoare acestor valori nu au fost trecute pe grafice deoarece sînt foarte apropiate de cele reprezentate. La scara figurii nu s-ar fi putut face distincţie între ele.

Din acest studiu se pot desprinde următoarele concluzii importante:

1. Pentru cazul $n \leqslant 1$, funcţiile $P[\lambda_1, \lambda_2, p(N)]$ şi $R[\lambda_1, \lambda_2, p(N)]$ pot fi extrapolate liniar, pentru $p(N) \to 0$, în tot domeniul de presiune situat sub $\sim 10^{-5}$ Torr. Domeniul de valori numerice ale mărimilor λ_1 şi λ_2, care se supune acestei concluzii, este suficient de larg pentru a acoperi practic toate situaţiile care se pot ivi în spectrometria de masă uzuală.

2. Dacă $n > 1$, atunci valorile lui a, pentru care este îndeplinită condiţia de extrapolare liniară a funcţiilor $P[\lambda_1, \lambda_2, p(N)]$ respectiv $R[\lambda_1, \lambda_2, p(N)]$, se deplasează către domeniul valorilor mai mici în comparaţie cu cazul $n \leqslant 1$. Se observă de asemenea că odată cu creşterea valorii numerice a mărimii λ_1 valoarea limită a parametrului a se deplasează către valori mai mari. În particular dacă $n = 10$, atunci în cazul funcţiei $P[\lambda_1, \lambda_2, p(N)]$, pentru $\lambda_1 = 10^4$ sec^{-1} se obţine $a = 2 \cdot 10^{-6}$ cm^{-1}, iar pentru $\lambda_1 = 10^7$ sec^{-1} se obţine $a = 10^{-5}$ cm^{-1}. În cazul funcţiei $R[\lambda_1, \lambda_2, p(N)]$

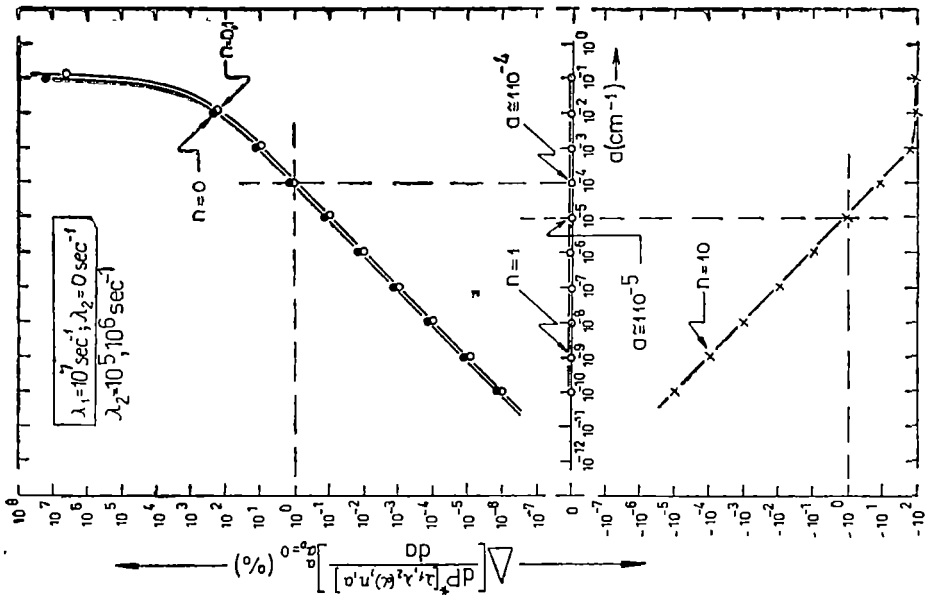
$\lambda_1=10^7 sec^{-1}; \lambda_2=0 sec^{-1}$
$\lambda_2=10^5;10^6 sec^{-1}$
n=0
n=0,1
n=1
n=10
$a\cong 110^{-4}$
$a\cong 110^{-5}$
a(cm^{-1})
$\Delta\left[\frac{dP^*(\lambda_1,\lambda_2(\kappa),n,a)}{da}\right]_{a=0}$ (%)

Fig. 2.

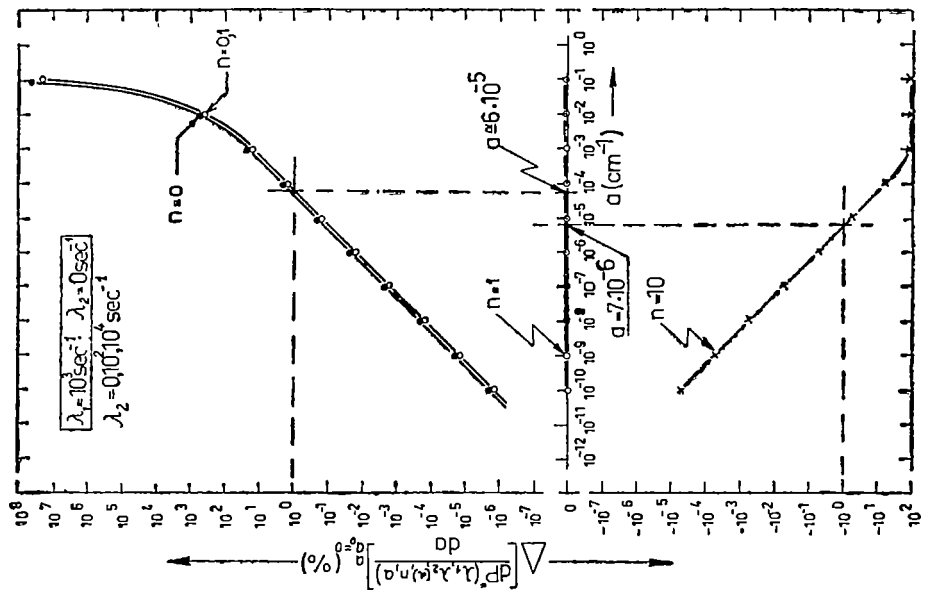
$\lambda_1=10^3 sec^{-1}; \lambda_2=0 sec^{-1}$
$\lambda_2=0;10;10^4 sec^{-1}$
n=0
n=0,1
n=1
n=10
$a\cong 6.10^{-5}$
$a=7.10^{-6}$
a(cm^{-1})
$\Delta\left[\frac{dP^*(\lambda_1,\lambda_2(\kappa),n,a)}{da}\right]_{a=0}$ (%)

Fig. 1.

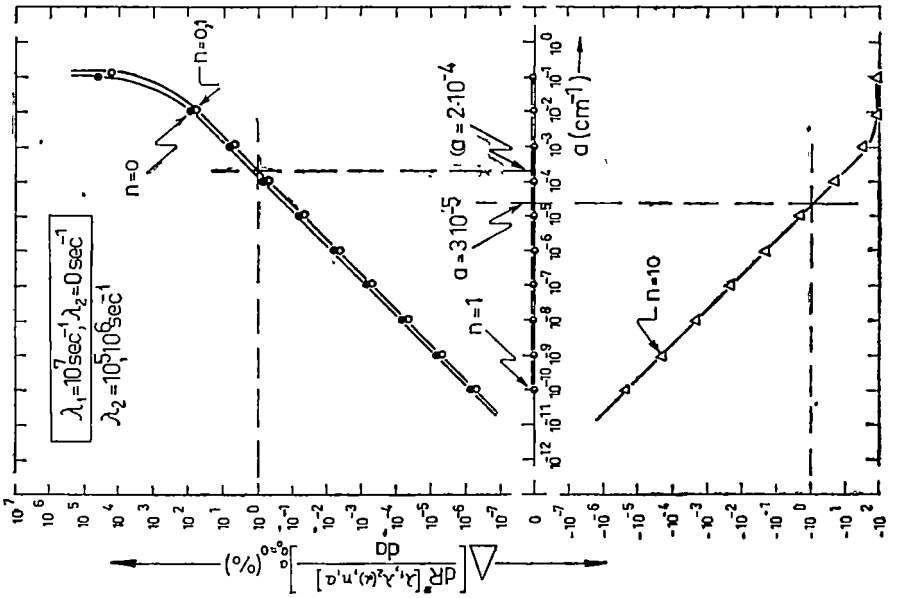
$\lambda_1=10^7 sec^{-1}, \lambda_2=0 sec^{-1}$
$\lambda_2=10^5, 10^6 sec^{-1}$
n=0
n=0,1
n=1
$a=3\,10^{-5}$
$a=2\cdot10^{-4}$
n=10
a (cm^{-1})
$\Delta\left[\frac{dR^*[\lambda_1,\lambda_2(\alpha),n,a]}{d\alpha}\right]_{\alpha\to0}$ (%)

Fig. 4.

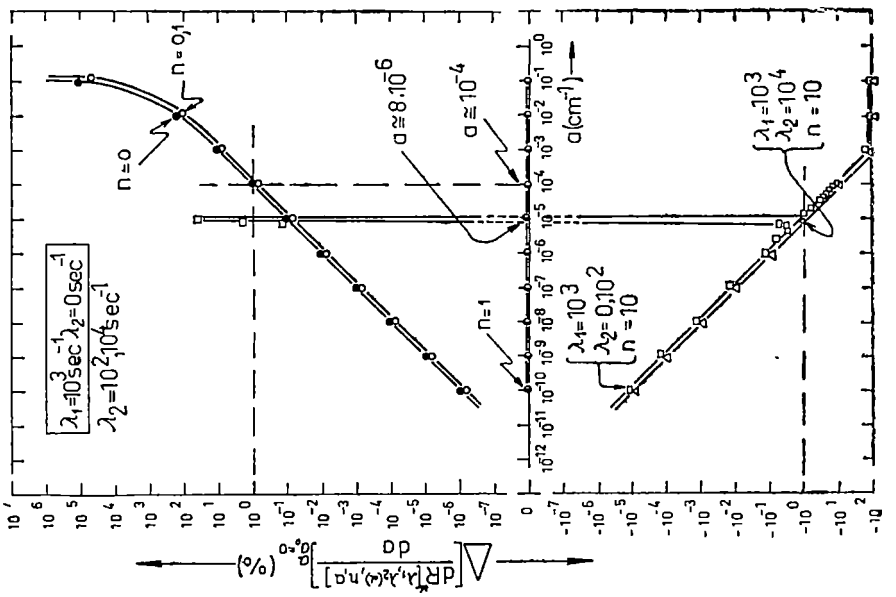
$\lambda_1=10^3 sec^{-1}, \lambda_2=0 sec^{-1}$
$\lambda_2=10^2, 10^4 sec^{-1}$
n=0
n=0,1
n=1
$a\cong8\cdot10^{-6}$
$a\cong10^{-4}$
$\lambda_1=10^3$
$\lambda_2=0,10^2$
n=10
$\lambda_1=10^3$
$\lambda_2=10^4$
n=10
a(cm^{-1})
$\Delta\left[\frac{dR^*[\lambda_1,\lambda_2(\alpha),n,a]}{d\alpha}\right]_{\alpha\to0}$ (%)

Fig. 3

dacă $n = 10$, atunci pentru valori mici ale lui λ_1 apar zone „periculoase" la valori ale parametrului a cuprinse între 10^{-5} și 10^{-4} cm^{-1}. Este vorba de zone în care funcția $\Delta[dR^*[\lambda_1, \lambda_2, n, a]/da]^{a}_{a_0=0}$ prezintă creșteri foarte puternice și abrupte, sub forma unor adevărate vîrfuri Din fericire aceste zone nu sînt prea largi. Ele vor trebui evitate în măsurătorile experimentale. De exemplu, pentru $\lambda_1 = 10^3$ sec^{-1}, funcția suferă un salt puternic, la $a = 10^{-5}$ cm^{-1}, de la valoarea de aproximativ — 1% pînă la valoarea de aproximativ + 100%

5. **Valorile limită ale funcțiilor P** $[\lambda_1, \lambda_2, 0]$ **și R** $[\lambda_1, \lambda_2, 0]$. În continuare vom discuta valorile limită ale funcțiilor $P[\lambda_1, \lambda_2, 0]$ și $R[\lambda_1, \lambda_2, 0]$ pentru cazurile cînd $\lambda_1 \to 0$, $\lambda_2 \to 0$ și $\lambda_2 \to \lambda_1$. În urma calculelor efectuate s-a ajuns la următoarele rezultate:

1. Dacă $\lambda_1 = 0$, atunci funcțiile $P[\lambda_1, \lambda_2, p(N)]$ și $R[\lambda_1, \lambda_2, p(N)]$ se extrapolează, pentru $p(N) \to 0$, exact prin originea sistemului de coordonate, pentru toate valorile lui λ_2 care îndeplinesc condiția $\lambda_2 \geqslant 0$. Situațiile $\lambda_1 = 0$, $\lambda_2 > 0$ și $\lambda_1 = 0$, $\lambda_2 = 0$ nu se pot distinge una de cealaltă după valorile extrapolatelor pentru $p(N) \to 0$.

2 Dacă $\lambda_2 = 0$ și $\lambda_1 > 0$ atunci extrapolatele funcțiilor definite la (10) și (11), pentru $p(N) \to 0$, sînt funcții exponențiale de λ_1. Ele iau numai valori pozitive

3. Dacă $\lambda_1 = \lambda_2 \neq 0$ funcția $P[\lambda_1, \lambda_2, p(N)]$ se extrapolează, pentru $p(N) \to 0$, cu o ordonată în origine egală cu $\lambda_1(t_2' - t_1') \cdot \exp\{-\lambda_1(t_6 - t_6')\} \cong \lambda_1(t_2' - t_1')$, iar funcția $R[\lambda_1, \lambda_2, p(N)]$ se extrapolează prin punctul cu ordonata în origine egală cu $\lambda_1(t_4 - t_3)$ Este vorba deci de ordonate în origine diferite de zero și pozitive

Considerațiile de mai sus au fost dezvoltate pentru valori fixe ale timpilor de zbor ale ionilor în spectrometru Baleajul valorilor acestor timpi între limite cît se poate de largi poate să aducă informații foarte prețioase asupra spectrului real de vieți medii care descrie disocierea metastabilă a unui ion molecular.

(*Intrat în redacție la 23 februarie* 1976)

BIBLIOGRAFIE

1 L. P Hills, J H. Futrell, A L Wahrhafting, J Chem. Phys, **51**, 5255 (1969)

2 J M Miller, G L. Wilson, Int J Mass Spectrom Ion Phys, **12**, 225 (1973).

3 J H Beynon, J W. Amy, T Ridley, W. E Baitinger, R G Cooks, *Pittsburg Conference on Analytical Chemistry and Applied Spectroscopy*, Cleveland, Ohio, March 1973, nr 239 și 240.

4 I Mastan, A Toderean, V. Mercea, Studia Univ. Babeș—Bolyai, Phys, 1, 12 (1977).

5 R. G. Cooks, J. H Beynon, R M Caprioli, G. R. Lesrte, *Metastable Ions*, — Elsevier Scientific Publishing Company, 1973.

6 I. Mastan, V Mercea, Z Naturforschg., **24a**, 1959 (1969)

THE DETERMINATION OF THE APPARENT RATE CONSTANTS AND CROSS SECTIONS OF THE METASTABLE DISSOCIATION OF MOLECULAR IONS (II)

Two steps consecutive dissociations

(S u m m a r y)

The using possibilities of a double focusing mass spectrometer for determination of the apparent values of the rate constants λ_1 and λ_2 and cross-sections σ_1 and σ_2 characterizing the two steps consecutive metastable dissociation process $m_0^+ \xrightarrow{\lambda_1,\sigma_1} m^+ \xrightarrow{\lambda_2,\sigma_2} m_1^+$ are discussed. The principle of the method consists in the following. The ratios between metastable peaks intensities of the m^+ ions and normal peak intensities of molecular parent ions are measured at several pressures From the values of these ratios the apparent cross-sections σ_1 and σ_2 of the collision-induced dissociations can be computed. The apparent rate constants λ_1 and λ_2 of the spontaneous dissociations can be computed taking into account the extrapolated values, to zero pressure, of these ratios. The conditions for which one can make a linear extrapolation to zero pressure of the named ratios are also discussed.

STUDIA UNIV BABEŞ—BOLYAI, PHYSICA, 2, 1977

THE THEORETICAL STUDY OF THE ANODIC OXIDATION OF HYDROGEN DISSOLVED IN A THIN PALLADIUM LAYER, BY ELECTROLYSIS IN CONSTANT CURRENT (III)

FELICIA BOTA

The reaction:

$$(H)_m \rightarrow (H)_{ads} \rightarrow H^+ + e^-$$

presented in fig 1 [1] serves to determine the dependence between potential and time.

The adsorbed hydrogen is in equillibrium with the absorbed one, supposing a linear isotherme:

$$[H]_{ads} = K[H]_{abs}$$

or

$$[H]_{ads} = K[H_{abs}]_{x=0}$$

It has been shown [2] that the dependence current — potential, for ireversible processes is:

$$I = z\mathcal{F}Sk_a^0[H_{ads}] \cdot \exp\left[\frac{\alpha z\mathcal{F}}{RT} \cdot \varepsilon_{Pd}(t)\right]$$

or

$$I = z\mathcal{F}Sk_a^0 \cdot K[H_{abs}]_{x=0} \cdot \exp\left[\frac{\alpha z\mathcal{F}}{RT} \cdot \varepsilon_{Pd}(t)\right]$$

But,

$$[H_{ads}]_{x=0} = C(0, t)$$

where $C(x, t)$ has been written in a dimensionless form in eq. (5) [3] and it can be expressed in physical quantities as it follows.

$$C(x, t) = C^0 - \frac{il}{z\mathcal{F}D} \cdot \frac{1}{2(1+m)}\left[\left(1 + \frac{x}{l}\right)^2 + \frac{2Dt}{l^2} - \frac{1+3m}{3(1+m)}\right]$$

and for $x = 0$:

$$C(0, t) = C^0 - \frac{il}{2zFD(1+m)}\left[1 + \frac{2Dt}{l^2} - \frac{1+3m}{3(1+m)}\right]$$

or

$$C(0. t) = C^0 - \frac{i}{z\mathcal{F}D}\left[\frac{l^2 + 2Dt}{2(l+K)} - \frac{l^2(l+3K)}{6(l+K)^2}\right]$$

When $t = \tau$, the concentration at the metal-solution interface becomes:

$$C(0, \tau) = 0$$

which leads to:

$$C^0 = \frac{i}{z\mathcal{F}D}\left[\frac{l^2 + 2D\tau}{2(l + K)} - \frac{l^2(l + 3k)}{6(l + K)^2}\right]$$

Thus,

$$C(0, t) = \frac{I}{z\mathcal{F}S(l + K)}(\tau - t)$$

and

$$I = z\mathcal{F}Sk_a^0K\,\frac{I}{z\mathcal{F}S(l + K)}(\tau - t) \cdot \exp\left[\frac{\alpha z\mathcal{F}}{RT} \cdot \varepsilon_{Pd}(t)\right]$$

The relationship for the potential is given by:

$$\varepsilon_{Pd}(t) = \frac{RT}{\alpha z\mathcal{F}}\ln\frac{l + K}{k_a{}^\circ K} - \frac{RT}{\alpha z\mathcal{F}}\ln(\tau - t)$$

The potential difference between palladium and a hydrogen normal electrode, during the electrolysis is:

$$E(t) = \varepsilon_{Pd} - \varepsilon_{Pt}$$

and when the electrolysis doesn't occur, it is:

$$E^0 = \varepsilon^0{}_{Pd} - \varepsilon_{Pt}$$

The difference between $E(t)$ and E° is called overvoltage. The variation of the potential vs. time is presented in fig. 1.

Thus,

$$\eta = \Delta E = E(t) - E^0 = \varepsilon_{Pd}(t) - \varepsilon^0_{Pd}$$

where

$$\varepsilon^0_{Pd} = \frac{RT}{z\mathcal{F}}\ln\frac{[H^+]}{[H^\circ_{ads}]} = \frac{RT}{z\mathcal{F}}\ln\frac{[H^+]}{KC^\circ}$$

Therefore

$$\Delta E = \frac{RT}{\alpha z\mathcal{F}}\ln\frac{l + K}{k_a{}^\circ K} - \frac{RT}{\alpha z\mathcal{F}}\ln(\tau - t) - \frac{RT}{z\mathcal{F}}\ln\frac{[H^+]}{KC^\circ}$$

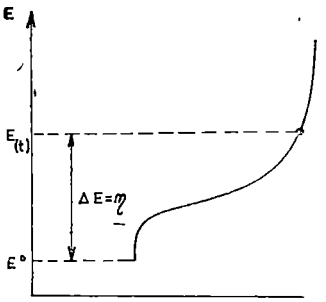

Fig. 1.

or

$$\Delta E = \frac{RT}{z\mathcal{F}} \ln\left[\left(\frac{l+K}{Kk_a^0}\right)^{1/\alpha} \cdot \frac{KC^\circ}{[H^+]}\right] - \frac{RT}{\alpha z\mathcal{F}} \ln(\tau - t) \qquad (1)$$

For reversible processes:

$$\varepsilon(t) = \frac{RT}{z\mathcal{F}} \ln \frac{[H^+]}{[H_{ads}(t)]}$$

$$\varepsilon_{Pd}^0 = \frac{RT}{z\mathcal{F}} \ln \frac{[H^+]}{[H_{ads}^0]}$$

and

$$\eta = \Delta E = \frac{RT}{z\mathcal{F}} \left[\ln \frac{[H^+]}{[H_{ads}^0]} - \ln \frac{[H^+]}{[H_{ads}(t)]}\right]$$

or

$$\Delta E = \frac{RT}{z\mathcal{F}} \ln \frac{C(0,\, t)}{C^\circ}$$

But

$$[H_{ads}^0] = KC^0$$

and

$$[H_{ads}(t)] = KC\ (0,t)$$

Because

$$C(0,\, t) = \frac{I}{zFS(l+K)} (\tau - t)$$

They obtain:

$$\Delta E = \frac{RT}{z\mathcal{F}} \ln \frac{I}{zFC^\circ S(l+K)} + \frac{RT}{z\mathcal{F}} \ln\ (\tau - t) \qquad (2)$$

They can notice that as much for the reversible processes, as for the irreversible ones, there is a linear dependence of the overvoltage on log $(\tau - t)$. The slope is positive for the reversible processes, and it is negative for the irreversible ones.

As the subject of this work is an irreversible process, the slope is negative and it doesn't depend on the initial concentration of hydrogen (deuterium) in palladium. It is possible to calculate the transfer coefficient α_H and α_D. Moreover, the plots of the intercept vs. the activity of hydrogen (deuterium) ions in solution are straight lines, which permit to calculate the rate constants $(k_a^0)_H$ and $(k_a^0)_D$.

(*Received March* 5, 1976)

REFERENCES

1. F. Bota, R V. Bucur, I. Covaci, Studia Univ. Babeş-Bolyai, Phys., 2, 61 (1974).
2. P. Delahay, T. Berzins, J. Am. Chem Soc, **75**, 2486 (1953).
3. F. Bota, I. Covaci, R. V. Bucur, Studia Univ. Babeş-Bolyai, Phys, 41 (1975).

STUDIUL TEORETIC AL OXIDĂRII ANODICE A HIDROGENULUI DIZOLVAT ÎN STRAT SUBŢIRE DE PALADIU, PRIN ELECTROLIZA LA CURENT CONSTANT (III)

(Rezumat)

Se determină dependenţa potenţialului în funcţie de timp, pentru procesele reversibile şi ireversibile.

STUDIA UNIV BABEŞ—BOLYAI, PHYSICA, 2, 1977

SPECTRELE DE ABSORBŢIE ŞI LUMINISCENŢĂ ALE ORTO, META ŞI PARA FENILENDIAMINEI ÎN MATRICE DE BENZEN LA 77°K

IRIMIE MILEA

Fenilendiamina este o substanţă de bază în sinteza multor compuşi organici. Corelarea spectrului de absorbţie şi mai ales cel de luminiscenţă cu spectrele I.R. şi Raman prezintă deci interes, contribuind la o mai bună cunoaştere a structurii acestei molecule.

Substanţa este destul de instabilă şi are o presiune de vapori mică, mai ales substituenţii para şi orto, motive care au determinat nereuşita unei analize complete a spectrului de vapori [1].

În prezenta lucrare se analizează spectrul de absorbţie şi luminiscenţă al fenilendiaminei înglobată în matrice de benzen la temperatura de 77°K.

Instalaţia experimentală folosită este descrisă în [2]. Spectrele au fost fotografiate pe plăci ORWO Blau Extrahart, timpii de expunere variind între 30 minute pentru absorbţie şi 3 ore pentru luminiscenţă.

Substanţele utilizate au fost produse de firma Merk şi au fost purificate prin recristalizări succesive din benzen. Puritatea s-a controlat prin verificarea punctului de topire.

Ca matrici s-au încercat o serie de parafine normale liniare, parafine ciclice şi alcooli superiori însă nu s-au obţinut rezultate care să se preteze la o analiză vibraţională decît în matrice de benzen. Îngheţarea s-a făcut încet prin imersarea în azot lichid a cuvei cu soluţie. Lărgimea benzilor, atît în spectrele de absorbţie cît şi în cele de luminiscenţă, variază între 6—10Å, deci chiar şi în cazul matricei de benzen nu se obţine o înglobare ideală existînd şi interacţiuni cu moleculele matricei [3]. Domeniul de concentraţii în care spectrul se structurează este aproximativ pentru absorbţie între $2M^{-2}$ şi $7M^{-3}$, iar pentru luminiscenţă între $2M^{-3}$ şi $8M^{-3}$.

Conform teoriei orbitalilor moleculari dezvoltată de R. N. Nurmuhamentov [4], probabil că la fenilendiamină tranziţiile $\pi\pi^*$ şi $n\pi^*$ se suprapun la absorbţie, ceea ce face ca spectrul să fie structurat, însă difuz. Luminiscenţa corespunde tranziţiilor de tip $\pi\pi^*$ şi este continuă la orto-fenilendiamină. Faptul că originea benzilor de absorbţie şi luminiscenţă nu coincide, duce la concluzia că este vorba de o fosforescenţă condiţionată de tranziţia $T_{\pi\pi^*} \rightarrow S_0$ datorată conversiei interne cu probabilitate mare $S_{n\pi^*} \rightarrow T_{\pi\pi^*}$.

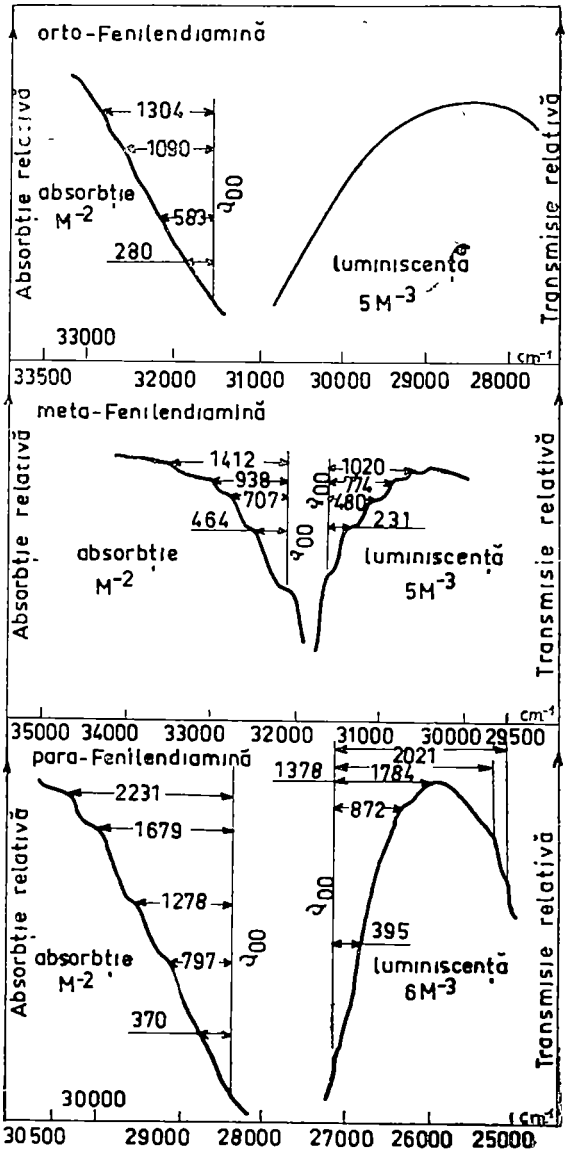

Fig. 1.

Aspectul spectrelor se observă în fig. 1, iar rezultatele măsurării pozițiilor benzilor de absorbție și luminiscență în comparație cu cele obținute prin efect Raman [5], [6], I.R. [7] și spectrul de vapori [1], sînt date în tabelul 1.

Tabel 1

Substituent	Efect Raman	I.R.	Vapori		În matrice de benzen				Interpretare
			stări de bază	stări excitate	stări de bază		stări excitate		
	$\Delta\nu cm^{-1}$	$\Delta\nu cm^{-1}$	$\Delta\nu cm^{-1}$	$\Delta\nu cm^{-1}$	νcm^{-1}	$\Delta\nu cm^{-1}$	νcm^{-1}	$\Delta\nu cm^{-1}$	$\Delta\nu cm^{-1}$
							31595		0—0
							31876	281	0+281
							32178	583	0+583
	775	746							
	870								
	1030						32685	1090	0+1090
		1205							
		1250							
	1270						32899	1304	0+1304
	1580	1595							
orto	1600								
					31532				
			211		31301	231	32087		0—0
				455			32551	464	0+464
					31052	480			
		599	537						
				715			32794	707	0+707
	757		758						
		780			30758	774			
	993	966		954			33025	938	0+2×464
	1065				30512	1020			
	1172								
				1205					
	1319	1330		1318					
							33499	1412	0+2×707
meta	1483			1565					
					27136		28284		0—0
					26741	395	28654	370	0+370
	421								
	469								
		520							
	646								
	691								
		733							
	750						29081	797	0+797
	845				26264	872			
		1015							
	1175								
	1264	1267					29562	1278	0+1278
	1348	1314			25818	1318			
		1522							
	1612	1640					29963	1679	0+1679
					25352	1784			
					25115	2021			
							30415	2231	0+2231
para	3045	3225							

Corelînd aceste rezultate cu domeniile de frecvențe pentru diferite vibrații ale derivaților orto meta și para disubstituiți ai benzenului [8], se pot elucida cîteva din modurile de vibrație ale moleculei de fenilendiamină.

În tabelul 2 se observă domeniile aproximative de absorbție ale substanței în stare de vapori și în matrice de benzen la 77°K.

Tabel 2

Substituent	Vapori Domeniul $\nu \cdot cm^{-1}$	Matrice de benzen Domeniul $\nu \cdot cm^{-1}$
orto	33333—35714	31595—32899
meta	32258—35842	32087—33499
praa	29585—32787	28284—30415

Evident că domeniile de absorbție în vapori conțin și benzile calde și din acest motiv lărgimea lor este mai mare, însă chiar și în aceste condiții se observă că deplasările sînt maxime pentru substituentul orto și minime pentru meta. Aceste deplasări fiind o măsură a interacțiunii moleculei cu matricea, se poate conclude că interacțiunea este mare la substituentul orto și mică la meta, care deci se apropie cel mai mult de condițiile ideale ale moleculei libere. Aceste concluzii sînt verificate și experimental, spectrul substituentului meta fiind mult mai net decît al substituentului orto, iar para fiind într-o situație intermediară Este probabil că un studiu la o temperatură mai joasă ar conduce la o structurare mai netă a benzilor și deci la o precizie mai ridicată a rezultatelor experimentale.

(*Intrat în redacție la 7 octombrie* 1976)

BIBLIOGRAFIE

1. Akira Sado, Tosinobu Anno, J Chem Phys **23**, 1970 1955.
2. T. Iliescu, H. Țintea, Studia Univ. Babeș—Bolyai, Physica, 24, 1976.
3 S Leach, Journal de Physique **28**, C_3—134, 1967
4. R N Nurmuhamentov, *Pogloscenie i luminiscentia organiceskih soedinenii*, Izd. Mira, Moskva, 1971
5. Landolt-Bornstein, *Zahlenwerte und Funktionen*, Springer-Verlag Tl 11, Berlin, 1951
6. M. Brigodiot, J. Marie Lebas, J de Chem. Phys et de Phy. Chem Biologique, **62**, 347, 1965.
7 G. Karagounis, O Peter, Z Elektrochem, **63**, 1120, 1959
8 G Varsanyi, S. Szoki, *Vibrational spectra of benzen derivatives*, Akademiai Kiado, Budapest, 1963

THE ABSORBTION AND LUMINISCENCE SPECTRA OF THE ORTO, META AND PARA PHENYLENEDIAMINE IN A MATRIX OF BENZENE AT 77°K

(Summary)

The absorbtion and luminiscence spectra of the phenylenediamine trapped in a matrix of benzene at 77°K is observed in the near ultraviolet region. A vibrational analysis is proposed A comparison is given with the results obtained by other authors.

STUDIA UNIV BABEŞ—BOLYAI, PHYSICA, 2, 1977

GERÄT FÜR OPTISCHE SPEKTROSKOPIEMESSUNGEN BEI VERÄNDERLICHEN TEMPERATURWERTEN

IRIMIE MILEA und WERNER MIESKES

Optische Spektroskopiemessungen bei tiefen Temperaturwerten von festen oder flussigen Substanzen benotigen unbedingt ein Kryostat. Kryostate konnen von zweierlei Art sein, (was den Aufbau anbelangt) undzwar, einerseits, wo die zu messenden Proben direkt in die Kuhlflussigkeit eingetaucht werden, anderseits wird das Abkuhlen der Probe durch Leitfähigkeit, durch Kontakt, erreicht, die zweite Methode ist vorteilhafter fur solche Falle wo das Spektrum photoelektrisch registriert wird.

Beide Arten von Kryostaten bestehen in erster Reihe aus Dewargefässen. Im ersten Fall ist eine Spezialanfertigung des Gefasses erforderlich, da Fenster angebracht werden und die Probe, welche an einer Kuvette an einem Eintauchstab befestigt ist, wird in die Kuhlflüssigkeit eingetaucht, Hiermit konnen die Messungen nur bei einem Temperaturwert durchgeführt werden und für einen bestimmten Wert des Druckes der Dampfe der Kühlflussigkeit [1] .(z.B. flussiger Stickstoff) Im zweiten Fall besteht die Gefahr des Verdampfens der Probe, durch den Einfluss des Kontaktes-Probe-Kuvette und Kuhlflüssigkeit [2].

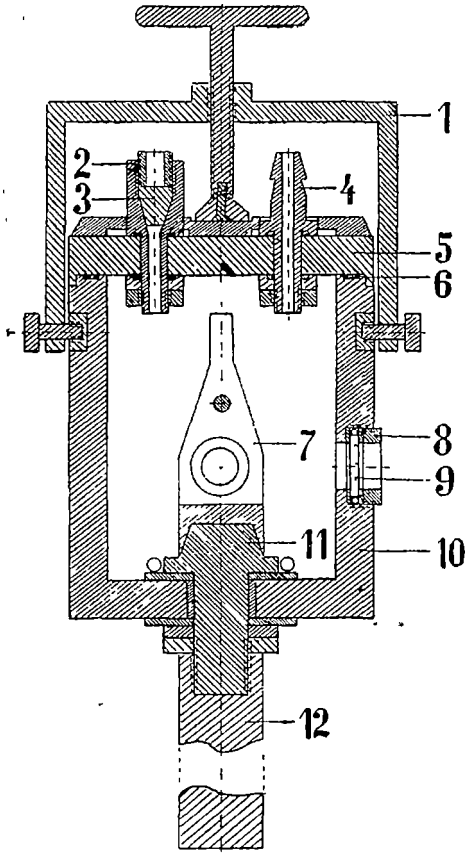

Abb 1

In diesem Bericht wird ein Gerat dargestellt wo die meisten Nachteile beseitigt werden Der Langsschnitt ermoglicht die Beobachtung der einzelnen Bestandteile (Abb 1).

Der Hauptteil (wo sich, die zu messenden Substanzen befinden) ist ein zylinderisches Gefäss (10) aus Aluminium Das Gefass wird mittels eines Deckels (5) und einem Doppelarm mit Schraube (1) verschlossen Um eine moglichst gute Abdichtung zu erziehlen wird eine ringformige Teflongarnitur benutzt. Der Deckel (aus Aluminium) wird mittels einer kreisför-

miger Platte mit Profil, auf welche die Schraube des Doppelarms wirkt, befestigt. Hierdurch wird ein gleichmässiges Andrücken des Deckels auf die Gefasswand erreicht. Im Deckel sind zwei Öffnungen vorgesehen für den Zugang in's Innere des Gefasses. An einer Öffnung ist mittels Teflongarnituren ein Stutzen (4) angebracht welcher mittels eines Gummischlauches mit einer Vakuumpumpe verbunden wird. Die zweite Öffnung dient zur Einführung eines Thermoelementes (3) aus Kupfer-Konstantan. Die Drahte des Thermoelementes werden durch einen Teflonstopfen gezogen. Der Stopfen wird der Lange nach halbiert und durch das feste Anziehen mittels einer ringformigen Mutter wird der Stopfen in die Offnung gepresst um auch hier eine gute Abdichtung im Innenraum zu haben.

Die Halterung (7) aus Abb. 1 (wird naher in Abb. 3 dargestellt) ermoglicht das Befestigen der flussigen Probe oder Festkorperprobe. Am Plattchen (2) wird das Thermoelement befestigt [3]. Die Halterung wird aus Kupfer hergestellt und wird auf eine kegelformige Basis (11) (Tragkorper) welche auch aus Kupfer ist, aufgesetzt Der kegelformige Tragkorper ist am unteren Teil des Gefässes befestigt und mittels Teflongarnituren von Aluminiumgefass isoliert. An den Tragkorper (11) wird die zylinderförmige Eintauchstange (12) angeschraubt, welche auch aus Kupfer ist. Die Eintauchstange (12) wird in die Kuhlflüssigkeit eingetaucht. Die Kuhlflüssigheit befindet sich in jedwelchem Dewargefass.

Das Gefäss besitzt vier Fenster (siehe Abb 2) so dass Fenster (1) u. (4) in gleicher Hohe und Linie sind, sie werden fur Absorbtionsspektren verwendet. Fester (3) und Fenster (2) sind auf 90° und 45° bezüglich der Axe der Fenster (1) und (4) angebracht. Mittels dieser Fenster kann man Luminiszenzspektren erhalten, Reflektion bei 45° oder 22,5° und

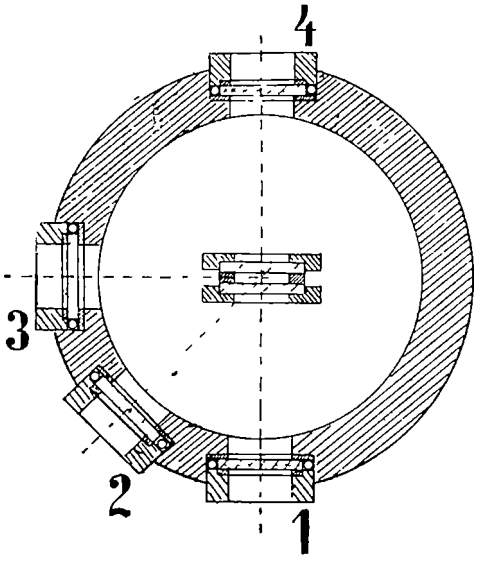

Abb. 2.

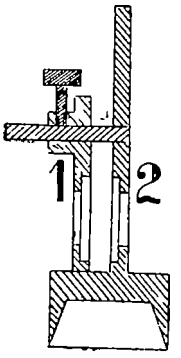

Abb. 3.

Absorbtion im Triplettstadium. Die Fenster werden aus Material hergestellt welches dem Spektralbereich endspricht (Z B Quarz).

Die Befestigung der Fenster ist ersichtlich aus Abb. 1, mit Hilfe einer ringformigen Aussenmutter wird das Fenster (9) an Ort und Stelle befestigt. Auch hier werden zur Abdichtung je zwei Teflongarnituren benützt. Um das „Anlaufen" oder Vereisung der Fenster zu vermeiden, werden diese mittels ringformigen Heizwiederständen geheizt. Die Heizwiederstande sind parallel geschaltet und werden mit einem Transformator 220/6 V gespiest

Die veranderliche Temperatur im Innenraum des Gefässes, also der Probe, wird mit Hilfe eines toroidformigen Heizwiederstandes geregelt. Der Wiederstand ist am Tragkorper (11) befestigt und wird mit einem Autotransformator gespeist. Ein Kontakt des Wiederstandes ist an dem Tragkorper bzw. Eintauchstange (12) befestigt und der andere Kontakt, am Aluminiumgefäss (10). Der Wiederstand heizt direkt die Halterung der Probe und der Temperaturbereich betragt 80K° bis 273K°.

Wahrend des Betriebes wird die Temperatur von 80K°, nach dem Eintauchen der Eintauchstange in flussigen Stickstoff, nach etwa 15 Minuten erreicht

Um den Wasserdampfniederschlag auf die Probe zu vermeiden muss im Innenraum des Gefasses, Vakuum sein. Die Abkuhlung der Probe geschieht relativ langsam, also demendsprechend auch der Niederschlag des Wasserdampfes, desshalb ist es angeraten die Vakuumpumpe erst nach dem Gefrieren der Probe einzuschalten. Hiermit wird auch die Gefahr einer eventuellen Verdampfung der flüssigen Probe, beseitigt. Trotzdem durch den geringen Vakuumbereich (1 mm Hg) nach 150—200 Minuten, im Inneraum setzt sich Schnee an die Oberflachen der Probe, dadurch ist die Dauer der Messungen begrenzt. Durch das Einsetzen eines Beutels mit Silikagel wird auch dieser Nachteil beseitigt.

Nach einer Zeitspanne von 40—50 Minuten überzieht sich die Oberfläche des Gefasses mit Schnee, dadurch werden die Messungen nicht behindert da alle 4 Fenster rein bleiben, durch ihre Heizung. Dieses Kondensieren kann verhutet werden durch einen Warmluftstrom oder das Einbauen der Gefasses in Polistiren.

In Sonderfällen, kann das Bestandteil fur den Durchgang des Thermoelementes (4), durch einen gleichen Stutzen (2) ersetzt werden und hiermit kann ein Stickstoffstrom (Dämpfe) im Inneren durchgefuhrt werden. Das Thermoelement wird entfernt und die verschiedenen Temperaturwerte werden mit dem Heizwiederstand erreicht oder durch Veränderung der Gasdurchflussmenge der Stickstoffdampfe.

Aus dem Bericht geht hervor dass die Konstruktion des Gefasses recht einfach ist und es kann jedwelches Dewargefass verwendet werden, Ausserdem nach Beendigung der Messungen wird das Gerat aus dem Dewar herausgehoben somit kann der flussige Stickstoff weiter aufbewahrt werden.

(Eingegangen am 22 Novembre, 1976)

LITERATUR

1. B Meyer, *Low temperature spectroscopy*, American Elsevier Publishing Company, Inc New York, 1971.
2. R. F. Broom und A. C. Rose-Innes, J. Sci. Instr., **33**, 420, (1965).
3. A. M. Boss und H. P Broida, *Formation and trapping of free radicals*, Academic Press, New York and London, 1960.

DISPOZITIV PENTRU STUDII DE SPECTROSCOPIE OPTICĂ LA TEMPERATURI VARIABILE

(Rezumat)

În lucrare se descrie un dispozitiv care permite variația continuă a temperaturii probei de la 80°K pînă la 273°K. Răcirea se face prin conducție.

STUDIA UNIV BABEŞ—BOLYAI, PHYSICA, 2, 1977

THE FREEZING PROPERTIES OF ADSORBED WATER ON SILICA SURFACE IN PRESENCE OF PARAMAGNETIC IONS

V. ZNAMIROVSCHI, O. COZAR and V.V. MORARIU*

It has been previously shown that the spectra of Cu^{2+} adsorbed on silica surface depends on the amount of adsorbed water [1].

The goal of this study is to further investigate the freezing properties of adsorbed water on silica surface in the presence of paramagnetic ions (VO^{2+}, Mn^{2+}).

At room temperature, the VO^{2+} ions in adsorbed state show the same spectra as in bulk solutions which consist from the eight hyperfine structure lines (fig. 1). This suggests that the $[VO(H_2O)_5]^{2+}$ complex is not influenced by the silica surface. The anisotropic interactions are averaged by the tumbling motion of the „microcrystals", the EPR parameters of this spectrum being $g = 1.988$ and $A = 95.2$ Gs.

On the other hand, the EPR spectrum obtained at 77 K (fig. 1) shows an axial symmetry of $[VO(H_2O)_5]^{2+}$ complex. It is characterized by $g_{\parallel} = 1.940$, $g_{\perp} = 2.007$, $A_{\parallel} = 190.5$ Gs and $A_{\perp} = 66$ Gs.

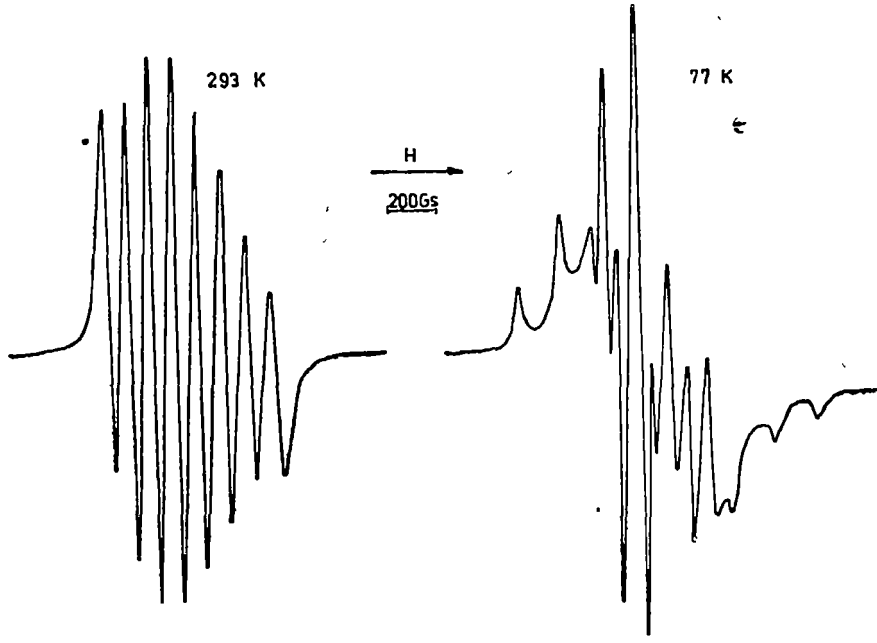

Fig. 1. E.P.R. spectra of VO^{2+} ion on silica surface.

* Stable Isotope Institute, Cluj-Napoca.

This result is similar to that obtained in glassy water-ethanol mixtures [2]. On the basis of this similarity we may conclude that the adsorbed water on silica surface freezes in an amorphous state and not in a common polycrystalline state. This fact is also confirmed by the E.P.R. spectrum of Mn^{2+} (fig 2), in a good agreement with the results obtained for adsorbed water on γ-alumina [3].

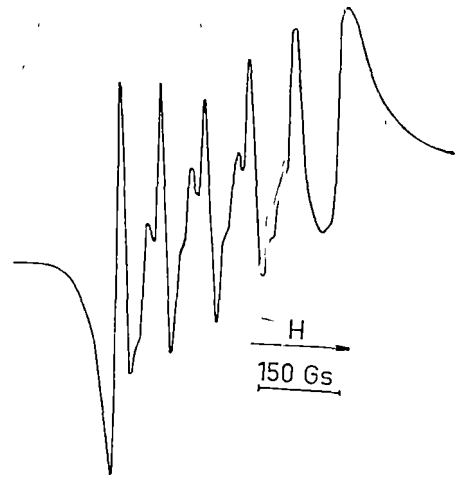

Fig. 2. E.P.R. spectra of Mn^{2+} on silica surface at 77K.

At room temperature the shape of E.P.R. spectra may be changed by partial dehydration, suggesting an axial symmetry. In the case of vanadyl ion, two groups of hyperfine lines corresponding to $g_{\parallel}$ and $g_{\perp}$ become evident (fig. 3). This may be explained in terms of a stronger interaction of the hydrated complex with the silica surface. The tumbling motion of the „microcrystal" is quenched and the anisotropic interactions are not completely averaged.

At 77 K the E.P.R. spectrum for VO^{2+} on silica dehydrated sample (fig. 3) is not much different from that obtained at room temperature, and the asymmetry of the complex is weaker than in fig. 1. In the case

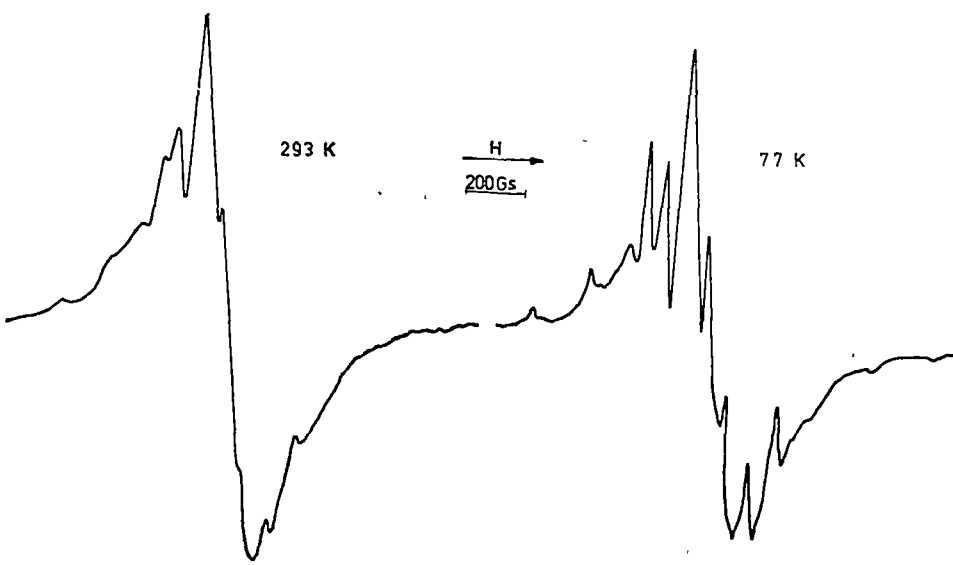

Fig. 3 E.P.R. spectra of VO^{2+} ion after partial dehydration.

of Cu^{2+} in adsorbed water on silica surface we have found that the spectrum of partially dehydrated sample (fig. 4) is similar to that obtained in bulk water at 77 K, where hyperfine structure is not evidenced [4].

These may lead to an interesting conclusion, that in the case of the partially dehydrated samples the adsorbed water on silica surface freezes in a polycrystalline state.

Therefore, the adsorbed water on silica surface seems to freeze in two distinct ways, depending on its amount. For high adsorbed water content (over two statistical monolayers) at room temperature, the studied hydrated complexes have the same behaviour as in adsorbed state of water as in bulk water.

The effect of the surface is evident only at low temperatures where the adsorbed water freezes in amorphous state, unlike bulk water which freezes in a polycrystalline state. In this case, the E.P.R. spectra are characterized by a strong axial symmetry component.

For smaller adsorbed water content (about one statistical monolayer) the water is more strongly bound by the silica surface and the mobility of hydrated complexes of paramagnetic ions decreases.

By freezing at 77 K the „microcrystals" are easy attached on the silica surface being not deformed by the structural network of water. In this case

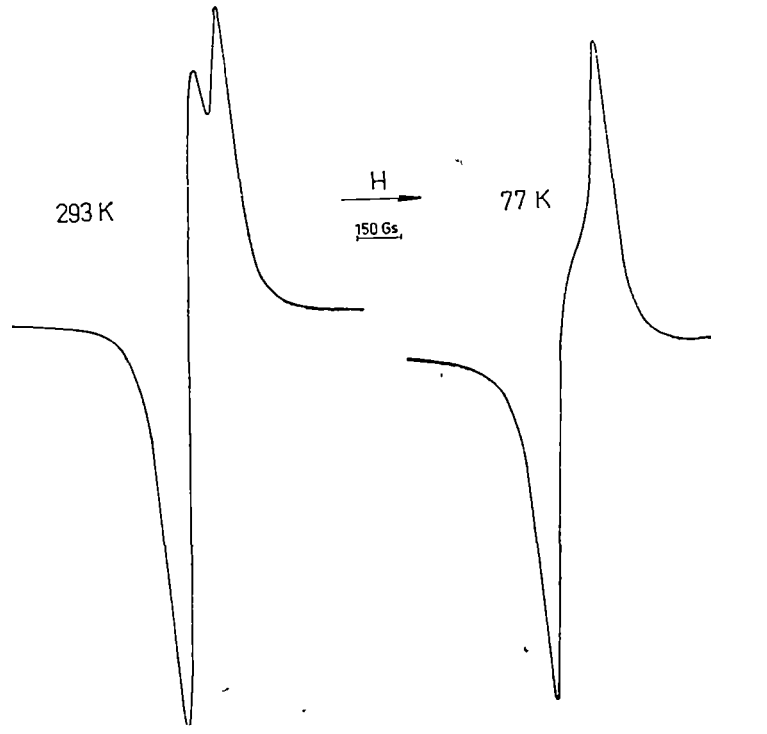

Fig. 4. E.P.R. spectra of Cu^{2+} after partial dehydration.

a freezing in a polycrystalline manner appears. The axial component is not well evidenced because of a small averaging effect.

In our experiments the adsorbent was a chromatographic silica manufactured by Mallinchrodt Chemical Works and designated as ARCC-4/100-200. The surface area measured by Kripton adsorption was found to be 600 m^2/g. The silica surface was impregnated with paramagnetic ions from aqueous solution. After drying, the impregnated silica was introduced in glass tubes which were sealed before E.P.R. measurements. The E.P.R. spectra were recorded with a JES-3B spectrometer, working at X-band frequencies with 100 Kc magnetic field modulation.

(Received October 9, 1976)

REFERENCES

1 O. Cozar, V Znamirovschi, V V Morariu, Rev. Roum. Phys,. **21** (6) 579 (1976).
2. V Znamirovschi, O. Cozar, Al. Nicula, Mol Phys , **27**, 273 (1974).
3 L. Burlamachi, J. C. S Faraday II, **1**, 54 (1975).
4 V Znamirovschi, O. Cozar, Al. Nicula, Isotopenpraxis, **1**, 29 (1972).

PROPRIETĂŢI DE ÎNGHEŢARE ALE APEI ADSORBITE PE SILICAGEL ÎN PREZENŢA IONILOR PARAMAGNETICI

(Rezumat)

În lucrare se face o investigare R.E.P. a proprietăţilor de îngheţare ale apei adsorbite pe suprafaţa pulberii SiO_2, folosindu-se ca senzori ionii paramagnetici VO^{2+} şi Mn^{2+}.

S-a găsit că forma spectrelor REP este dependentă de cantitatea de apă adsorbită, evidenţiindu-se la 77°K două situaţii distincte. Atunci cînd există mai mult de două straturi statistice monomoleculare de apă adsorbită, se obţine o îngheţare a acesteia în stare amorfă, iar atunci cînd există o cantitate mai mică, în jur de un monostrat, apa îngheaţă în stare policristalină.

STUDIA UNIV BABEŞ—BOLYAI, PHYSICA, 2, 1977

THE HYBRIDISATION IN TRANSITION METALS (I)

V. CRIŞAN, M. MUREŞAN

The description of the electronic energy levels of ferromagnetic transition metals, has been developed using the interpolation scheme of H o d g e s and all [1] in order to obtain the influence of hybridisation in the density of states.

The electronic specific heat, the Pauli susceptibility, the transport properties and the presence or absence of ferromagnetism, all depend on the density of states at the Fermi level $\eta(E_F)$. We are interested in the density of states, to perform self consistent band calculation in order to find the appropiate values for hybridisation parameters for spin waves in transition metals calculation.

The many-electron Hamiltonian is:

$$H = H_{\text{band}} + H_{\text{corr}} \tag{1}$$

where H_{band} is the ordinary band Hamiltonian and H_{corr} is the correlation Hamiltonian and it is given by:

$$H_{\text{corr}} = U^{d-d} \sum_{i\mu} n_{i\mu\uparrow} n_{i\mu\downarrow} + U^{d-d} \sum_{i\sigma\sigma'} n_{i\mu\sigma} n_{i\mu'\sigma'}$$
$$- J^{d-d} \sum_{\substack{i\sigma \\ u \neq u'}} n_{i\mu\sigma} n_{i\mu'\sigma} - J^{s-d} \sum_{i\sigma k\mu} n_{i\mu\sigma} n_{ik\sigma} \tag{2}$$

in H u b b a r d [2] approximation. The first term describes the intra-atomic Coulomb repulsion between two antiparallel d electrons in the same orbital μ on the same atom site i, and the second the Coulomb repulsion betwe en d electrons in different orbitals on the same atom. The third and fourth terms correspond, respectively, to exchange interactions among d orbitals and between d and s orbitals. We assume the polarization of the conduction electrons to arise purely from the magnetisation of the d electrons via a Hund's-rule coupling (J^{s-d}).

We shall represent the unhybridized d bands in terms of linear combinations of atomic orbitals φ_μ:

$$b_{k\mu}(\vec{r}) = \langle \vec{r} | \vec{k}\mu \rangle = N^{-\frac{1}{2}} \sum_l e^{i\vec{k}\vec{R}_l} \varphi_\mu(\vec{r} - \vec{R}_l) \quad \mu = , \ 1 \ldots, 5 \tag{3}$$

where the $\varphi_\mu(\vec{r} - \vec{R}_e)$ are atomic d orbitals centered at the site $\vec{R}_e$ and N is the number of atoms in the solid. The atomic orbitals have the form:

$$\varphi_1(\vec{r}) = \left(\frac{15}{4\pi}\right)^{\frac{1}{2}} xyf^{T_{2g}}(r)/r^2$$

$$\varphi_2(\vec{r}) = \left(\frac{15}{4\pi}\right)^{\frac{1}{2}} yzf^{T_{2g}}(r)/r^2$$

$$\varphi_3(\vec{r}) = \left(\frac{15}{4\pi}\right)^{\frac{1}{2}} zxf^{T_{2g}}(r)/r^2 \tag{4}$$

$$\varphi_4(\vec{r}) = \left(\frac{15}{16\pi}\right)^{\frac{1}{2}} (x^2 - y^2)f^{Eg}(r)/r^2$$

$$\varphi_5(\vec{r}) = \left(\frac{15}{16\pi}\right)^{\frac{1}{2}} (3z^2 - r^2)f^{Eg}(r)/r^2$$

and satisfy:

$$[(P^2/2m) + U(\vec{r})]\varphi(\vec{r}) = E_{\text{atomic}}\,\varphi(\vec{r})$$

$U(r)$ is the atomic potential and $f^\mu(r)$ are the normalized radial function of the isolated atom.

The conduction bands in a nearly-free electron approximation is described by OPW method. The OPW's have the form:

$$b_{kK}(\vec{r}) = \langle\vec{r}\,|\vec{k} + K\rangle = \chi[\langle\vec{r}\,|k + K\rangle - \sum_\mu \langle\vec{r}\,|\vec{k}\mu\rangle\langle\vec{k}\mu\,|\vec{k} + \vec{K}\rangle] \tag{5}$$

where the k are reciprocal lattice vectors and χ the normalization factor. The wave functions $\langle\vec{r}\,|\vec{k} + \vec{K}\rangle$ are plane waves.

$$\langle\vec{r}\,|\vec{k} + \vec{K}\rangle = (Nv_{\text{atomic}})^{-1/2}\, e^{i(\vec{k}+\vec{K})\vec{r}}. \tag{6}$$

The appropiate OPW's for the 1/48 of the Brillouin zone are formed from four plane waves $\langle\vec{r}\,|\vec{k} + \vec{K}\rangle$ where $\vec{K}_1 = (0, 0, 0)$ $K_2 = \frac{2\pi}{a}(0, 2, 0)$, $\vec{K}_3 = \frac{2\pi}{a}(1, 1, 1)$ and $\vec{K}_4 = \frac{2\pi}{a}(1, 1, 1)$.

The interpolation scheme will use as basis functions the LCAO, s defined in Eq(3) and the plane waves given by (6). The energy eigenvalues are given by the solution of the secular equation

$$\det\,|\langle\vec{k}\nu\sigma\,|H\,|\vec{k}\nu'\sigma\rangle - E\langle\vec{k}\nu\sigma\,|\vec{k}\nu'\sigma\rangle\,| = 0$$

where ν includes the d and conduction band indices: μ and K. In the paramagnetic case the $\uparrow\uparrow$ and $\downarrow\downarrow$ blocks are identical and only a 9×9 matrix must be considered, but in ferromagnetic case the secular determinant is 18×18.

Using the Hodges numerical values for interpolation parameters we obtained the ferromagnetic band structure of Ni along Σ symmetry line (fig. 1).

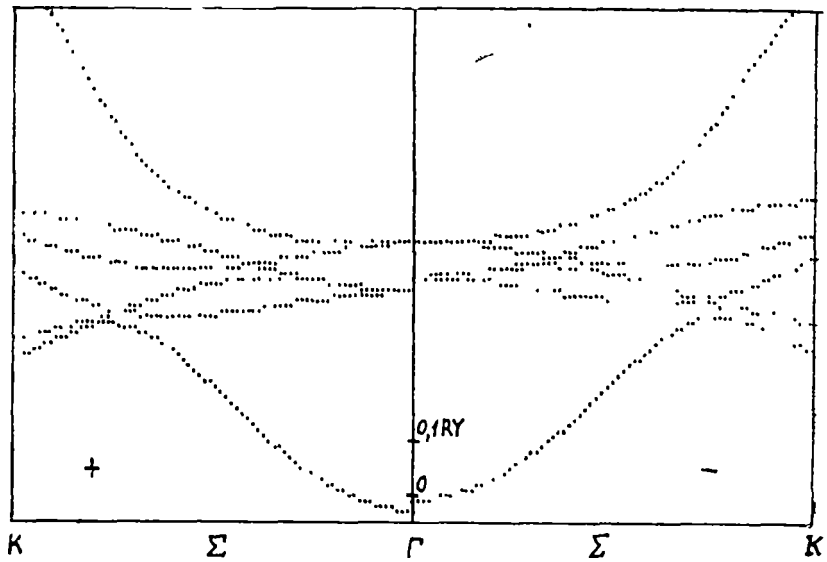

Fig. 1.

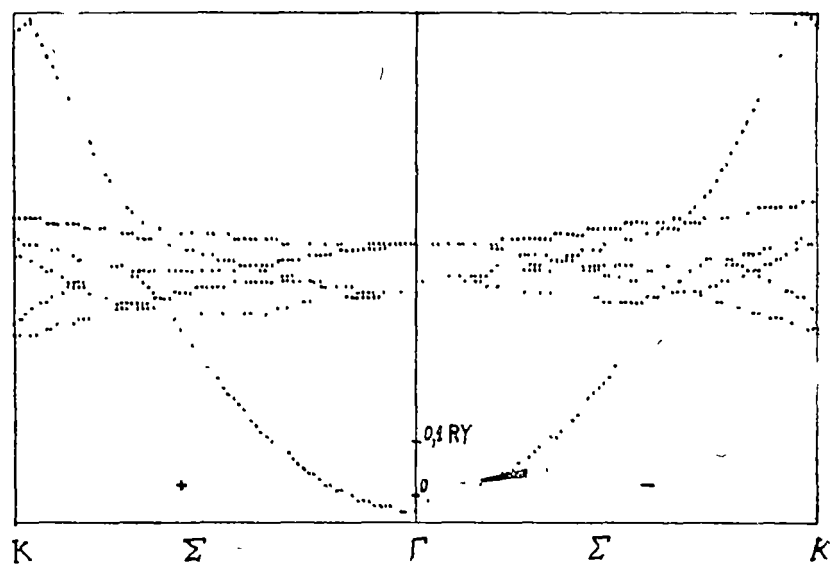

Fig. 2,

+ and — means the majority and minority spin bands. The hybridisation matrix elements depend on the radial function of the atoms $f(r)$. We have made modifications in the numerical values of hybridisation matrix elements taking different values for numerical parameters containing the radial functions. The results are shown in fig. 2, fig. 3, fig. 4.

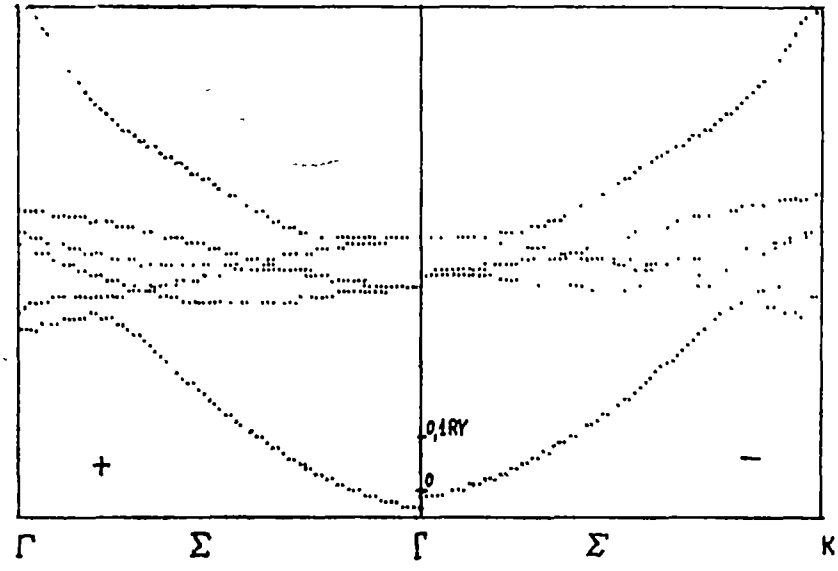

Fig. 3,

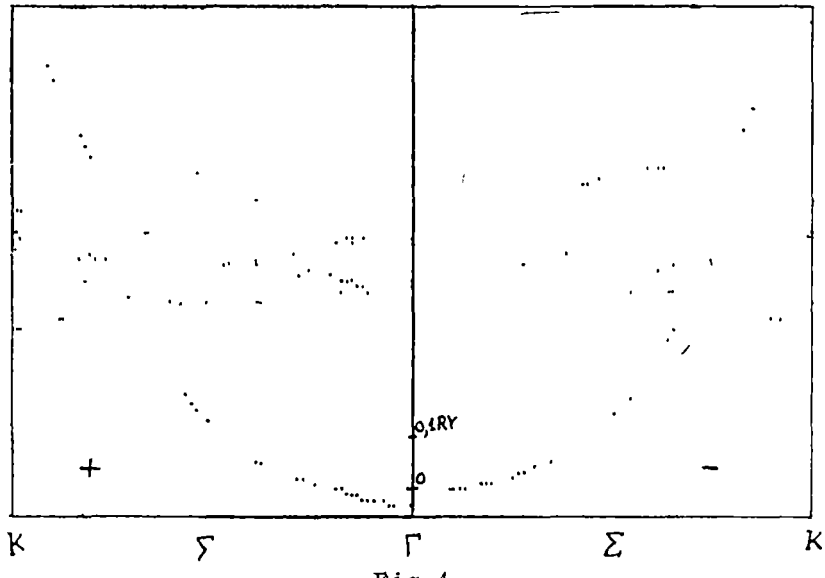

Fig. 4,

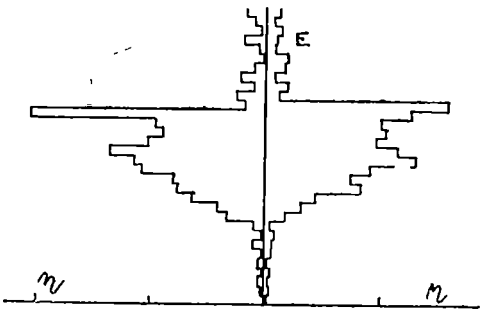

Fig 5

The parameter was twice smaller (fig. 2) twice bigger (fig. 4) and 0,5 bigger (fig. 3), than that used in Hodges papers. It is easy to see that the forms of hybridised bands are changed showing different k dependences for all four cases. In general the forms of bands are unchanged in the centre and the boundary of the Brillouin zone. Changing the hybridisation parameters, not only the hyridized bands are changed. Strong modifications show the unhybridised d bands near the boundary zone too.

We have calculated the density of states for the bands of fig 2.

Using Burdick k — points in Brillouin zone and the following formula:

$$\eta(E) = \frac{\sum_{nk,\,|En(k)-E|<\frac{1}{2}\Delta E} W(k)}{\Delta E \sum_{k} W(k)} \tag{7}$$

where $W(k)$ is the number of k vectors in the star of k, and $\Delta E = 0.03$. we obtained the density of states which is slightly different from the Hodges one.

In spite of the fact that some physical properties, like electronic specific heat, are not in total agreement with that derived from this band calculation, this interpolation scheme is appropriate for the study of the mixing of d with $s-(p)$ states in transition metals.

The numerical calculations were made using an original program on the Romanian computer Felix C-256 for which the authors want to thank the stuff of CTCE.

(Received January 18, 1977)

REFERENCES

1. Hodges, L., Phys. Rev. **152**, 505 (1966).
2 Hubbard, J, Proc. Roy. Soc. (London), A**276**, 238 (1963).

HIBRIDIZAREA ÎN METALE DE TRANZIŢIE (I)

(Rezumat)

Lucrarea şi-a propus studierea fenomenului de hibridizare folosind schema de interpolare propusă de Hodges şi Ehrenreich. S-au urmărit efectele modificări elementelor de matrice din blocul OPW—LACO în forma benzilor de energie şi în densitatea de stări.

STUDIA UNIV BABEŞ—BOLYAI, PHYSICA, 2, 1977

LARGE KCl SINGLE CRYSTAL PREPARATION

AL. DARABONT, P. FITORI and AL. NICULA

I. **Introduction.** KCl has such optical properties which permit its application as prisms and windows in ultraviolet and infrared spectroscopy. It is one of the best materials for the apparatuses and experimental equipments which have utilizations in the infrared region from 2 to 18 μm. For this reason the obtaining of large KCl single crystals has a great importance. The present information gives experimental details with respect to the large KCl single crystal growing in our laboratory for proper purposes.

The KCl single crystals have been yet obtained by many authors with different techniques. From the great number of references we have selected a few. Wagner [1] prepared little single crystals of KCl by sublimation in vacuum. Botsaris [2], Steinike [3], Schnerb and Bloch [4], Schock [5] have studied the growing process of KCl from aqueous solution with or without impurities. The crystal growing mechanism was also studied by Batchelder and Vaughan [6] and by Shikiri et al. [7], whereas the rate of growing by Peibst and Noak [8]. These two methods usually give little single crystals and a larger one needs a long time of growing.

Crystals of large dimensions can be obtained in a relatively short time from the melt. So Franks [9] obtained single crystals of KCl by slow cooling of the melt in stationar crucible [10, 11]. Grassano and Jacobs [12], Grundig and Wasserman [13] grew doped and pure single crystals of KCl by Bridgman-technique [14, 15]. Gründig [16], Pauly and Süe [17] purified and grew KCl single crystals by zone melting technique. Kanzaki et al. [18] and Warren [19] purified and obtained KCl crystals in Cl_2 and HCl atmosphere by zone melting technique. Schonherr [20] grew pure KCl single crystals with low dislocation densities by Kyropoulos technique [21]. Butler et al. [22] obtained high purity KCl single crystals by Czochralski technique [23].

We used the Kyropoulos technique because of its following advantages.

— it is useful in large crystal growing especially from alkali halides

— it was the easiest to achieve in our conditions

— the crystal growing process is observable all the time of growing and the appearance of the defects can be remedied

— the crystal is growing free and the tension creation probabilities are smaller than in the case of Bridgman-method or in the case of slow cooling of the melt in stationar crucible.

As the cooling is realised along the crystal, it contributes to the appearance of the tensions due to the temperature gradient, which is a disadvantage.

2 **Experimental equipment.** The experimental equipment used by us is composed of the following parts

1) A resistance furnace with kanthal A heating wires, constructed by us, from two parts · the lateral is a cylindrical one, the inferior is a flat one.

2) The power supply is composed of two adjustable power transformers both of 3 kW.

3) A porcelain crucible of 12 cm diameter

4) The cooling system for the crystal and the crystal holder is composed of a double walled stainless steel tube, permitting the circulation of the cold water or of the air flow, and the crystal holder

5) The reducing gear system providing the permanent rotation and the periodic ascension of the crystal

The temperature was measured by the Pt—Pt(Rh) thermocouple

The starting material was polycrystalline KCl from „Reactivul Bucureşti" or K_2CO_3 („Reactivul Bucureşti") and hydrochloric acid (from Turda) of reagent grade purity.

3. **Experimental procedure.** Approximately 3—4 kg of polycrystalline KCl were put in the porcelain crucible and this in the furnace Then the temperature of the furnace was increased slowly (1 day) up to approx. 800 °C The melt was kept at this temperature for about 6—12 hours for sedimentation of the insoluble impurities and elimination of the gas bubbles After this period the melt is perfectly transparent In this time the furnace was covered.

After the clarifying of the melt, the seed crystal fastened in the crystal holder was brought slowly near to the melt and was introduced in it By regulation of the cooling of the continuously rotated seed crystal (3—4rot/min) and of the temperature of the melt, we selected the optimum temperature and cooling conditions when an intimate contact between the seed crystal and the melt was realised. Then by increase of the cooling of the seed crystal, by lowering the temperature of the furnace and by periodical climbing of the crystal we have got the wanted and possible dimensions (limited by the dimensions of the crucible). All the time of the growing we have tried to maintain a uniform crystal diameter by furnace temperature and cooling regulation.

After the growing process was finished the obtained crystal was slowly cooled from 700 °C to the room temperature in the covered furnace in 48 hours.

The seed crystal of approximately $1 \times 1 \times 5$ cm^3 dimensions was obtained by Czochralski-technique.

The picture of the crystal during the growing process is represented in fig. 1.

4. **The experimental results.** After the above mentioned conditions in 20—24 hours we succeeded to obtain KCl single crystals of 9 5 cm in diameter, weighting about 2 kg and their picture can be seen in fig. 2. From this crystal we could cut windows for IR equipments, especially for those using CO_2 laser radiation.

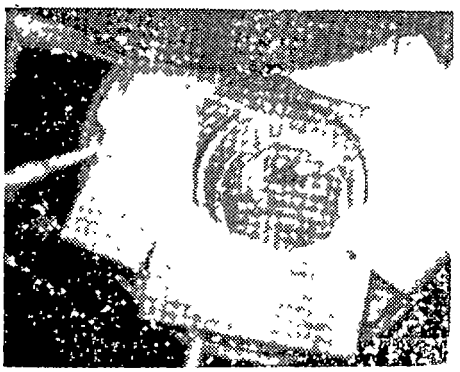

Fig 1 The picture of the crystal during the growing process

Fig 2 The picture of the crystals obtained by the authors

To assure the crystal perfection we strove for the perfection of the seed crystal selected from nearly perfect crystals. This fact is necessary to avoid the transfer of the seed crystal defects to the growing crystal.

About 1 kg of the starting material remains in the crucible This part of the melt contains the majority of the soluble impurities from the starting material. The use of this part for growing process without previous purification contributes to the lowering of the crystal quality.

The rotation of the crystal causes the agitation of the melt and promotes the polyedrical growing form [24], while the case of the fixed crystal favours the cylindrical form [25]

(Received January 25, 1977)

REFERENCES

1 W U Wagner, Z Naturforsch, **19a,** 1490—1497 (1964).
2 G D Botsaris, E A Mason and R. C. Reid, J chem Physics, **45,** 1893—1899 (1966); **46,** 192—198 (1967), AIChEJ, **13,** 764—768 (1967).
3 U Steinike, Z anorg allg Chem, **317,** 186—203 (1962), Kristall u. Techn, **3,** K5—K8 (1968)
4 I Schnerb and M. R. Bloch, Bull. Res. Council Israel, **7A,** 179—185 (1958).
5 H. H. Schock, Contr. Mineral. Petrol, **13,** 161—180 (1966).
6 F. W. von Batchelder and W. H. Vaughan, Rep NRL Progr. S. 1—13 (1965); Proc Int. Conf on Cryst Growth Boston, 405—411 (1966)
7. T. Shikiri, H Kinoshita and N Kato, Proc. Int Conf on Cryst. Growth Boston, 385—388 (1966).
8 H. Peibst and J. Noack, Z physik Chem **221,** 115—120 (1962).
9 J Franks, Brit. J appl Physics, **4,** 377—378 (1953).
10 J Strong, Physic. Rev. **36,** 1663—1666 (1930)
11 F Stöber, Z Kristallogr., **61,** 299—314 (1925)
12. U M Grassano and P. W. M. Jacobs, J appl. Physics, **35,** 2391—2397 (1964).
13 H Grundig and E Wassermann, Z Physik, **176,** 293—304 (1963).
14 P W Bridgman, Proc. Amer. Acad Arts Sci. **60,** 305 (1925).
15. D C Stockbarger, Rev. Sci. Instrument, **7,** 133 (1936); J. Opt. Soc. America, **27,** 416—419 (1937), Rev. Sci. Instrument, **10,** 205 (1939).

16. H. Grundig, Z Physik, **158**, 577—594 (1960).
17. J Pauly and P. Sue, C R hebd Séances Acad. Sci, Sér **C244**, 2722—2725 (1957).
18. H Kanzaki, K Kido and T Ninomiya, J appl. Physics, **33**, 482—486 (1962); J. Physics Chem. Solids, **22**, 309—315 (1961).
19. R. W. Warren, Rev. Sci Instruments, **36**, 731—737 (1965)
20. E. Schönherr, Physics Letters, **20**, 241—242 (1966), Proc. Second Int. Conf on Crystal Growth, Birmingham, 265—267 (1968)
21. S Kyropoulos, Z. Physik, **63**, 849 (1930)
22 C. T. Butler, J. R. Russel, R B Quincy Jr. and D E LaValle, J chem. Physics **45**, 968—975 (1966).
23. J. Czochralski, Z physik Chem, **92**, 219—221 (1917)
24. I. Tarján and Gy. Turchányi, Acta physica Acad. Sci Hung **5**, 533—535 (1956).
25 I Tarján, Gy Turchányi, R Voszka, Magyar Fizikai Folyóirat, Vol II, 1—10 (1954)

CREȘTEREA MONOCRISTALELOR KCl DE DIMENSIUNI MARI

(Rezumat)

Informarea de față prezintă datele privind obținerea monocristalelor mari de KCl pentru scopuri spectroscopice. Cristalele obținute cu metoda Kyropoulos într-un creuzet de porțelan $\varnothing = 12$ cm cîntăresc aprox 2 kg, cu diametrul maxim de 9,5 cm și prezintă formă poliedrică

STUDIA UNIV BABEŞ—BOLYAI, PHYSICA, 2, 1977

ÉTUDE EXPÉRIMENTALE DES FACTEURS ISOTOPIQUES H—D DANS LES SPECTRES DE MASSE DU MÉTHANE

E. CONSTANTIN et O. COZAR

1. **Introduction.** Le but du présent travail consiste à établir la répartition de deutérium dans les fragments ioniques du méthane et les changements de cette répartition avec l'énergie des électrons. Les spectres de masse ont été obtenus avec un spectromètre de masse de type CH4/58. L'énergie des électrons ionisants a été comprise entre 13 et 70 eV. L'abondance relative des ions superposés a été calculée en utilisant les relations de Turchevich [1]. On a séparé ainsi les courants ioniques à $m/e = 14$ (CD^+ et CH_2^+), $m/e = 15$ (CH_3^+ et CDH^+), $m/e = 16$ (CD_2^+, CDH_2^+). Ayant les intensités relatives pour chaque type d'ion nous avons calculé les facteurs isotopiques B, C définis de la manière suivante [2, 3]·

$$B = \frac{\left[\frac{D}{H}\right]_{IF}}{\left[\frac{D}{H}\right]_{IM}} \qquad C = \frac{\left[\frac{D}{H+D}\right]_{IF}}{\left[\frac{D}{H+D}\right]_{IM}}$$

IM = ion moléculaire, IF = ion fragment, et:

$$\mathrm{D/H} = \frac{\sum_i iCD_iH_{m-i}}{\sum_i (m-i)CD_iH_{m-i}}$$

$$\mathrm{D/(H+D)} = \frac{\sum_i iCD_iH_{m-i}}{\sum_i mCD_iH_{m-i}}$$

2 **Résultats et discussions.** a) *Les ions* CX_3^+, CX_2^+, $CX^+(X = H, D)$. Sur la fig. 1 on a représenté la dépendance de B de la concentration initiale en deutérium pour 25 eV. Cette courbe montre que chaque type d'ion CX^+, CX_2^+, CX_3^+ présente un maximum avec une position caractéristique par rapport à l'abscisse Ainsi, pour les ions CX_3^+, la valeur maximale correspond à $n = 3$ à toutes les énergies. Pour les ions CX_2^+ il y a aussi un maximum avec une position stable, il se trouve à $n = 2$ En

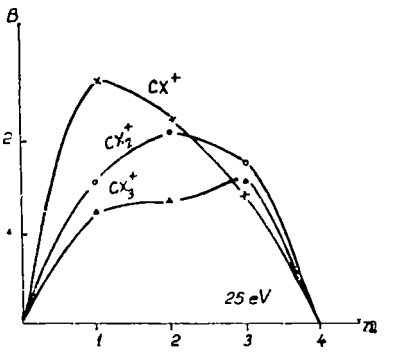

Fig. 1 La dépendances des facteurs B du nombre d'atomes de deutérium contenus par l'ion moléculaire.

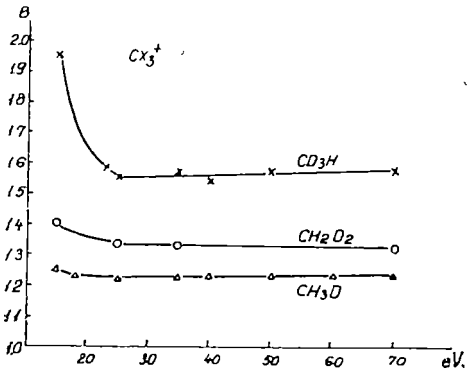

Fig 2 Variation du facteur $B(CX_3^+)$ avec l'énergie des électrons ionisants pour les ions provenants de CD_3H, CH_2D_2 et CH_3D

ce qui concerne les ions CX^+ il paraît que la position du maximum est dépendante de l'énergie des électrons ionisants, à mesure que l'énergie diminue, le sommet se déplace vers de faibles concentrations Par exemple, si à 70 eV il correspond à $n = 2$, pour 25 eV on le trouve à $n = 1$

Comme les valeurs de B sont supérieures à l'unité il en résulte que le nombre d'atomes de deutérium dans les fragments augmente par rapport au nombre D dans l'ion moléculaire

En traçant les graphiques pour B en fonction de l'énergie des électrons, on obtient des courbes du type donné sur la fig 2 Ces courbes montrent que si l'énergie diminue, il y a une décroissance jusqu'à ≈ 25 eV d'où les rapports augmentent légèrement pour CX_3^+ et plus fortement pour CX_2^+

Nous avons comparé sur la fig 3 les rapports C fonction du nombre des atomes D de l'ion primaire (70 eV). Le pointillé marque les valeurs de C pour les ions moléculaires On peut voir que les courbes s'éloignent progressivement du pointillé, l'écart maximal étant atteint par les ions CX^+ et celui minimal par CX_3^+

Pour expliquer le comportement des courbes ci-dessus présentées, il est nécessaire de considérer la différence entre la probabilité de séparation de D et H de la même molécule et le changement de cette probabilité d'une molécule à l'autre aussi bien que sa dépendance de l'énergie des électrons

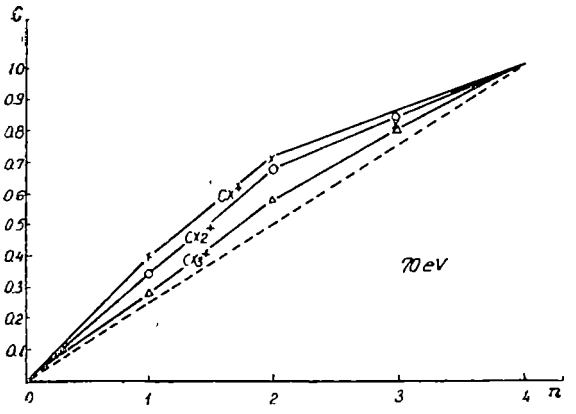

Fig 3 Les facteurs C (à 70 eV) fonction de nombre d'atomes de deutérium dans l'ion moléculaire

Ainsi, on a vu que la courbe $B(CX_3^+)$ passe par un maximum (fig. 1) On peut atribuer cette allure à l'augmentation de la différence entre la probabilité de rompre un atome H ou D dans le sens CH_3D, CD_3H De la même manière, la croissance de $B(CX_2^+)$ de CH_3D vers CH_2D_2 peut être considérée comme le résultat d'une diminution plus rapide de la probabilité de formation de CH_2^+ par rapport à celle de CHD^+. En ce qui concerne

$B(CX^+)$, les probabilités de formation pour CD^+ et CH^+ croissent différemment de CD_3H^+ vers CH_3D^+, celui de CD^+ augmentant plus vite

Pour pouvoir expliquer l'évolution des courbes B en fonction de l'énergie, il faut connaître l'espèce ionique qui change plus sensiblement B. On a obtenu l'ordre suivant d'influence sur le rapport $CX^+(CH^+, CD^+)$, $CX_2^+(CH_2^+, CHD^+, CD_2^+)$, $CX_3^+(CH_3^+, CDH_2^+, CD_2H^+, CD_3^+)$ Le comportement est donc déterminé spécialement par les ions ayant le minimum de nombre d'atomes de deutérium. Pour le groupe CX_3^+, ces ions résultent de l'ion moléculaire par la perte de D La croissance des courbes vers les faibles énergies correspond par suite à l'augmentation de la probabilité de perte de H par rapport à la perte de D

b) *Les ions H^+, D^+, H_2^+, HD^+, D_2^+. La comparaison des valeurs du B pour les fragments lourds et légers.* Pour voir la répartition de deutérium dans les fragments légers les rapports B et C ont été calculés Sur la fig 4 on peut poursuivre la variation de B avec le contenu en deutérium de l'ion primaire pour H^+, D^+ (courbe 1) et H_2^+, HD^+, D_2^+ (courbe 2). On a également représenté la valeur moyenne de B (courbe M). Sur la fig. 5 on a porté les valeurs de B fonction de l'énergie pour CH_3D et CD_3H. Les observations essentielles faites à propos de ces courbes peuvent se résumer comme il suit :

— on remarque que les valeurs de B pour H^+, D^+, d'une part, et celles pour H_2^+, HD^+, D_2^+ d'autre part, diffèrent d'habitude, elles deviennent égales pratiquement seulement pour CD_3H. La plus grande différence correspond à la molécule CH_2D_2

— la valeur maximale de B moyenne se déplace de CD_3H vers CH_2D_2 si l'énergie diminue de 70 eV à 25 eV ;

— si l'énergie augmente, il y a une légère croissance de l'enrichissement en deutérium autant pour les fragments atomiques que pour ceux moléculaires

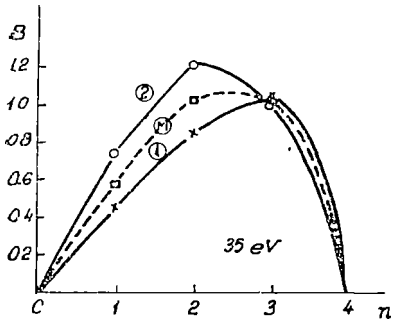

Fig. 4 Les facteurs $B(X+)$, $B(X_2^+)$ $X = H$, D fonction de concentration en deutérium

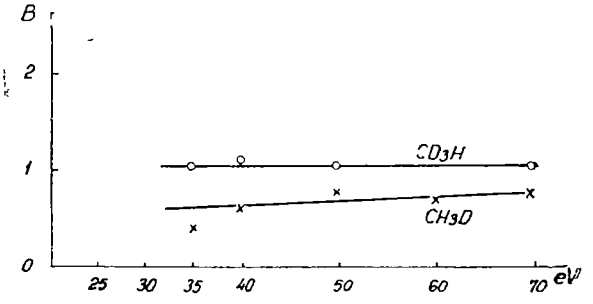

Fig 5 Les valeurs de $B(X+)$ fonction de l'énergie.

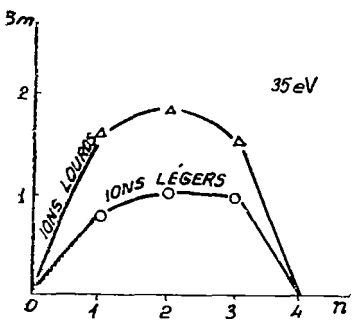

Fig. 6. Les valeurs moyennes B_m à 35 eV fonction de nombre d'atomes de deutérium contenu par l'ion moléculaire.

La plupart des valeurs sont inférieures à l'unité, excepté celles pour CD_3H et CH_2D_2 aux faibles énergies. Par conséquent on peut affirmer que les ions légers concentrent moins le deutérium que les ions lourds. La même conclusion résulte en considérant les courbes du type donné sur la fig. 6.

Le comportement des ions lourds et légers montre également l'accumulation de l'hydrogène dans les fragments neutres d'autant plus que l'énergie des électrons diminue sous 25 eV.

3. **Conclusions.** Le présent travail donne une autre image sur les effets isotopiques H—D impliqués dans le processus de fragmentation du méthane. La manière de calcul [2] met en évidence la séparation partielle de deutérium par son préférence pour les fragments lourds. Le processus de séparation dépend de l'énergie des électrons ionisants aussi bien que de l'ion qui dissocie.

(Manuscrit reçu le 26 janvier 1977)

BIBLIOGRAPHIE

1. D. O. Schissler, S O. Thompson, J. Turchevich, Disc Far Soc, **10**, 46 (1951).
2. E. Constantin, J. Ch Abbé, Rev. Roum. Chimie, **20**, 1329 (1975).
3. E Constantin, Int J Mass Spectrom. Ion Phys, **13**, 343 (1974)

STUDIUL EXPERIMENTAL AL FACTORILOR IZOTOPICI H-D DIN SPECTRUL DE MASĂ AL METANULUI

(Rezumat)

Prezenta lucrare urmăreşte modul de repartizare al deuteriului în fragmentele ionice rezultate din disocierea metanilor deuteraţi. Disocierea este produsă de electroni avînd energia în domeniul 13—70 eV. Se constată o preferinţă de acumulare a deuteriului în fragmentele CX_3^+, CX_2^+, CX^+ (X = H, D) comparativ cu ionu de hidrogen X^+, X_2^+. Distribuţia depinde de energia electronilor ionizanţi şi de specia deuterată care se fragmentează.

STUDIA UNIV BABEŞ—BOLYAI, PHYSICA, 2, 1977

ELECTRICAL RESISTIVITY OF THE ITINERANT-ELECTRON ANTIFERROMAGNET NEAR T_N

M. CRIŞAN, D. DĂDÎRLAT

I. **Introduction.** The study of transport properties at magnetic phase transitions, and of the electrical resistivity in particular, has received a good deal of attention. The case of ferromagnetic metals has been studied by Fisher and Langer [1], Takada [2] and recently by Geldart and Richard [3]

There are still several questions which have not yet been satisfactorily classified in connection with the critical behavior in the electrical resistivity of itinerant-electron antiferromagnet and its alloys.

Experimental data for itinerant-electron antiferromagnet (Cr) and its alloys obtained by Arajs [4] pointed out that the critical exponents of Cr and its alloys are not very different from the values calculated using mean-field approximation. On the other hand from the specific heat measurements one can conclude that a λ — transition appears at $T_N = 311$ K and for this reason the critical exponent of specific heat (C) is very small ($\alpha \to 0$).

The paramagnetic-antiferromagnetic transition has been studied by Feders—Martin [5]. Rice [6] Nakanishi and Maki [7] Fenton [8], Crişan [9] using the electron-hole pairing model.

In this paper we are going to study the contribution of electron-fluctuation scattering on the electrical resistivity of the itinerant-electron antiferromagnet (II) in the molecular field (1) and static scaling approximations (2).

In section III we analyse the temperature behavior of the effective number near the critical temperature T_N.

II. **Electrical resistivity in the critical region.** The general expression for the contribution to the electrical resistivity given by electron-fluctuation scattering is

$$\rho(\tau) = \frac{m}{n_{eff} \cdot e^2} \frac{1}{T_r} \tag{1}$$

where

$$\frac{1}{T_r} = I_m \Sigma_\sigma(p) \tag{2}$$

In order to calculate (2) we define the fluctuation propagator

$$D(\vec{r},\ t) = \langle T\Delta(\vec{r},\ t)\Delta(0,\ 0)\rangle \tag{3}$$

with the Fourier transform

$$D(\vec{q},\ \omega_n) = [\tau - \Pi(\vec{q},\ \omega_n)]^{-1} \tag{4}$$

$$\Pi(\vec{q},\ \omega_n) = T\sum_m \int \frac{d^3p}{(2\pi)^3} G(\vec{p},\ \omega_m)G(\vec{q},\ -\vec{p}\,;\ \omega_n - \omega_m) \tag{5}$$

where G is the Green function of the electrons

The self-energy $\Sigma_\sigma(\vec{p}, \omega_n)$ is defined by

$$G^{-1}(\vec{p}, \omega_n) = G_0^{-1}(\vec{p}, \omega_n) - \Sigma(\vec{p}, \omega_n) \tag{6}$$

and Σ will be calculated using the relation

$$\Sigma_\sigma(\vec{p}, \omega_n = 0) = -T\sum_q \Gamma(p, q)D(q)G_{-\sigma}(q - p) \tag{7}$$

Γ being the electron-fluctuation vertex function, and for $D(q)$ we will use

$$D_0(q) = [\tau + \xi^2 q^2]^{-1} \tag{7a}$$

Using these general results the ,,mean-field approximation'' and the ,,scaling'' approximation will be discussed.

1. *The mean field approximation* In order to obtain the self energy we approximate (7) as

$$\Sigma_\sigma = A^2 G_{-\sigma} \qquad A^2 = 4T\sum_q \Gamma(p, q)D(q, \tau) \tag{8}$$

and from (6) we get

$$\Sigma_\sigma(p) = \frac{(\imath\omega_n - \varepsilon)\sqrt{\omega_n^2 + \varepsilon^2} - \sqrt{\omega_n^2 + \varepsilon^2 + A^2}}{4\sqrt{\omega_n^2 + \varepsilon^2}}$$

and

$$I_m\Sigma(p) = \frac{A}{4\varepsilon} \tag{9}$$

In the mean-field approximation A^2 is given by

$$A^2 = 4T\int \frac{d^3q}{\tau(2\pi)^3}\frac{1}{\tau + q^2} \simeq 4T\ const\ |\tau| \tag{10}$$

where

$$\tau = (T - T_N)/T_N$$

The electrical resistivity ρ expressed by (1) is

$$\rho(\tau) = \text{const}\int \frac{d^3p}{(2\pi)^3}\frac{1}{T_r(p)} \tag{11}$$

which gives

$$\rho(\tau) = \text{const}\ |\tau|^{1/2} \tag{12}$$

2 *Static scaling approximation* In this approximation we take the vertex function as

$$\Gamma = \tau^{-\zeta}g(q\xi),\ D = \tau^{-\gamma}f(q\xi) \tag{13}$$

where ζ and γ are the critical index, ,,d'' dimensionality of the system, g and f the universal functions

Following the same way as in the „mean field approximation" we get

$$\rho(\tau) = \text{const } \tau^{\frac{d\nu-\gamma-\zeta}{2}} \tag{14}$$

and if we take $\zeta = 0$, $\nu = \frac{2\gamma}{d}$ a good agreement of the relation (14) is obtained if $\gamma/2 = 0\,67$

This result is in agreement with $\gamma = 1\,33$ obtained by T a k a d a [2].

III **Temperature dependence of the effective number of electrons.** The calculation of the temperature dependence of the effective number n_{eff} from (1) will be performed using [10]

$$n_{eff} = n_0 \left[1 + \frac{\partial \mathrm{Re}\,\Sigma(\vec{k}, \varepsilon_0)}{\partial k^2}\right]^{-1}_{|\vec{k}|=k_0} \tag{15}$$

where

$$\Sigma(k) = \int \frac{d^3p}{(2\pi)^3} D(k-p)G(p) \tag{16}$$

In the self-energy (16) we have two contributions and

$$\Sigma = \Sigma_l + \Sigma_s \tag{17}$$

where Σ_l is the long-range contribution and Σ_s is the short-range contribution

The expressions for Σ_l and Σ_s have been calculated by A u s l o o s [11] as

$$\Sigma_l = -xZ(x)G(\tilde{p}), \quad \Sigma_s = \tau^{-\alpha+1} \tag{18}$$

where $x = \tau^{\nu}$ and $Z(x) = \tau^{-\gamma+2\nu}$ and ν, γ are the usual critical index.

Using for the Green function [2]

$$G(\tilde{p}, \tilde{\omega}_m) = [i\tilde{\omega}_m - \varepsilon(\tilde{p})]^{-1} \tag{19}$$

we get

$$\frac{\partial R_e \Sigma_l(k, \varepsilon_0)}{\partial k^2} = -\frac{1}{4}\frac{m}{k_0^4}\left(1 \mp \frac{k_0}{k}\right)\tau^{-\gamma+3\nu} \tag{20}$$

and

$$n_{eff} = n_0(1 + C\tau^{3\nu-\gamma})^{-1}$$
$$C \equiv \frac{4m}{k_0}\left(\frac{k_0}{k} - 1\right) = \begin{cases} C_+ > 0, & k < k_0 \\ C_- < 0 & k > k_0 \end{cases} \tag{21}$$

Finally we obtain for $\rho(\tau)$ from (1) and (14)

$$\rho(\tau) = \text{const} \frac{\tau^{\gamma/2}}{1 + C_{\pm}\tau^{3\nu-\gamma}} \tag{22}$$

which is identical with (14) if $k = k_0$.

A more detailed effect of the Fulde—Ferrel state on the resistivity will be discussed in connection with the recent result obtained by Crişan and Anghel [12] about the magnetic susceptibility near T_N.

*

The authors would like to thank Dr. M. Ausloos from the International Center for Solid State Physics (Liège) for providing us with his recent results in this problem, and prof. S Arajs lor useful correspondence.

(Received January 26, 1977)

REFERENCES

1. M E Fisher, J S Langer, Phys Rev. Lett **20**, 665 (1968).
2 S Takada, Prog Theor Phys, **46**, 15 (1971)
3. D J. W Geldart, T G Richard, Phys. Rev B **12**, 5175 (1975).
4 S Arajs, K V Rao, H U. Astrom, T F de Young, Physica Scripta, **8**, 109 (1973)
5 P A Feders, P C Martin, Phys Rev. **143**, 243 (1966).
6 T M Rice, Phys Rev. **B2**, 3619 (1970)
7. Nakanishi, K Maki, Progr. Theor Phys, **48**, 1059 (1772)
8 E W Fenton, J. Low, Temp. Phys **13**, 525 (1973)
9 M Crişan, Phys Rev. **B9**, 4838 (1974)
10. H Miwa, Prog Theor. Phys., **29**, 477 (1963)
11. M Ausloos, J Phys. F., Metal Phys, **6**, 1723 (1976).
12 M Crişan, Al. Anghel, Phys. Rev (will be pulished in 1977).

REZISTIVITATEA ELECTRICĂ A ANTIFEROMAGNETULUI DE BANDĂ ÎN APROPIEREA TEMPERATURII CRITICE

(Rezumat)

Lucrarea studiază comportarea rezistenţei electrice a metalelor antiferomagnetice în apropierea temperaturii critice.

Se arată că ipoteza „scaling" dă rezultate apropiate de cele obţinute prin calculul în aproximaţia cîmpului molecular

STUDIA UNIV BABEŞ—BOLYAI, PHYSICA, 2, 1977

ISOTOPE EFFECTS IN THE METASTABLE DISSOCIATION OF THE CH^+ AND CD^+ IONS

I. MASTAN, A. TODEREAN, N. PALIBRODA*

1. **Introduction.** The occurrence of the metastable dissociation process $CH^+ \rightarrow C^+ + H$ in the mass spectrum of acetylene was mentioned without details in an early paper by C. E. Melton et. al. [1] It is specified that this process is only collision-induced. More recently a careful experimental and theoretical study on the metastable dissociations of the CH^+ and CD^+ ions has been performed [2—4]. In these papers it was established that for low pressures in the mass spectrometer analyser the metastable dissociation of the CH^+ and CD^+ ions appears as a unimolecular process. For large pressures in the apparatus on spontaneous dissociations the collision-induced ones are superposed. The lifetimes of the order of 10^{-7} s were measured for spontaneous dissociations. The electronic predissociation strongly forbidden by some selection rules has been suggested [2, 3] as mechanism for metastable dissociations of the CH^+ and CD^+ ions

In the present paper we shall give some results on H—D isotope effects appearing in the metastable dissociations of the CH^+ and CD^+ ions. The measurements were performed in the methane and deuteromethane mass spectrum

2. **Experimental.** The experimental measurements on metastable dissociations of the CH^+ and CD^+ ions

$$CH^+ \rightarrow C^+ + H \tag{1}$$

$$CD^+ \rightarrow C^+ + D \tag{2}$$

in the methane and deuteromethane mass spectrum have been performed using a double-focussing mass spectrometer with inverted geometry. A schematic picture of the ionic path in the apparatus is given in fig. 1.

The method of direct analysis of the daughter ions (DADI) was used for the detection of the metastable transitions. The recorded metastable peaks are due to metastable dissociations (1) and (2) taking place in the second field free region of the mass spectrometer. This region is situated between the magnetic and electrostatic analysers. The energy of the ionizing electrons was of about 70 eV. For the whole ionic beam an accelerating voltage of 3000 V has been used. The ion source repeller was maintained to a negative voltage of $-4 \div -5$V.

The pressure dependence of the intensity of the metastable transitions (1) and (2) has been studied in order to know their nature. The obtained results are given in figs. 2 and 3.

* Institute for Stable Isotops, Cluj-Napoca.

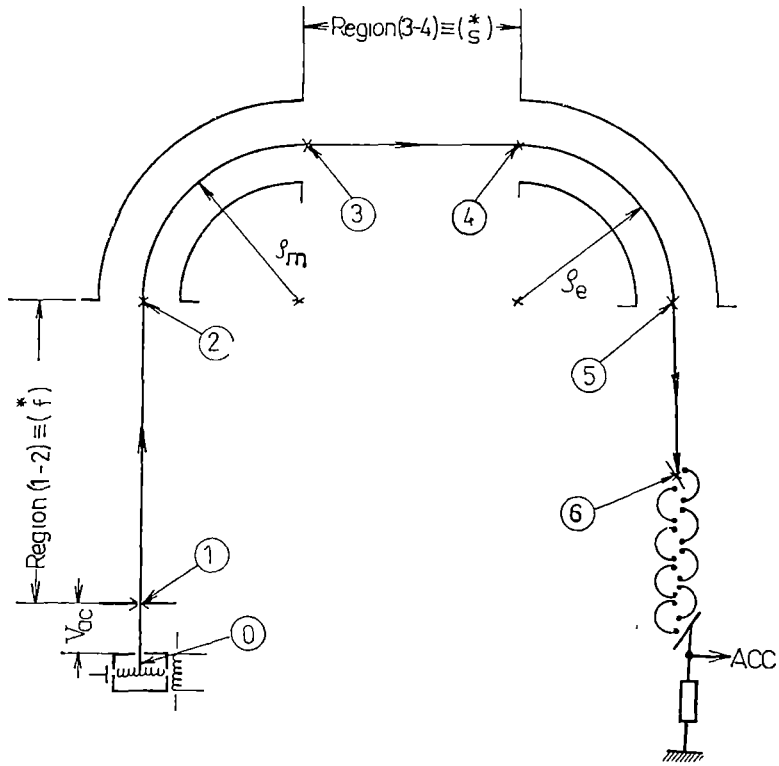

Fig 1

Here there are plotted the ratios between metastable and parent peaks in arbitrary units against the pressure in the mass spectrometer analyser. From figs. 2 and 3 it can be seen that for low pressures the metastable dissociations (1) and (2) are spontaneous For large pressures the spontaneous metastable dissociations and collision-induced ones are superposed. Therefore, for large pressures in the mass spectrometer analyser, the metastable dissociations (1) and (2) could be written as follows

$$CH^+ \xrightarrow{\lambda_H} C^+ + H \quad \Big| \xrightarrow{\sigma_H} C^+ + H \tag{1a}$$

$$CD^+ \xrightarrow{\lambda_D} C^+ + D \quad \Big| \xrightarrow{\sigma_D} C^+ + D \tag{2a}$$

Here by λ_H, λ_D and σ_H, σ_D *the apparent rate constants of the spontaneous dissociations* and *the cross-sections of the collision-induced* ones for the CH^+ and CD^+ ions were respectively denoted In the next part we shall estimate these values.

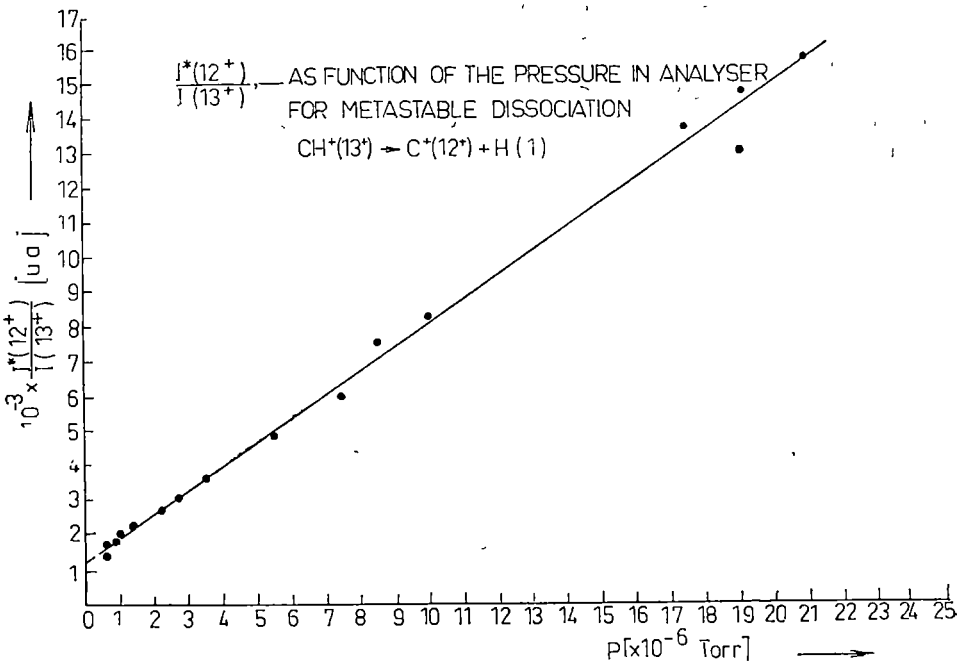
$\frac{I^*(12^+)}{I(13^+)}$, — AS FUNCTION OF THE PRESSURE IN ANALYSER
FOR METASTABLE DISSOCIATION
$CH^+(13^+) \rightarrow C^+(12^+) + H(1)$
$10^{-3} \times \frac{I^*(12^+)}{I(13^+)}$ [ua]
P[x10^{-6} Torr]

Fig. 2

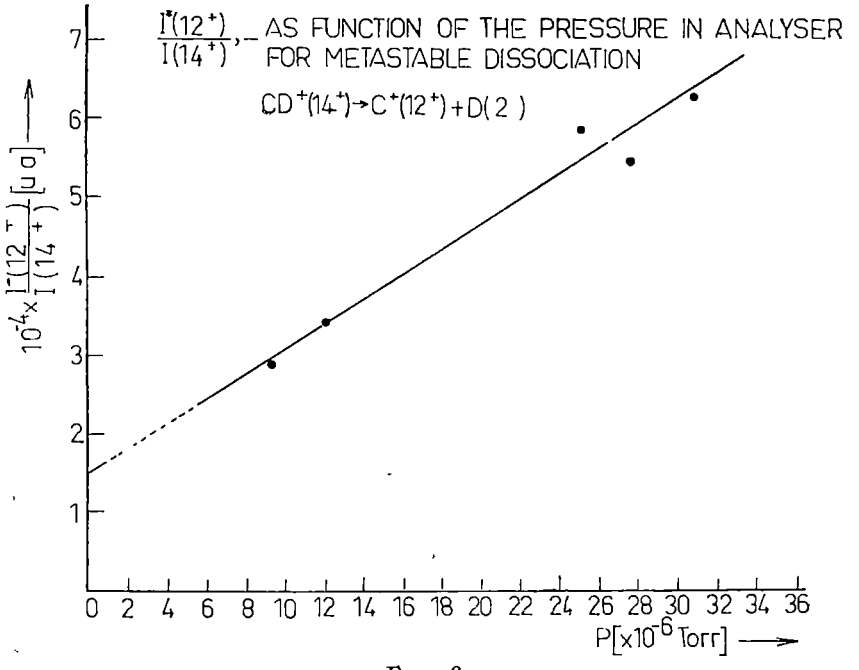
$\frac{I^*(12^+)}{I(14^+)}$, — AS FUNCTION OF THE PRESSURE IN ANALYSER
FOR METASTABLE DISSOCIATION
$CD^+(14^+) \rightarrow C^+(12^+) + D(2)$
$10^{-4} \times \frac{I^*(12^+)}{I(14^+)}$ [ua]
P[x10^{-6} Torr]

Fig. 3.

3. **Estimation of the values λ_H, λ_D, σ_H and σ_D. Discussion.** The method for estimation of the apparent rate constants of the spontaneous dissociations (generally denoted by λ) and of the cross-sections of the collision-induced dissociations (generally denoted by σ) has been described in detail in a previous paper [5]. Here we shall give only those equations and experimental parameters that are necessary to estimate the λ and σ values.

When the DADI method is used the following function in which the λ and σ unknown are correlated with experimental results and parameters can be introduced

$$R[\lambda,\ p(N)] = I_S^*/I_6 = \\ = \frac{\exp\{-\lambda t_3\} \cdot exp\{-\sigma N x_3\} - \exp\{-\lambda t_4\} \cdot \exp\{-\sigma N x_4\}}{\exp\{-\lambda t_6\} \cdot \exp\{-\sigma N x_6\}} \tag{3}$$

Here I_S^* is the intensity of the metastable peak which is yielded in the second field free region, I_6 is the intensity of the parent peak, x_i the covered path by the ionic beam from source to the $i (i = 3, 4, 6)$ point of the trajectory, t_i the necessary time of the ions to reach the i point of the trajectory and N the pressure in the flight region of the apparatus expressed in molecules/cm^3. For very low pressures ($N \to 0$) in the mass spectrometer analyser the equation (3) can be written as follows

$$R[\lambda,\ 0] = \frac{\exp\{-\lambda t_3\} - \exp\{-\lambda t_4\}}{\exp\{-\lambda t_6\}} \tag{4}$$

The estimation of the apparent rate constant λ and of the cross-section σ may be performed starting from the transcendental equations (4) and (3) where $R[\lambda, 0]$ and $R[\lambda, p(N)]$ were beforehand replaced by the corresponding experimental values. For the mass spectrometer used by us are known $x_3 = 59{,}6$ cm, $x_4 = 79{,}6$ cm and $x_6 = 117{,}3$ cm. Using this method and the experimental results plotted in figs 2 and 3 for the metastable dissociation processes (1a) and (2a) the following values have been estimated

$$\tau_H = 1/\lambda_H = 7{,}64 \cdot 10^{-4}\ s, \qquad \sigma_H = 1{,}087 \cdot 10^{-15}\ \text{cm}^2,$$
$$\tau_D = 1/\lambda_D = 6{,}59 \cdot 10^{-3}\ s; \qquad \sigma_D = 2{,}36 \cdot 10^{-17}\ \text{cm}^2$$

One can observe that $\lambda_H/\lambda_D = 8{,}63$ and $\sigma_H/\sigma_D = 46{,}1$. That is to say that the CH^+ ion dissociates spontaneously with a rate constant eight times greater and collision-induced with a cross-section of about forty six times greater than the CD^+ ion. Hence, the metastable dissociation of the CH^+ and CD^+ ions is accompanied by large enough H—D isotope effects.

The electronic predissociation strongly forbidden by some selection rules has been proposed as mechanism for metastable dissociation of the biatomic ions. This idea already appears in the earlier papers by J. A. Hipple et al. [6] and J. Momigny [7, 8]. In the framework of this mechanism A. J. Lorquet et al [2, 3] have computed the theoretical

values of the lifetimes for the metastable dissociation process (1) of the CH^+ molecular ion. The computed lifetimes are comprised between about 10^{-4} s and 10^{-11} s. The experimental values of the order of 10^{-7} s for the lifetimes of the metastable dissociation processes (1) and (2) have been reported in the papers [2—4]. It is appreciated that such experimental lifetimes are long for the metastable dissociation of a biatomic molecular ion. For metastable dissociations having lifetimes of the order of 10^{-7} s and longer, as a possible mechanism has been suggested the electronic predissociation by tunneling effect. The tunneling is assumed to take place through the potential barrier appearing owing to the crossing between an attractive potential curve and a repulsive one. It is likely that long lifetimes and large H—D isotope effects measured by us can be associated with the electronic predissociation by tunneling effect. In a recent paper [9] about the metastable dissociations appearing in the methane and deuteromethane mass spectrum the measurement of some very slow metastable transitions whose lifetimes reach values of 10^{-1} s has been reported.

(Received January 26, 1977)

REFERENCES

1. C. E. Melton, M M. Bretscher, R. Baldock, J. Chem Phys, **26**, 1302 (1957).
2. A J. Lorquet, J. C Lorquet, J Momigny, H Wankenne, J Chim. Phys, **67**, 64 (1970)
3. A. J Lorquet, J. C. Lorquet, H. Wankenne, H. Lefebvre-Brion, J. Chem Phys, **55**, 4053 (1971).
4. A. S Newton, A F. Sciamanna, J. Chem, Phys., **58**, 1292 (1973).
5. I. Mastan, A. Todereau, V Mercea, Studia Univ. Babeş—Bolyai, Phys, **1**, 12. (1977).
6. J A Hipple, R. E Fox, E. U. Condon, Phys. Rev., **69**, 347 (1946).
7. J. Momigny, Bull. Soc. Chim. Belg., **70**, 291 (1961).
8. J. Momigny, Mém. Soc. Roy Sci. Liège, **13**, 138 (1966).
9. R. D. Smith, Int. J. Mass Spectrom. and Ion Phys., **20**, 425 (1976).

EFECTE IZOTOPICE LA DISOCIEREA METASTABILĂ A IONILOR CH+ ŞI CD+

(Rezumat)

În lucrare au fost estimate valorile aparente ale vitezelor de disociere spontană λ_H şi λ_D şi ale secţiunilor eficace de ciocnire σ_H şi σ_D pentru procesele de disociere metastabilă $CH^+ \xrightarrow{\lambda_H, \sigma_H} C^+ + H$ şi $CD^+ \xrightarrow{\lambda_D, \sigma_D} C^+ + D$ din spectrul de masă al metanului şi deuterometanului. A fost pusă în evidenţă existenţa unor efecte izotopice H—D considerabile, anume $\lambda_H/\lambda_D = 68{,}3$ şi $\sigma_H/\sigma_D = 46.1$,

STUDIA UNIV BABEŞ—BOLYAI, PHYSICA, 2, 1977

L'APPLICATION DE LA THÉORIE DES GROUPES AU CALCUL DES COEFFICIENTS DU DICHROISME CIRCULAIRE MAGNÉTIQUE

I. BOSKOVITZ et E. TĂTARU

Introduction. Ces dernières années on a prouvé la capacité du dichroisme circulaire magnétique (D.C.M.) de fournir des informations qualitatives et quantitatives sur les états quantiques de divers systèmes et sur les transitions qui ont lieu entre ces états. En conséquence, l'utilisation du D.C.M. comme moyen d'investigation structurale est de plus en plus répandue. Les spectres D.C.M. nous fournissent des informations similaires aux ceux qui résultent des études de l'effet Zeeman, mais ils ont l'avantage que, à la différence des premières, on peut les mettre en évidence même dans la zone des bandes d'absorption larges, caractéristiques à la majorité des systèmes qui se trouvent dans l'état condensée.

L'interprétation du dichroisme circulaire magnétique consiste dans l'évaluation des constantes $\mathcal{A}$, $\mathcal{B}$, $\mathcal{C}$ du D.C.M. celles-ci étant fonctions de certains paramètres quantiques, les valeurs desquels peuvent être ensuite déterminées en comparant la courbe calculée avec la courbe expérimentale.

Dans ce qui suit nous présentons les problémes généraux qui se posent dans le calcul des constantes de la courbe de D.C.M. La difficulté du calcul direct a fait qu'on a recours à des méthodes grafiques d'évaluation [1] ou à exprimer en lieu de cettes constantes les moments de D C.M. Dans le cas d'un champ cristallin avec une symétrie T_d, S c h w a r t z [2] exprime les constantes en fonction des éléments de matrice réduite du opérateur moment dipolaire électrique. D o b o s h [3] détermine en utilisant la méthode des tensors irréductibles les expressions des ces constantes pour le cas de la symétrie octaédrique. Dans le présent travail on applique cette méthode à un cas dans lequel la symétrie est de type C_{3v}, en montrant aussi le mode dans lequel ont été employés les résultats de la théorie des groupes à la détermination du diagramme des niveaux d'énergie et des fonctions d'onde dans ce cas.

Théorie. Dans l'analyse théorique [4, 5] de la dispersion du dichroisme circulaire magnétique dans la zone des bandes d'absorption on introduit les constantes $\mathcal{A}(A \rightarrow J)$, $\mathcal{B}(A \rightarrow J)$ et $\mathcal{C}(A \rightarrow J)$, qui sont indépendantes de la pulsation, température et champ magnétique, et qui sont caractéristiques pour le système quantique étudié. Avec A et J sont notés les états quantiques entre lesquels a lieu la transition électronique qui est responsable de l'absorption. Dans le cas où l'axe optique est parallèle au faisceau lumineux et au champ (Oz) les expressions de ces constantes sont [4]:

$$\mathcal{A}(A \rightarrow J) = (3/d_A) \sum_{a^\circ, j^\circ} Im \left(< a^\circ | m_x | j^\circ > < j^\circ | m_y | a^\circ > \right) \cdot \left(< j^\circ | \mu_z | j^\circ > - \right.$$

$$\left. - < a^\circ | \mu_z | a^\circ > \right) \qquad (1)$$

$$\mathfrak{B}(A \to J) = (3/d_A) \sum_{a^\circ, j^\circ} Im \left[\sum_{K \neq J} (< a^\circ | m_x | j^\circ > < k^\circ | m_y | a^\circ > - \right.$$

$$\left. - < a^\circ | m_y | j^\circ > < k^\circ | m_x | a^\circ >) < j^\circ | \mu_z | k^\circ > \hbar \omega^\circ_{KJ} + \sum_{K \neq A} (< a^\circ | m_x | j^\circ > \cdot \right.$$

$$\left. \cdot < j^\circ | m_y | k^\circ > - < a^\circ | m_y | j^\circ > < j^\circ | m_x | k^\circ >) < k^\circ | \mu_z | a^\circ > | \hbar \omega^\circ_{KA} \right.$$

$$\mathcal{C}(A \to J) = (3/d_A) \sum_{a_0 j_0} Im \, (< a^\circ | m_x | j^\circ > < j^\circ | m_y | a^\circ >) < a^\circ | \mu_z a^\circ >$$

où K symbolise les états que le champ magnétique vient de mêler aux états A et J ; par $|a^\circ>$, $|j^\circ>$ et $|k^\circ>$ on a noté les groupes de fonctions d'état correspondants aux états A, J respectivement K et qui sont ainsi choisis qu'ils diagonalisent l'hamiltonien de l'interaction du système avec le champ magnétique extérieur $\mathcal{H} = - \vec{\mu} \cdot \vec{H}$; d_A représente le degré de dégénération de l'état fondamental A, et m_x, m_y, m_z et μ_z sont les composantes des opérateurs moment dipolaire électrique $\vec{m} = \sum_i e_i \vec{r}_i$ respectivement magnétique $\vec{\mu} = \sum_i \frac{e_i}{2m_i c} [(\vec{r}_i \times \vec{p}_i) + 2 \vec{s}_i]$.

Des expressions ci-dessus il résulte que pour calculer les constantes du D.C.M. il faut préalablement déterminer les niveaux énergetiques et les fonctions d'onde de l'ion responsable de D.C.M. et puis il faut calculer les éléments de matrice des opérateurs $\vec{m}$ et $\vec{\mu}$.

Pour trouver les fonctions d'onde d'ordre zéro, c'est à dire celles qui correspondent aux états obtenus par la réduction d'un seul terme de symétrie sphérique, dans le cas d'un champ cristallin faible, on cherche des combinaisons des vecteurs $|JM>$ qui se transforment les unes dans les autres à toutes les opérations appartenant au groupe de symétrie locale. Dans le cas du champ moyen les fonctions se construisent en multipliant les combinaisons des vecteurs orbitaux $|LM_L\rangle$ avec les vecteurs des états de spin.

Au calcul des éléments de matrice nous voulons mettre en évidence deux problèmes. Le premier s'en réfère au fait qu'il est possible que la transition étudiée vienne lier des états électroniques dans lesquels le champ cristallin actionne différemment. Ainsi on aboutit qu'un des états soit décrit par des vecteurs $|LSJM\rangle$ et l'autre par des vecteurs $|LM_L SM_S\rangle$. Dans des cas pareils l'évaluation directe des éléments de matrice d'un opérateur de transition n'est pas possible et on a recours à l'exprimation préalable d'un type de vecteurs comme une combinaison linéaire de ceux d'autre type :

$$|LSJM\rangle = \sum_{M_L M_S} (LSM_L M_S | JM) | LSM_L M_S \rangle \qquad (2)$$

Les coefficients du développement, nommés coefficients Wigner se calculent avec la relation [7]:

$$(jj'mm'|JM) = \left[\frac{(j+j'-J)\,!(j+J-j')\,!(j'+J-j)\,!(2J+1)}{(j+j'+J+1)\,!}\right]^{1/2} \delta^{M}_{m+m'} \times$$

$$\times \sum_{r} (-1)^{r} \frac{[(j+m)\,!(j-m)\,!(j'+m')\,!(j'-m')\,!(J+M)\,!(J-M)\,!]^{1/2}}{(j-m-r)\,!(J-j'+m+r)\,!(j'+m'-r)\,!(J-j-m'+r)\,!r\,!(j+j'-J-r)\,!} \tag{3}$$

où la somme s'effectue après toutes les valeurs entières du r pour lesquelles les arguments des factoriels ne deviennent pas négatifs.

Le deuxième problème s'en réfère à la difficulté de calculer complètement les éléments de matrice de l'opérateur moment dipolaire électrique, qui est issu principalement de la nécessité d'exprimer explicitement la part radiale de la fonction d'onde. Pour éviter cette difficulté nous avons fait recours à l'exprimation des éléments conformément au théorème Wigner — Eckart [7]·

$$\langle j_1\ m_1|\,T^{k}_{m}|j_2 m_2\rangle = (-1)^{j_1+k+m_1} \frac{\langle j_1||T^{(k)}||j_2\rangle}{(2k+1)^{1/2}} (j_1 j_2 - m_1 m_2|k - m) \tag{4}$$

où $T^{(k)}_{m}$ est un opérateur tensoriel d'ordre k, et $\langle j_1\|T^{(k)}\|j_2\rangle$ est l'élément de matrice réduite de l'opérateur T calculé entre les états de moments cinétiques j_1 et j_2. Si des composantes m_x, m_y, m_z on construit les combinaisons

$$m_1 = -\sqrt{\frac{1}{2}}\,(m_x + i m_y)$$

$$m_{-1} = \sqrt{\frac{1}{2}}\,(m_x - i m_y) \tag{5}$$

$$m_0 = m_z$$

elles forment un opérateur tensoriel de premier ordre à qui on peut appliquer le théorème ci-dessus.

Ce^{3+}: LaMN

La configuration électronique d'ion Ce^{3+} dans l'état fondamental présente une seule couche incomplète — la couche 4f — avec un seul électron. En conséquent $L = 3$ et $S = 1/2$, et le terme Russel-Saunders correspondant est ^2F. L'interaction spin — orbite scinde le terme en deux multiplets avec $J = 5/2$ respectivement $7/2$, le premier représentant l'état fondamental.

Le champ cristallin a la symétrie C_{3v} [8]. Pour l'électron $4f$, qui est entouré par les couches fermées $5s^2$ et $5p^6$, il représente un champ faible qui n'empêche pas le couplage spin-orbite mais qui amène à scinder les

multiplets. De l'état fondamental il résulte, en utilisant les tableaux de réduction [6] trois doublets

$$D_{5/2} \xrightarrow[C_{3v}]{} ({}^1\Gamma_4^- + {}^1\Gamma_5^-) + {}^2\Gamma_6^- + {}^2\Gamma_6^- \tag{6}$$

De ceux-ci, un niveau ${}^2\Gamma_6^-$ représente le niveau fondamental; il suit le doublet $({}^1\Gamma_4^- + {}^1\Gamma_5^-)$ situé à $\Delta_1/k = 34°K$, et puis le doublet ${}^2\Gamma_6^-$ à $\Delta_2/k \approx 200°K$ [9].

À la conséquence de l'absorption, l'électron passe de la couche $4f$ sur la couche $5d$. Sur cet électron le champ cristallin agit comme un champ moyen qui scinde le terme ${}^2D(L = 2,\ S = 1/2)$ de la manière suivante:

$$D_2 \xrightarrow[C_{3v}]{} {}^2\Gamma_3^+ + {}^1\Gamma_1^+ + {}^2\Gamma_3^+ \tag{7}$$

l'état inférieur étant de type ${}^2\Gamma_3^+$ [10]. L'interaction spin-orbite amène à la décomposition de cet état en deux doublets:

$${}^2\Gamma_3^+ \xrightarrow[\times {}^2\Gamma_6 \xrightarrow[C_{3v}]{}]{s-0} ({}^1\Gamma_4^+ + {}^1\Gamma_5^+) + {}^2\Gamma_6^+ \tag{8}$$

Le diagramme partiel des niveaux énergetiques des ions Ce^{3+} dans LaMN est présenté dans la fig 1.

Les opérations du groupe de symètrie C_{3v} sont: P — une rotation d'angle $2\pi/3$ autour de l'axe O_z et Q — réflexion vis-à-vis d'un plan vertical. Il résulte immédiatement que toute combinaison

$$\psi = C_1 \,|5/2,\ m> \pm \pm C_2 \,|5/2,\ m - k> \tag{9}$$

dans laquelle $k = 3$, est invariante à P. En cherchant des groupes de deux combinaisons de type (9) qui soit invariants à Q il résulte pour l'état fondamental

$$|a_1\rangle = b\,|5/2,\ -1/2\rangle + c\,|5/2,\ 5/2\rangle$$
$$|a_2\rangle = b\,|5/2,\ 1/2\rangle - c\,|5/2,\ -5/2\rangle \tag{10}$$

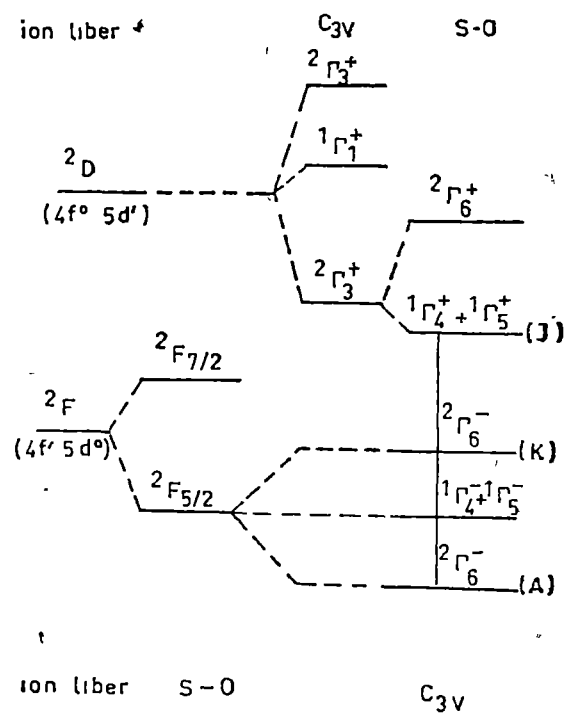

Fig. 1.

Pour déterminer les coefficients b et c nous avons employé les relations qui existent, entre eux et les paramètres $g_{\parallel}$ et $g_{\perp}$ [11]

$$g_{\parallel} = \frac{6}{7}(b^2 - 5c^2)$$
$$g_{\perp} = \frac{18}{7} b^2 \tag{11}$$

en tenant simultanément compte de la condition

$$b^2 + c^2 = 1 \tag{12}$$

Puisqu'on connait [12] les valeurs $g_{\parallel} = 0{,}023$ et $g_{\perp} = 1{,}826$, et en cherchant à déterminer les coefficients ainsi que les facteurs g calculés soyent plus proches à facteurs expérimentaux, nous avons choisi les solutions $b = 0{,}915$ et $c = 0{,}403$. Avec ces valeurs la relation (12) est satisfaite avec une précision de 10^{-4}, $g_{\parallel} = 0{,}018$ ez $g_{\perp} = 2{,}151$.

En conséquence pour l'état fondamental nous avons obtenu

$$|a_{1,2}\rangle = 0{,}915\,|5/2,\ \mp 1/2\rangle \pm 0{,}403\ |5/2, \pm 5/2\rangle \tag{13}$$

L'autre doublet $^2\Gamma_6^-$ aura comme fonctions d'onde autres deux combinaisons de type (13), mais avec de tels coefficients qu'ils forment un groupe orthogonal avec celui formé par $|a_1\rangle$ et $|a_2\rangle$.

$$|k_{1,2}\rangle = 0{,}403\,|5/2,\ \mp 1/2\rangle \mp 0{,}915\,|5/2,\ \pm 5/2\rangle \tag{14}$$

Pour le doublet $(^1\Gamma_4^- + {}^1\Gamma_5^-)$ nous avons choisi

$$|k_{3,4}\rangle = |5/2, \pm 3/2\rangle \tag{15}$$

Dans les états correspondants à la configuration $5d$ on détermine les vecteurs d'état en tenant compte du fait que le moment cinétique orbital $L = 2$. En procédant comme ci-dessus on obtient

$$|\varphi_{1,2}(L, M_L)\rangle = d\,|2, \pm 2\rangle \mp e\,|2, \mp 1\rangle$$

N'ayant pas à la disposition des dates relativement à la structure de cet état, nous avons choisi les coefficients d et e en admettant $g = 2$. De ces vecteurs, par multiplication avec les vecteurs de spin $|\psi(S, M_s)\rangle = |1/2, \pm 1/2\rangle$, on obtient les fonctions propres correspondantes au niveau $(^1\Gamma_4^+ + {}^1\Gamma_5^+)$:

$$|j_{1,2}\rangle = \frac{1}{\sqrt{3}}\,|2, \pm 2\rangle\,|1/2, \mp 1/2\rangle \mp \sqrt{\frac{2}{3}}\,|2, \mp 1\rangle\ |1/2, \mp 1/2\rangle \tag{16}$$

Pour pouvoir calculer les éléments de matrice qu'interviennent dans (1), en utilisant (2) et (3) nous avons transformé les fonctions (13) et (14) dans :

$$|a_{1,2}\rangle = 0{,}915\left(\pm\sqrt{\frac{3}{7}}\,|3{,}0\rangle|1/2, \mp 1/2\rangle \mp \sqrt{\frac{4}{7}}\,|3, \mp 1\rangle|1/2, \pm 1/2\rangle + \right. \tag{17}$$

$$\left. + 0{,}403\left(\sqrt{\frac{6}{7}}\,|3, \pm 3\rangle|1/2, \mp 1/2\rangle - \sqrt{\frac{1}{7}}\,|3, \pm 2\rangle|1/2, \pm 1/2\rangle\right.\right.$$

$$|k_{1,2}\rangle = 0{,}403\left(\pm\sqrt{\frac{3}{7}}\,|3{,}0\rangle|1/2, -1/2\rangle \mp \sqrt{\frac{4}{7}}\,|3, \mp 1\rangle|1/2, \pm 1/2\rangle + \right. \tag{18}$$

$$\left. + 0{,}915\left(\frac{1}{\sqrt{7}}\,|3, \pm 2\rangle|1/2, \pm 1/2\rangle - \sqrt{\frac{6}{7}}\,|3, \pm 3\rangle|1/2, \mp 1/2\rangle\right.\right.$$

Avec ces fonctions d'onde, en utilisant les relations (1), (4) et (5) on peut obtenir les expressions des coefficients $\mathcal{A}$, $\mathcal{B}$ et $\mathcal{C}$ en fonction de l'élément de matrice réduite $\langle 3||m||2\rangle$:

$$\mathcal{A} = -\frac{3\beta}{49}\,|\langle 3||m||2\rangle|^2 \cdot 0{,}1452$$

$$\mathcal{B} = -\frac{3\beta}{49}\,|\langle 3||m||2\rangle|^2 \cdot \frac{0{,}23862}{\hbar\omega_{KA}} \tag{19}$$

$$\mathcal{C} = -\frac{3\beta}{49}\,|\langle 3||m||2\rangle|^2 \cdot 0{,}001319$$

En conclusion il résulte qu'en utilisant la théorie des groupes il est possible de construire le diagramme énergetique et celui des vecteurs d'état pour le système Ce^{3+}: LaMN · D'un cas à l'autre, en fonction de l'intensité du champ cristallin, ces vecteurs seront exprimés par le moment cinétique total ou par les produits des moments orbitaux et de spin. L'utilisation de la méthode des opérateurs tensoriels irréductibles permet l'exprimation des éléments de matrice de l'opérateur dipolaire électrique en fonction de l'élément de matrice réduite sans la nécessité de déterminer la part radiale des fonctions d'onde.

L'expression théorique complète de la courbe de D.C.M pour Ce^{3+}: : LaMN, l'interprétation du phénomène et l'analyse des constantes de D.C.M. dans ce cas fait l'objet d'un autre travail.

(Manuscrit reçu le 27 Janvier, 1977)

BIBLIOGRAPHIE

1. B. Badoz, M. Billardon, A. C. Boccara, B. Briat, Symp of Faraday Soc. **3**, 27 (1969).
2. R. W. Schwartz, P. N. Schatz, Phys. Rev., 3, **8**, 3229 (1973).
3. P. A. Dobosh, Mol. Phys., **27**, 689 (1974).
4. A. D Buckingham, P. J. Stephens, Am. Rev Phys. Chem., **17**, 399 (1966).
5. P. J. Stephens, J. Chem. Phys, **52**, 3489 (1970)
6. Th, Kahan, *Théorie des Groupes en Physique Classique et Quantique*, Tome III, Dunod, Paris, 1972.
7. V. Heine., *Teoria Grup v Qvantovoi Mehanike*, Izd. Inostr. Lit., Moskva, 1963.
8. A. Abragam, B. Bleaney., *Electron Paramagnetic Resonanace of Transition Ions.* Clarendon Press, Oxford, 1970.
9. R. H. Ruby, H. Benoit, C. D. Jeffries., Phys. Rev., **127**, 51 (1962).
10. L. A. Alekseyeva, N. V. Starostin., OiS, **24**, 72 (1968).
11. B. R. Judd, Proc. Roy. Soc., **A232**, 458 (1955).
12. G. H. Larson, C. D. Jeffries, Phys. Rev, **145**, 311 (1966).

APLICAREA TEORIEI GRUPURILOR LA CALCULUL COEFICIENȚILOR DE DICROISM CIRCULAR MAGNETIC

(Rezumat)

Lucrarea prezintă modul de construire a diagramei energetice și a vectorilor de stare pentru sistemul $Ce^{+}: La_2Mg_3(NO_3)_2 \cdot 12H_2O$ (LaMN), utilizînd rezultatele teoriei grupurilor. Apoi se prezintă și se aplică la sistemul studiat metoda operatorilor tensoriali ireductibili folosită pentru calcularea elementelor de matrice ale operatorului moment dipolar electric.

STUDIA UNIV BABEŞ—BOLYAI, PHYSICA, 2, 1977

MAGNETIC PROPERTIES OF $U_{1-x}Dy_xCu_5$ INTERMETALLIC COMPOUNDS

MARIN COLDEA, IULIU POP, ALIN GIURGIU

1. **Introduction.** The intermetallic compounds $U_{1-x}Dy_xCu_5$ have the crystalline structure of $AuBe_5$ type [1]. The unit cell of these compounds contains four formula units and the space group is $F\bar{4}3m$.

Magnetic susceptibility measurements do not indicate any localized magnetic moment of 5*f* electrons in the lighter actinide metals, but rather point out a Pauli — paramagnetism type of behaviour [2, 3]. On the other hand, the magnetic results on the uranium intermetallic compounds have shown either a localized band [4] or a partially localized one [5, 6].

The purpose of this paper is to investigate, through the magnetic susceptibility measurements, the nature of 5*f* electrons in the $U_{1-x}Dy_xCu_5$ compounds.

2. **Experimental.** The investigated compounds used in this paper (UCu_5, $U_{0.2}Dy_{0.8}Cu_5$ and $U_{0.3}Dy_{0.7}Cu_5$) were prepared by melting stoichiometric amounts of the element in a high frequency field using a cold boat method. The starting components were of very high purity.

The formation of the compounds was verified by X-ray analysis.

The magnetic susceptibility was measured between 90 K and 700 K, in a 9450 Oe magnetic field, with a Faraday type of magnetic balance, having 10^{-8} e.m.u./g sensitivity [7].

3. **Results and discussion.** The curves of reciprocal susceptibility versus temperature of these compounds are shown in figs. 1 and 2.

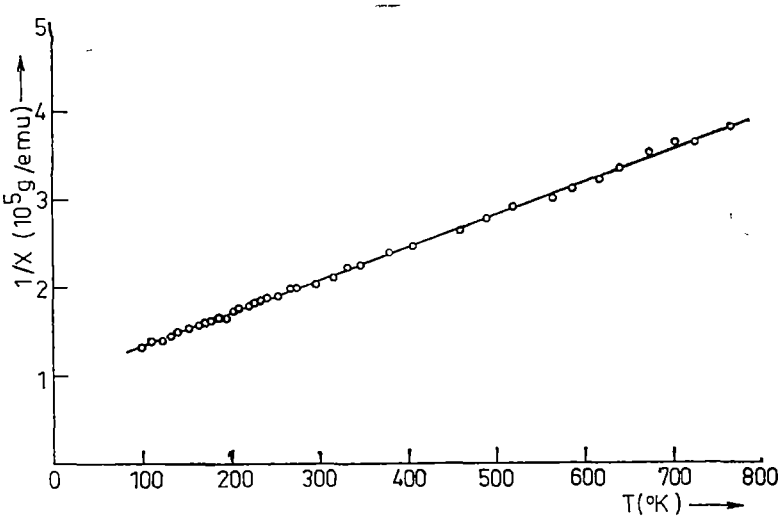

Fig. 1. The reciprocal sucesptibility versus temperature for UCu_5.

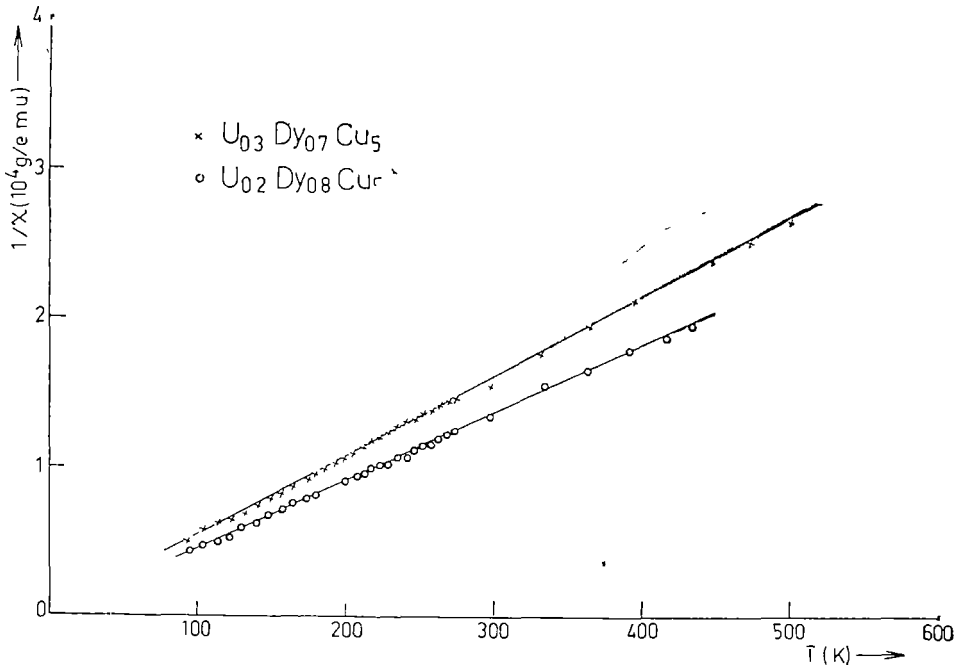

Fig. 2. The reciprocal susceptibility versus temperature for $U_{0.3}Dy_{0.7}Cu$ and $U_{0.2}Dy_{0.8}Cu_5$.

The experimental data fit a Curie-Weiss term, expressing the paramagnetism of the localized *f*-electrons, plus a temperature — independent one according to

$$\chi = \frac{C}{T - \theta_p} + \chi_0 \tag{1}$$

A summary of some of the magnetic characteristics obtained for these compounds is given in table 1. The values for $DyCu_5$ compound are those obtained by B u s c h o w et al. [8].

Table 1

Values of densities, effective moments and Curie temperatures for the $U_{1-x}Dy_xCu_5$ compounds

Compound	M	ρ(g/cm³)	θ_p(°K)	μ_{ef} of U^{3+} and Dy^{3+} ions (μ_B)		calc. $\mu_{ef}(\mu_B)$
UCu_5	555.72	10.74	−260	3.46	3.69	—
$U_{0.3}Dy_{0.7}Cu_5$	502 85	9.55	−2	8.7	—	9
$U_{0.2}Dy_{0.8}Cu_5$	495,30	9.41	0	9,37	—	9.57
$DyCu_5$	480.20	9.29	+2	10.9	10.59	—

The table lists the density calculated with four formula units per unit cell, the Curie temperatures θ_p and the effective magnetic moments μ_{ef} calculated from the slope of the $1/\chi$ versus temperature curves.

The effective magnetic moment value of $3 \cdot 46\mu_B^*/U$ atom in UCu_5 compound is near the value of $3 \cdot 69\mu_B^*$ [9] calculated for the free-ion, U^{3+} (state $^4I_{9/2}$), with all $5f^3$ localized electronic states. Consequently our measurements have revealed a strong localization of $5f^3$ electrons in contrast with the pure metallic uranium, which is a Pauli paramagnet.

If we take for the effective magnetic moments of U and Dy in $U_{0.3}$ $Dy_{0.7}$ Cu_5 and $U_{0.2}$ $Dy_{0.8}$ Cu_5 the corresponding values of trivalent ions given in table 1, then the estimated values of the effective magnetic moments per unit formula are

$$\mu_{ef}^{calc} = \sqrt{f_1\mu_U^2 + f_2\mu_{Dy}^2} \tag{2}$$

where f_1 and f_2 are the molar ratios. The good agreement between the experimental values of the effective magnetic moments in these compounds and the calculated ones confirm the above-mentioned assumption. This means that the state of uranium $5f^3$ electrons does not change by replacing the U atoms with Dy atoms.

Figure 3 shows that the effective magnetic moment per unit formula in these compounds increases linearly as the Dy content is increasing, which means that the $5f$ electronic state of the U atoms in these compounds is unaffected by their substitution with Dy atoms.

In order to confirm the abovementioned state of U 5f electrons in these compounds we have also calculated all the contributions in the temperature-independent term χ_0, obtained experimentally by fitting. The temperature-independent susceptibility χ_0, given in table 2, may be expressed as

$$\chi_0 = \chi_p + \chi_{orb}^{5d^1} + \chi_{orb}^{6d^1} + \chi_{VV}^{4f^8} + \tag{3}$$

$$+ \chi_{VV}^{5f^2} + \chi_L + \chi_{dia}$$

where χ_p is the Pauli paramagnetism of the conduction electrons, $\chi_{orb}^{5d^1}$ and $\chi_{orb}^{6d^1}$ are the orbital contributions of the $5d^1$ and $6d^1$ electrons of Dy and U atoms, $\chi_{VV}^{4f^8}$ and $\chi_{VV}^{5f^2}$ are the van Vleck paramagnetic contributions of the $4f^9$ and $5f^3$

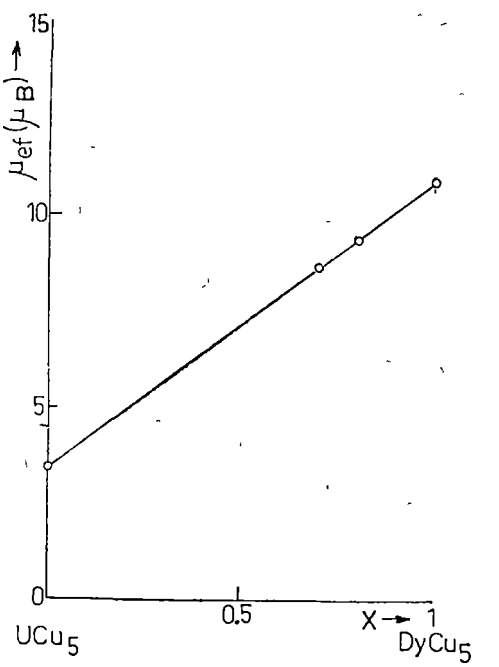

Fig. 3. The effective magnetic moments per unit formula in $U_{1-x}Dy_xCu_5$ compounds versus the Dy content.

electrons localized on Dy and U atoms, respectively, $\chi_L = -1/3\chi_p$ is the Landau diamagnetism of the conduction electrons and χ_{dia} is the diamagnetism of U, Dy and Cu atomic cores.

Table 2

Calculated values of all contributions to the susceptibility for the $U_{1-x}Dy_xCu_5$ compounds (all values are given in 10^{-6} e.m.u./mol)

Compound	χ_0 (exp)	χ_p	χ_L	χ_{dia}	$\chi_{orb}^{5d^1}$	$\chi_{orb}^{6d^1}$	$\chi_{VV}^{4f^8}$	$\chi_{VV}^{5f^2}$	$h\nu$ (cm^{-1})
UCu_5	40	51 48	−17.16	−106	—	38 8	—	72 8	4434
$U_{0.2}Dy_{0.8}Cu_5$	70	52 30	−17 43	−77.1	27 16	11 64	61 4	22.	4402
$U_{0.3}Dy_{0.7}Cu_5$	74	52 30	−17 43	−84 4	31 04	7.76	70 17	14 6	4422

Assuming that the Cu 4*s* electrons form with the U 6*d* and 7*s* and with the Dy 5*d* and 6*s* electrons a conduction band the Pauli paramagnetism for the free electrons gives the susceptibility [10]

$$\chi_p = 1\,86 \times 10^{-6} \left(\frac{M}{\rho}\right)^{2/3} n^{1/3} e \; m \; u/mol \tag{4}$$

where M is the molar mass, ρ the density and n the number of conduction electrons per molecule.

Calculation of the $\chi_{orb}^{5d^1}$ and $\chi_{orb}^{6d^1}$ was performed with the following expression [11]

$$\chi_{orb} \simeq 4N_A\mu_B^2 \; n_d \left(1 - \frac{n_d}{10}\right) \frac{1}{\overline{\Delta E_d}} \tag{5}$$

where $\overline{\Delta E_d} \simeq 3$ eV and n_d is the number of the 5*d* and 6*d* electrons per atom.

The localization of the Dy 4*f* electrons and the fact that the temperature independent van Vleck paramagnetism does not contribute appreciably to the f electron susceptibility allows us to use for $\chi_{VV}^{4f^8}$ the value calculated on the basis of the free — ion model [12] with the relation:

$$\chi_{VV} = \frac{N_A\mu_B^2}{6(2J+1)} \left[\frac{F(J+1)}{h\nu(J+1;\,J)} + \frac{F(J)}{h\nu(J-1;\,J)}\right] \tag{6}$$

where

$$F(J) = \frac{1}{J}[(S+L+1)^2 - J^2][J^2 - (S-L)^2]$$

All the above mentioned contributions are given in table 2.

The values for the susceptibility $\chi_{VV}^{5f^2}$ result from eq. (3) and are also given in table 2. Supposing that the $5f^2$ electrons are well localized on U atoms in all studied compounds we have used the eq. (6) for the cal-

culation of $h\nu(J+1;J)$ using the obtained values for $\chi_{VV}^{5f^3}$. The values calculated in this way are given in the last column of table 2. One can see that these values are very nearly between them and also with the value of the free ion U^{3+} obtained from optical absorption spectra, namely $h\nu = 4560\ cm^{-1}$ [13]. This result confirms once again that the $5f^3$ electronic shell of U stoms in $U_{1-x}Dy_xCu_5$ intermetallic compounds is strongly localized.

4. **Conclusions.** The magnetic susceptibility measurements indicate strong localization of the $5f^3$ electronic shell of U atoms in $U_{1-x}Dy_xCu_5$ compounds, in contrast with the delocalization of the 5f shell in elemental U and also in some actinide intermetallic compounds.

One can underline that the magnetic behaviour of U atoms in $U_{1-x}Dy_xCu_5$ compounds is analogous with that of rare-earth elements in intermetallic compounds.

*

The authors are very indebted to Prof. W. E. Wallace and Dr. K. S. V. L. Narasimhan from Pittsburg University, Pennsylvania for the samples studied in this paper.

(Received January 27 1977)

REFERENCES

1. W. B. Pearson, *A Handbook of Lattice Spacing and Structures of Metals and Alloys*, Pergamon Press, vol 2, 1967, p. 67.
2. B Johansson, Phys. Rev, B **11**, 2740 (1975).
3 M. B Brodsky, *Rare Earths and Actinides*, the Institute of Physics London, 1971, p 75.
4 W. B. Lewis, S. W Rabideau, N H Krikorian, W. G Witteman, Phys. Rev, **170**, 455 (1968).
5. A. C. Gossard, V. Jaccarino, J H Wernick, Phys. Rev., **128**, 1038 (1962).
6. V U. S Rao and R. Vijayaraghavan, J. Phys Chem Solids, **29**,, 123 (1968).
7. Iuliu Pop, V. I. Cecernikov, Prib i Tekh. Eksper., **5**, 180 (1964).
8. J. H. J Buschow, A. S van der Goot, J. Birkhan, J. Less-Common Metals, **19**, 433 (1969).
9. E. R. Jones, Jr., M E. Hendricks, J A Stone, D. G. Karraker, J Chem. Phys, **60**, 2088 (1974).
10. J. A. Seitchik, A. C Gossard, V. Jaccarino, Phys Rev, **136**, A 1119 (1964).
11 W. E. Gardner, J. Penfold, Phil. Mag, **11**, 549 (1965).
12 J H van Vleck, *The Theory of Electric and Magnetic Susceptibilities*, edited by R. H. Fowler, P. Kapitza, N F. Mott and E C Bullard, Oxford University Press, 1932.
13 W T. Carnall, B G. Wybourne, J. Chem Phys, **40**, 3428 (1964)

PROPRIETĂȚILE MAGNETICE ALE COMPUȘILOR INTERMETALICI $U_{1-x}Dy_xCu_5$

(Rezumat)

Susceptibilitatea magnetică a compușilor intermetalici $U_{1-x}Dy_xCu_5$ ($x = 0; 0{,}2; 0{,}3$) a fost măsurată în intervalul de temperatură 80—700 K. Variația susceptibilității paramagnetice în funcție de temperatură poate fi descrisă de o lege de tip Curie-Weiss, care exprimă paramagnetismul electronilor f localizați din benzile $4f$ și $5f$ a atomilor de Dy și U, afectată de un termen independent de temperatură pentru care au fost estimate toate contribuțiile

STUDIA UNIV BABEŞ—BOLYAI, PHYSICA, 2, 1977

ON THE PROPERTIES OF ALUMINA PROMOTED WITH METALLIC DIOXIDES (I)

Aluminium Hydroxides and aluminium oxides

I. POP, N. DULĂMIȚĂ, V. CRIȘAN, R. GOOSS

1. **Introduction.** The aluminium oxides are much studied because they are used as abrasives, adsorbents, catalysts etc. The modern investigation methods: X ray diffraction, I.R. spectroscopy, textural determinations and others, identified several crystalline forms of active alumina and explained the formation mechanism of such forms [1—7].

The X ray diffraction spectra for different crystalline forms of aluminium oxides are quite different from one author to the other, because obtaining chemically pure and especially crystallographically pure aluminium oxides is still a difficult problem [8—13]. Very often phase mixtures with different crystallinity degrees are obtained, the composition of which is sensitive to minor variations of the preparation method [14—15]. That is why we study here the relationship between the preparation method of aluminium oxides and their physico-chemical properties.

2. **Experimental.** 2.1. Samples preparation. The aluminium hydroxide samples: 1*a*, 1*b*, 1*c* were obtained from a solution of aluminium nitrate and a 20% solution of ammonia, in a chemical reactor Symax, in identical precipitation, slirring, sluicing and desiccation conditions.

The sample 1*a* was obtained at 22°C, sample 1*b* at 22°C and 20% glicol and sample 1*c* at 55°C and 20% glicol.

The aluminium oxides 2*a*, 2*b*, 2*c* were obtained after thermal treatment of 1*a*, 1*b* and 1*c* at 550°C for four hours.

2.2. Roentgenographic determinations. The powder pattern of each specimen was obtained by the Debye Scherrer method, using the filtered CuK radiation, $\lambda = 1{,}5418$Å. The results are shown in tables 1 and 2.

2 3 I.R spectroscopy. The I R. spectra (fig. 1) were recorded using a Karl Zeiss UR10 spectrometer.

2.4. Textural determinations. The specific surface and microporosity was determined using a BET installation, for the domain 5—300Å through nitrogen adsorption at a temperature of —196°C. The pores between 150—75 000Å were calculated from the curves recorded using a Carlo-Erba type mercury porosimeter, between 1—1000 atmospheres. The results are listed in table 3.

3. **Results and discussion.** The X-ray diffraction spectrum of sample 1*a* shown in table 1 has the lines 1, 2, 3, 5, 7, 8, 9 and 13 identical to those of bayerite. The line with d = 2,68Å cannot be attributed to any crystalline form. The 1,46Å line is from boehmite. Instead of the 2,06Å and 2,14Å lines from the literature we recorded a line at 2,10Å. The lines 1, 2, 7, 9, 10, 11 and 13 of sample 1*b* are the lines of bayerite,

Table 1

Aluminium hydroxides

	1*a*		1*b*		1*c*	
	d(Å)	I	d(Å)	I	d(Å)	I
1	4,77	m·b	4,77	m	4,87	v·v
2	4,33	m·b	4,39	m	4,37	w
3	3,19	w·b	3,12	m	—	—
4	—	—	2,84	w	—	—
5	2,70	v·w	—	—	2,74	m
6	2,68	v·w	2,64	s	2,66	v·w
7	2,44	s	2,45	v s	2,48	v·s
8	2,36	m	2,40		2,40	s
9	2,20	m·b	2,23	s	2,21	v·w
10	2,10	w	2,11	m	2,14	m
11	—	—	1,99	v·w	—	—
12	—	—	1,88	m·b	1,91	v·w
13	1,70	m·b	1,73	m	1,74	v·w
14	1,46	s	1,46	m	1,46	m
15	—	—	1,34	s	1,34	w

Table 2

Aluminium oxides

Sample	2*a*		2*b*		2*c*	
	d(Å)	I_{rel}	d(Å)	I_{rel}	d(Å)	I_{rel}
	4,57	w·b	4,62	v·s	—	—
	—	—	4,22	v·s·b	3,48	v·v·w
	—	—	—	—	3,20	v·v·w
	2,81	w	2,84	w	2,88	v·v·w
	2,60]	v·w	—	—	—	—
	2,42	m	2,41	s	2,41	v·s
	2,14	v·w	—	—	2,12	s
	1,99	s	1,99	v·s	1,82	v·s·b
	1,68	w	—	—	1,67	w
	1,60	v·w	—	—	1,58	w
	1,53	w	1,53	w	—	—
	—	—	—	—	1,46	s
	1,39	v·s	1,40	v·s	1,40	v·w
	—	—	—	—	1,34	v
	1,20	w·b	—	—	1,22	s
	1,14	w	1,15	v·v	1,16	s

with the difference that the lines 7 and 10 are more intense. Instead of the 2,69Å line we recorded two lines, at 2,64Å and 2,84Å. The lines 3 and 14 belong to boehmite and the 2,40Å line has no explanation. For the sample 1*c* the lines 2, 5, 6, 7, 8, 9, 10, 12, 13 coincide as position with the interlayer distances for bayerite. The lines 13, 14, 15 belong to boehmite. The lines 2, 7, 8, 9 do not coincide as intensity with those of bayerite.

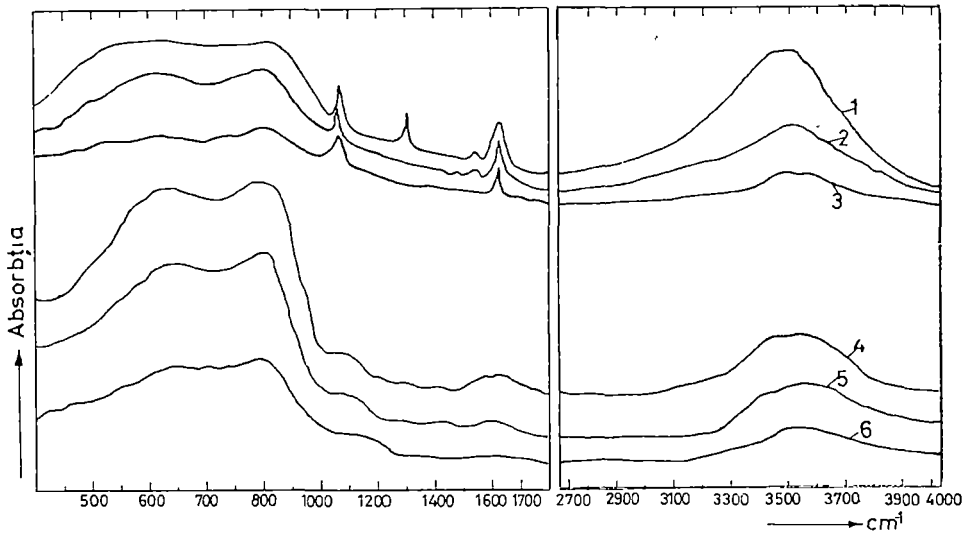

Fig. 1.

Table 3

Textural measurements

		Sample		
		2a	*2b*	*2c*
Specific surface (m^2/g)		206,0	228,0	134,6
Total volume of pores (5—75000Å) cm^3/g		0,6887	0,5682	0,4870
	Pore radii Å			
	5—25	18,42	9,83	—
	25—50	15,18	25,85	53—85
Pore radius distribution	50—100	36,84	23,02	33,32
%	100—300	11,96	25,44	2,26
	300—1000	14,02	11,91	5,05
	1000—10.000	2,83	3,04	4,61
	10000—75 000	0,91	—	0,91

The sample 2*a* contains the forms η, γ and δ of aluminium oxide. The η form of Al_2O_3 crystallizes in the cubic system Fd3m, having the lattice constant 7,94Å. The line from 4,57Å is diffuse and broad. The 1,99Å line indicates the presence of the γ form with a = 7,96Å and b = 7,82Å. The 2,60Å line belongs to the δ form of Aluminium oxide (Stumpf).

The sample 2*b* presents almost the same lines as the sample 2*a*.

The sample 2c does not present the characteristic lines of the forms η and γ. The lines can be attributed to a mixture of two crystalline forms: cubic with the lattice parameter $a = 3,66$Å and tetragonal with $a = 3,22$Å, $b = 2,995$Å.

The IR spectra [16, 17] for the samples 1*a* and 1*b* (curves 1—3 in fig. 1) show the presence of the oxidrilic groups, of the adsorbed molecular water and of the Hydrogen, bound by Hydrogen bonds onto their surface.

At 3440—3520 cm^{-1} a large vibrational band is observed, which indicates that there is a mixture of bayerite and boehmite.

The great absorbtion of these bands shows the presence of strong Hydrogen bonding.

The band from 1640 cm^{-1} corresponds to the vibration of the water molecules, meaning that there is an amorphous form in mixture with boehmite and bayerite.

The large band from 600—800 cm^{-1} corresponds to the vibration of the hydroxil groups and to the vibration of the aluminium-oxygen valence bonds.

The water content which was determined by heating the samples at 1000°C is 36,57% for 1*a* and 38,18% for 1*b*, consistent with the presence of a larger amount of bayerite, as compared with the boehmite and the amorphous forms.

The water content for sample 1*c* is 26,44% showing the presence of a large amount of boehmite impurified with bayerite and pseudoboehmite.

The absorbtion bands of sample 1*c* (curve 3) are weaker than for 1*a* and 1*b* (curves 1 and 2).

The IR spectra for samples 2*a* and 2*b* (curves 4 and 5) show the almost complete disappearance of the amorphous form. The same affirmation is valid for boehmite as, the 1075 cm^{-1} peak has disappeared. The absorbtion of the valence band has decreased because of the disappearance of Hydrogen bonding. The spectrum of the sample 2*c* (curve 6) shows that a complete dehydration took place during the thermal treatment

Analysing the textural data presented in table 3 for the samples 2*a* and 2*b* we realize that the presence of glicol in sample 2*b* determined a 22 m^2/g increase in the specific surface and a 0,12 cm^3/g decrease in the pores volume. Sample 2*c* was obtained with glicol at 55°C. This resulted in the decrease of both the specific surface (by 72 m^2/g) and the pores volume (by 0,20 cm^2/g).

(Received January 28 1977)

REFERENCES

1. B C. Lippens, *Thesis*, Delft, 1961.
2. G Yamagucki, H. Yanagida, S Ono, Bull Chem Soc Japan., **37**, 752 (1964)
3. U. Hauschild, Z. anorg allg Chemie, **324** (1—2), 15 (1963).
4 L. Stoica, Rev. Chimie, **18** (9), 543 (1967)
5. H. Saalfeld, Z. Krist, **112**, 88 (1959).
6. V. Alevra, D. Ciomîrtan, M Ionescu, Rev Roumaine Chim. **17** (7), 1163 (1972); **17** (8), 1379 (1972)
7. B. C. Lippens, J J. Stegerda, în *Physical and Chemical Aspects of Adsorbents and Catalysts*, Ed. B. G Linsen, Academic Press, London-New York, 1970, p. 171.

8. D. Papeé, R. Tertian, R. Biais, Bull. Soc. Chim. France, **1958**, 1301; **1955**, 983.
9. H. C. Stumpf, A. I. Russell, J. W. Newsime, C. M. Tucker, Ind Eng. Chem. **42**, 1398 (1950).
10. M. K. B. Day, V. J. Hill, J. Phys. Chem. **57**, 946 (1953).
11. R. Tertian, D. Pappeé, J. Chim. Phys. **55**, 341 (1958)
12. K. Torkar, Monatsh, Chem. **95**, 110 (1963).
13. H. P. Rooksby, in *The X-Ray Identification and Crystal structures of Clay Minerals*, G. W. Brindley, Ed. London, 1951.
14. T. Sato, J Appl Chem, **14**, 339 (1964).
15. H. Ginsberg, W. Huttig, G. Stunk-Lichtenberg, Z anorg allg Chem. **293**, 205 (1957).
16. N. M. Dobrst, E. I. Khazanov, Zh. Prikl. Khim. (Leningrad) **42** (6), 1244 (1969).
17. S. A. Shcherban, K. N. Nurmagambetov, Zh Prikl Spektrosk. **13**(3), 566 (1970).

PROPRIETĂȚILE ALUMINELOR PROMOTATE CU DIOXIZI METALICI (I)

Hidroxizi de aluminiu și oxizi de aluminiu

(Rezumat)

Lucrarea își propune analiza prin raze X, spectroscopie în IR și măsurători de porozitate, a proprietăților oxizilor de aluminiu obținuți în trei condiții diferite. Deoarece s-a observat o dependență mare a proprietăților structurale de modul de preparare a acestor oxizi, s-au studiat și hidroxizii de aluminiu utilizați

STUDIA UNIV BABEŞ—BOLYAI, PHYSICA, 2, 1977

CONDITIONS FOR THREE-WAVE RESONANCES IN A COLLISIONLESS PLASMA

MARIA CRISTEA

Nonlinear wave-wave interactions play an important role in dispersive media. Sometimes such an interaction is called resonant wave-wave scattering or decay instability [7], [9].

The nonlinear wave-wave interaction between three plasma waves has been intensively studied in the past few years [1], [3]—[9]. This process is such that an incident wave (the pump wave) drives two other waves through coupling provided by the plasma, or interact with two other waves already existing in the plasma.

If the pump wave drives two waves, both secondary waves being of a different character from the pump wave, this decay is called an *absorptive instability*. The absorptive instabilities appear as an efficient mechanism of energy exchange between wave modes. The electromagnetic energy of the pump wave is converted into energy of plasma oscillations. Then this energy is transferred by absorption to the plasma particles, resulting an anomalous heating of the plasma.

The starting point for the study of absorptive instabilities is the fulfilment of the conditions of three-wave resonance:

$$\vec{k}_0 = \vec{k}_1 + \vec{k}_2, \quad \omega_0 = \omega_1 + \omega_2. \tag{1}$$

Subscript o refers to the transverse pump wave, and subscripts 1, 2 refer to the driven longitudinal waves. All ω's are taken to be positive [3], [5].

The purpose of this paper is to investigate the conditions of existence of three-wave resonances. We consider a collisionless, unbounded electron plasma. No constant magnetic field is present. The electromagnetic pump wave drives two Langmuir oscillations (*photon* decays into *plasmon* plus *plasmon* [1]). The transverse, linearly-polarized pump wave has the dispersion relation

$$\omega_0^2 = \omega_p^2 + k_0^2 c^2, \tag{2}$$

where ω_p is the electron plasma frequency

$$\omega_p^2 = \frac{N_0 e^2}{\varepsilon_0 m}. \tag{3}$$

N_0 is the nonperturbed plasma density.

The longitudinal driven waves have the dispersion relations

$$\omega_1^2 = \omega_p^2 + \gamma k_1^2 V_e^2, \quad \omega_2^2 = \omega_p^2 + \gamma k_2^2 V_e^2; \tag{4}$$

γ is the ratio of specific heats, and V_e is the thermal velocity of electrons

$$V_e^2 = \frac{KT_e}{m}, \tag{5}$$

where K is the Boltzmann constant and T_e is the electron temperature.

The frequency condition (1) can be written as

$$\omega_0 = \sqrt{\omega_p^2 + \gamma k_1^2 V_e^2} + \sqrt{\omega_p^2 + \gamma k_2^2 V_e^2}. \tag{6}$$

If we note $X = \omega_0/\omega_p$ and introduce the (squared) electron Debyelength

$$\lambda_D^2 = V_e^2/\omega_p^2 \tag{7}$$

equation (6) becomes

$$X = \sqrt{1 + \gamma k_1^2 \lambda_D^2} + \sqrt{1 + \gamma k_2^2 \lambda_D^2}. \tag{8}$$

After somewhat algebra this equation can be put approximately into the form

$$\gamma \lambda_D^2 (k_1 \pm k_2)^2 = X^2, \tag{9}$$

which is equivalent to the following two equations

$$k_1 + k_2 = Q \tag{10}$$

$$|k_1 - k_2| = Q \tag{11}$$

with $Q^2 = X^2/\gamma\lambda_D^2$. Obviously, these two equations cannot be satisfied simultaneously, unless $k_1 = 0$ or $k_2 = 0$.

On the other hand, the wave-vector resonance condition (1) yields

$$|k_1 - k_2| \leqslant k_0 \leqslant k_1 + k_2. \tag{12}$$

Comparison of (12) with (10) and (11) shows that only (10) holds. Equation (11) would imply $k_0 \geqslant Q$, relation equivalent to $\gamma KT_e > mc^2$. This inequality can hold only if $T_e \gg 10^8\,°K$. Such a temperature is much larger than the solar plasma temperature in the corona [2]. Thus relation (11) does not correspond to a realistic situation, at least for a laboratory plasma.

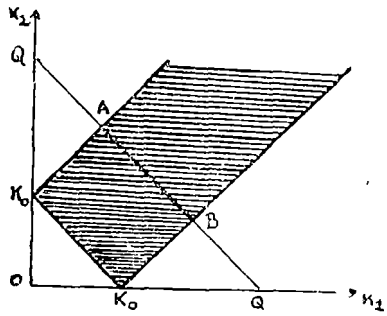

Fig 1.

Therefore the absolute values of vectors $\vec{k}_1$ and $\vec{k}_2$ must satisfy (10) and (12). Figure 1 illustrates the conditions for the existence of three-wave resonances, concerning the absolute values of wave-vectors. The shaded region in the k_1 k_2 plane corresponds to (12) and the heavy segment AB indicates the possible combinations of k_1 and k_2 when both (10) and (12) are satisfied. It can be seen that

$$\frac{Q - k_0}{2} \leqslant k_i \leqslant \frac{Q + k_0}{2} \qquad (i = 1, 2) \tag{13}$$

In order to specify the directions of $\vec{k}_1$ and $\vec{k}_2$ we notice that the three vectors $\vec{k}_0$, $\vec{k}_1$ and $\vec{k}_2$ are co-planar. So we can write

$$k_1 \cos\theta_1 + k_2 \cos\theta_2 = k_0 \cos\theta_0 \tag{14}$$

$$k_1 \sin\theta_1 + k_2 \sin\theta_2 = k_0 \sin\theta_0 \tag{15}$$

where the notations are obvious. If we choose the co-ordinate axis so that $\theta_0 = 0$, then from (14) and (15) we obtain

$$k_1 = -k_0 \frac{\sin\theta_2}{\sin(\theta_1 - \theta_2)},$$

$$k_2 = k_0 \frac{\sin\theta_1}{\sin(\theta_1 - \theta_2)}. \tag{16}$$

It follows that

$$\sin\theta_1 \geqslant 0, \quad \sin\theta_2 \leqslant 0, \quad \sin(\theta_1 - \theta_2) \geqslant 0, \tag{17}$$

or

$$\sin\theta_1 \leqslant 0, \quad \sin\theta_2 \geqslant 0, \quad \sin(\theta_1 - \theta_2) \leqslant 0. \tag{18}$$

The inequalities (17) and (18) are symmetric with respect to θ_1 and θ_2, so we can use only the set (17), that is

$$0 \leqslant \theta_1 \leqslant \pi, \quad -\pi \leqslant \theta_2 \leqslant 0 \tag{19}$$

Obviously

$$\sin\theta_1 + \sin\theta_2 \leqslant \sin\theta \leqslant \leqslant \sin\theta_1 - \sin\theta_2, \tag{20}$$

where $\theta = \theta_1 - \theta_2$ is the angle between the vectors $\vec{k}_1$ and $\vec{k}_2$.

If $\theta_1 = \theta_2 = 0$, from (14) it follows that $k_1 + k_2 = k_0$, hence $Q = k_0$. But this case is not of interest, as we have already indicated.

If $\theta_1, \theta_2 \neq 0$, some forbidden values of θ can occur. In figures 2, 3 and 4, $F_1 = \sin\theta_1$ and $F_2 = \sin\theta_2$ are plotted as functions of θ. In figure 2 the values $k_1 = (Q - k_0)/2$, $k_2 = (Q + k_0)/2$ are considered. In figure 3, $k_1 = k_2 = Q/2$, and in figure 4 we

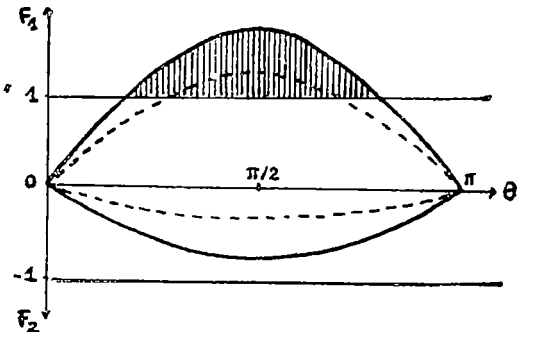

Fig 2.

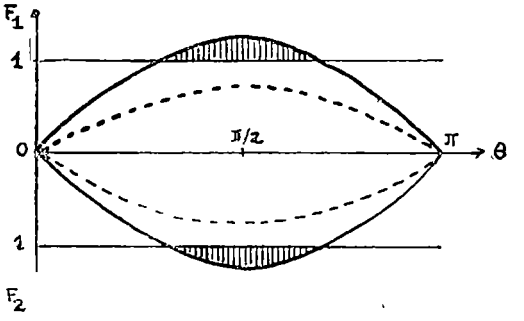

Fig. 3.

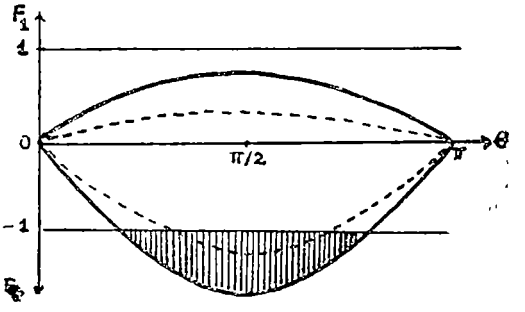

Fig. 4.

have $k_1 = (Q + k_0)/2$ and $k_2 = (Q - k_0)/2$. The full-line curves correspond to $Q = 5k_0/2$ and the dotted lines correspond to $Q = 3k_0/2$.

The values of θ corresponding to shaded domains are forbidden. The width-range of forbidden values will increase with increasing Q. Only if $k_1 = k_2 = Q/2$ and $Q \leqslant 2k_0$, the entire range of values $0 \leqslant \theta \leqslant \pi$ is allowed. Resonances are possible for any values of Q only if θ is close to 0 or π. This statement is in agreement with Hruska's result: the wave 0 delivers energy to waves 1 and 2 at the maximum rate when $\theta_1 \sim 3\pi/4$ and $\theta_2 \sim -\pi/4$.

In short, the resonance conditions for the process involved here (the transverse pump wave drives two other longitudinal waves) imply some restrictions concerning absolute values of vectors $\vec{k}_1$ and $\vec{k}_2$ and values of angle θ. The absolute values of wave-vectors must satisfy the relations (10) and (13), where Q depends on both pump wave frequency and plasma parameters (ratio of specific heats, electron temperature). The directions of the two wave-vectors have been inferred only qualitatively. The most probable values of their angle are lying in the neighbourhood of 0 and π, and the least probable in the vicinity of $\pi/2$. Actually, the value $\pi/2$ is not allowed, except the case $k_1 = k_2 = Q/2$ with $k_0 \leqslant Q \leqslant 2k_0$.

(Received January 28, 1977)

REFERENCES

1 Bornatici, M J Plasma Phys, **14**, 105 (1975)
2. Dungey, J. W., *Cosmic Electrodynamics*, University Press, Cambridge, 1958.
3. Galloway, J. J, Kim, H, J Plasma Phys, **6**, 53 (1971).
4. Giles, M. J, Plasma Phys, **16**, 99 (1974).
5. Hruška, A, J. Plasma Phys, **14**, 93 (1975)
6. Jackson, E. A, Phys Rev., **153**, 235 (1967)
7. Sagdeev, R. Z, Galeev, A A., *Nonlinear Plasma Theory*, Benjamin Inc, New York, 1969.
8. Stenflo, J. Plasma Phys, **16**, 677 (1974).
9. Tsytovich, V N, *Nonlinear Effects in Plasma* (In Russian), Nauka, Moscow, 1967.

CONDIŢII PENTRU REZONANŢA A TREI UNDE ÎNTR-O PLASMĂ FĂRĂ CIOCNIRI

(Rezumat)

În lucrare sînt discutate condiţiile de rezonanţă a trei unde într-o plasmă electronică fără ciocniri, în absenţa cîmpului magnetic. Se consideră cazul în care o undă transversală generează două unde longitudinale. Atît valorile absolute cît şi orientările reciproce ale vectorilor de undă ai undelor longitudinale sînt supuse unor restricţii. Se determină domeniile valorilor permise pentru aceste mărimi

STUDIA UNIV BABEŞ—BOLYAI, PHYSICA, 2, 1977

SUR L'INSTABILITÉ MAGNÉTOHYDRODYNAMIQUE D'UN FLUIDE IONISÉ ET STRATIFIÉ, DOUÉ D'UNE CONDUCTIVITÉ ÉLECTRIQUE FINIE. L'ÉQUATION DE DISPERSION (I)*

MIRCEA VASIU

1. **Introduction.** Dans le présent mémorie nous proposons de déduire l'équation de dispersion d'un fluide ionisé, compressible, non visqueux, ionisé et stratifié, doué d'une conductivité électrique finie. Le fluide se trouve sous l'action d'un champ magnétique, $\vec{B}_0$, dirigé d'après l'axe Ox (nous choisirons comme système de référence un système de coordonnées cartésiennes x, y, z) et aussi sous l'action d'accélération gravitationnelle $\vec{g}$, dirigée d'après l'axe Oz. On suppose une transformation thermodynamique isotherme du fluide. Pour simplifier le problème, nous négligerons le procès de conductivité thermique, le procès de transfert de radiation. On suppose que dans l'état d'équilibre le fluide possède une vitesse nulle. Nous utilisons les résultats obtenus par Ţerkovnikov [1], Hines [2], et Yu [3]. Nous établirons une équation de dispersion plus générale que l'équation de dispersion obtenue par Yu [3] pour un fluide ionisé et stratifié, doué d'une conductivité électrique infinie.

2. **Equations fondamentales pour le fluide.** Dans les suppositions ci-dessus, le système des équations s'écrit de la manière suivante

$$\rho\left[\frac{\partial\vec{v}}{\partial t}+(\vec{v}\cdot\nabla)\vec{v}\right]=-\Delta p+\rho\vec{g}+\frac{1}{\mu}(\nabla\times\vec{B})\times\vec{B}, \tag{1}$$

$$\frac{\partial\rho}{\partial t}+\nabla\cdot(\rho\vec{v})=0, \tag{2}$$

$$\frac{\partial\vec{B}}{\partial t}=\nabla\times(\vec{v}\times\vec{B})+\nu_m\Delta\vec{B}\,;\ \nu_m=\frac{1}{\mu\sigma} \tag{3}$$

$$\frac{\partial p}{\partial t}+(\vec{v}\cdot\nabla)p=\frac{\gamma p}{\delta_0}\left[\frac{\partial\delta_0}{\partial t}+(\vec{v}\cdot\nabla)\rho_0\right], \tag{4}$$

$$\frac{d}{dz}\left(p+\frac{B^2}{2\mu}\right)=-\rho_0 g \tag{5}$$

$$\rho_0=\rho e^{-z/L} \tag{6}$$

où ρ_0 est la densité du fluide, $\vec{v}$ est le vecteur vitesse d'un élément du fluide, p est la pression du fluide, $\vec{g}$ est le vecteur d'accélération gravitationnelle (g est la valeur d'accélération gravitationnelle), $\vec{B}$ est le vecteur

---

* Communication faite à la session scientifique de la Faculté de physique de l'Université de Cluj-Napoca, décembre, 1976.

champ magnétique, γ_m est le coefficient adiabatique, ν_m est le coefficient de viscosité magnétique du fluide σ est la conductivité électrique du fluide, μ est la perméabilité magnétique du fluide, ∇ est l'opérateur *nabla*, ∇x est l'opérateur *rotation* (rot), ρ est la densité du fluide pour $z = 0$, L définit une distance caractéristique pour le fluide.

3. **E'état perturbé du fluide.** Admettons maintenant que de petites perturbations de la vitesse, de la pression, de la densité et du champ magnétique se superposent à l'état d'équilibre du fluide. Les perturbations étant supposées suffisamment petites, leurs carrés et leurs produits peuvent être négligés. On suppose que les perturbations se propagent dans le fluide sous la forme des ondes monocromatiques planes

$$\varphi' = \varphi_0' e^{i(\vec{k}\cdot\vec{r}-\omega t)} \tag{7}$$

ou φ' représente la perturbation d'une grandeur quelconque, $\vec{k}$ est le vecteur nombre d'onde, ω est la pulsation, $\vec{r}$ este le vecteur de position d'un point dans l'espace. La substitution des perturbations (7) dans les équations (1)—(5), faisant les calculs d'une manière analogue avec celle qui est utilisée dans notre mémoire [4], permet d'écrire l'équation (1) sous la forme

$$\rho_0 \frac{\partial^2 \vec{\xi}}{\partial t^2} = \nabla[(\vec{\xi}\nabla\cdot)p_0 + V_s^2\rho_0\nabla\cdot\vec{\xi}] - \vec{g}\nabla\cdot(\rho_0\vec{\xi}) + \\ + \frac{1}{\mu}[(\nabla\times\vec{B}_0)\times\vec{B}' + (\nabla\times\vec{B}')\times\vec{B}_0] \tag{8}$$

où $\vec{\xi}$ est le vecteur de déplacement infinitésimal $\left(v' = \frac{\partial\xi}{\partial t}\right.$, où $\left.\vec{v}'\right.$ est le vecteur perturbation vitesse$\Big)$, $V_s^2 = \frac{\gamma p_0}{\delta_0}$ est la vitesse du son dans le fluide et

$$\vec{B}' = \frac{1}{\Omega_m^2}\nabla\times(\vec{\xi}\times\vec{B}_0) \tag{9}$$

$$(\nabla\times\vec{B}_0)\times\vec{B}' = \vec{i}\frac{1}{\Omega_m^2}B_0\frac{dB_0}{dz}ik_x\xi_z + \vec{\tilde{k}}\frac{1}{\Omega_m^2}\left(\frac{dB_0}{dz}ik_yB_0\xi_y + \right. \\ \left. + ik_xB_0\xi_x + \frac{dB_0}{dz}\xi_z\right) \tag{10}$$

$$(\nabla\times\vec{B}')\times\vec{B}_0 = \vec{j}(ik_xB_0B_y' - ik\ B_0B_x') + \vec{\tilde{k}}(ik_xB_0B_z' - ik_zB_0B_x') \tag{11}$$

$$(\vec{\xi}\cdot\nabla)p_0 = \xi_z\frac{dp_0}{dz} = \rho_0\left(\frac{1}{2}\frac{dV_A^2}{dz} - g\right)\xi_z \tag{12}$$

$$\vec{g}\nabla\cdot(\rho_0\vec{\xi}) = \rho_0\vec{g}\left(\nabla\cdot\vec{\xi} - \frac{1}{L}\xi_z\right) \tag{13}$$

$$B_0 \frac{dB_0}{dz} = \mu \rho_0 \frac{V_A^2}{2L} \tag{14}$$

$$\frac{d\rho_0}{dz} = -\frac{1}{L}\ \rho_0 \tag{15}$$

$$\frac{1}{2}\frac{dV_A^2}{dz} = \frac{V_A^2}{2L}\ ;\ \frac{d}{dz}\left[\frac{1}{2}\frac{dV_A^2}{dz}\right] = \frac{V_A^2}{2L^2} \tag{16}$$

où

$$\Omega_m^2 = 1 + \frac{\nu_m}{i\omega} k^2\ ; \qquad V_A^2 = \frac{B_0^2}{\mu\rho_0}\ , \tag{17}$$

V_A est la vitesse Alfvén.
On peut écrire l'équation (8) sous la forme suivante

$$\begin{aligned} -\rho_0\omega^2\vec{\xi} = \nabla\Big[\rho_0\Big(\frac{1}{2}\frac{dV_A^0}{dz} - g\Big)\xi_z + V_s^0\rho_0(ik_x\xi_x + \\ + ik_y\xi_y + ik_z\xi_z)\Big] - \rho_0\vec{g}(ik_x\xi_x + \\ + ik_y\xi_y + ik_z\xi_z - \frac{1}{L}\xi_z) + \vec{i}\Big(\frac{1}{\Omega_m^2}\rho_0\frac{V_A^2}{2L}ik_x\xi_2\Big) + \\ + \vec{j}\Big\{-\frac{1}{\Omega_m^2}\rho_0\Big[V_A^2(k_x^2\xi_y + k_y^2\xi_y + k_yk_z\xi_z) + \\ + \frac{V_A^2}{2L}ik_y\xi_z\Big]\Big\} + \vec{\tilde{k}}\Big\{\frac{1}{\Omega_m^2}\rho_0\frac{V_A^2}{2L}\Big(ik_y\xi_y + \\ + ik_z\xi_z + \frac{1}{2L}\xi_z\Big) - \frac{1}{\Omega_m^2}\rho_0V_A^2\Big[(k_x^2 + k_z^2)\xi_z + \\ + k_yk_z\xi_y + \frac{1}{2L}ik_z\xi_z\Big]\Big\} \end{aligned} \tag{18}$$

ou $\vec{i}$, $\vec{j}$, $\vec{\tilde{k}}$ sont les verseurs des axes $Oxyz$. On parvient au système suivant d'équations différentielles pour les déplacements ξ_x, ξ_y, ξ_z :

$$\begin{aligned} (\omega^2 - V_s^2k_x^2)\xi_x - V_s^2k_xk_y\xi_y - \Big[V_s^2k_xk_z + ik_xg - \\ - \frac{V_A^2}{2L}\Big(1 - \frac{1}{\Omega_m^2}\Big)ik_x\Big]\xi_z = 0 \end{aligned} \tag{19}$$

$$-V_s^2 k_x k_y \xi_x + \left[\omega^2 - V_s^2 k_y^2 - \frac{V_A^2}{\Omega_m^2}(k_x^2 + k_y^2)\right] \xi_y -$$

$$-\left\{i\left[\left(g - \frac{V_A^2}{2L}\left(1 - \frac{1}{\Omega_m^2}\right)\right] k_y + \left(V_s^2 + \frac{V_A^2}{\Omega_m^2}\right) k_y k_z\right\} \xi_z = 0 \tag{20}$$

$$\left[-i\left(g + \frac{V_s^2}{L}\right) k_x - V_s^2 k_x k_z\right] \xi_x + \left[-i\left(g + \frac{2V_s^2 - V_A^2\left(\frac{1}{\Omega_m^2}\right)}{2L}\right) k_y\right) -$$

$$-\left(V_s^2 + \frac{V_A^2}{\Omega_m^2}\right) k_y k_z\Big] \xi_y + \left[\omega^2 - \left(V_s^2 + \frac{V_A^2}{\Omega_m^2}\right) k_z^2 + \frac{1}{\Omega_m^2} \frac{V_A^2}{4L^2} + \right. \tag{21}$$

$$\left. + i \frac{V_A^2 - 2V_s^2}{2L} k_x - 2ik_z g - \frac{V_A^2}{\Omega_m^2} k_x^2\right] \xi_z = 0.$$

4. **L'équation de dispersion.** L'équation de dispersion s'obtient par l'annulation du déterminant formé par les coefficients des grandeurs ξ_x, ξ_y, ξ_z :

$$\begin{vmatrix} \omega^2 - V_s^2 k_x^2 & -V_s^2 k_x k_y & -V_s^2 k_x k_z - ik_x g + \\ & & + \frac{V_A^2}{2L}\left(1 - \frac{1}{\Omega_m^2}\right) ik_x \\ -V_s^2 k_x k_y & \omega^2 - V_s^2 k_y^2 - \frac{V_A^2}{\Omega_m^2}(k_x^2 + k_y^2) & -ik_y\left(g - \right. \\ & & \left. - \frac{V_A^2}{2L}\left(1 - \frac{1}{\Omega_m^2}\right) + \right. \\ & & \left. + \left(V_s^2 + \frac{V_A^2}{\Omega_m^2}\right) k_y k_z \right. \\ -i\left(g + \frac{V_s^2}{L}\right) k_x - V_s^2 k_x k_z & -i\left(g + \frac{2V_s^2 - V_A^2\left(\frac{1}{\Omega_m^2}\right)}{2L}\right) k_y - & \omega^2 - \left(V_s^2 + \frac{V_A^2}{\Omega_m^2}\right) k_z^2 + \\ & - (V_s^2 + & + \frac{V_A^2}{\Omega_m^2 4L^2} - 2igk_z - \\ & + \frac{V_A^2}{\Omega_m^2}) k_y k_z & - \frac{V_A^2}{\Omega_m^2} k_z^2 + i \frac{V_A^2 - 2V_s^2}{2L} k_z \end{vmatrix} = 0$$

(Manuscrit reçu le 29 janvier, 1977)

BIBLIOGRAPHIE

1. A. Ţerkovnikov, D.A.N. **130,** 295 (1960).
2. C. Hines, Can J. Phys., **38,** 1441, (1960).
3. C. Yu, Phys. of Fluids, **8,** 650, (1965); **9,** 412 (1966).
4. M. Vasiu, Stud. Cercet. Mat., **4,** 635 (1967).

ASUPRA INSTABILITĂŢII MAGNETOHIDRODINAMICE A UNUI FLUID IONIZAT ŞI STRATIFICAT, CU CONDUCTIVITATE ELECTRICĂ FINITĂ. ECUAŢIA DE DISPERSIE (I)

(Rezumat)

Se stabileşte ecuaţia de dispersie pentru un fluid ionizat şi stratificat, cu conductivitate electrică finită. Fluidul se găseşte sub acţiunea unui cîmp magnetic B_0 dirijat după axa Ox, precum şi sub acţiunea acceleraţiei gravitaţionale. Fluidul se consideră stratificat, astfel încît densitatea fluidului ρ_0 se consideră dependentă de coordonata z (stratificarea fluidului se consideră de-a lungul axei Oz), sub forma: $\rho_0 = \rho e^{-Z/L}$. Pentru stabilirea ecuaţiei de dispersie se aplică metoda „micilor perturbaţii". Ecuaţia de dispersie obţinută generalizează ecuaţia de dispersie obţinută de Yu pentru cazul fluidului ionizat şi stratificat, cu conductivitate electrică infinită

STUDIA UNIV BABEŞ—BOLYAI, PHYSICA, 2, 1977

COMPTEUR D'ÉCLAIRS À TRANSISTORS

STELA GÎJU*

1. **Introduction.** Dans les nuages d'orage s'engendrent d'immenses quantités d'électricité, à cause des décharges électriques atmosphériques, c'est-à-dire des éclairs. Un éclair ne décharge pas d'habitude toute la charge électrique accumulée dans le nuage et c'est pourquoi, après certain temps, on peut s'attendre à des décharges répétées dans le même canal de décharge. Ces décharges puissantes, dans un canal créé, constituent la base de la formation des ondes électromagnétiques sous forme d'impulsions, nommées aussi atmosphériques (ou sphériques), qui contiennent des oscillations électromagnétiques dans une large gamme de fréquences, ayant le maximum d'énergie dans le domaine VLF (Very low frequency) [1—5].

2. **La description de l'appareil.** Pour le comptage électronique des atmosphériques radiées par les éclairs, nous avons construit un compteur d'éclairs à transistors (fig. 1).

Les signaux électriques radiés par les éclairs sont reçus par une antenne horizontale longue de 20 m. À noter, à l'entrée, le filtre et le

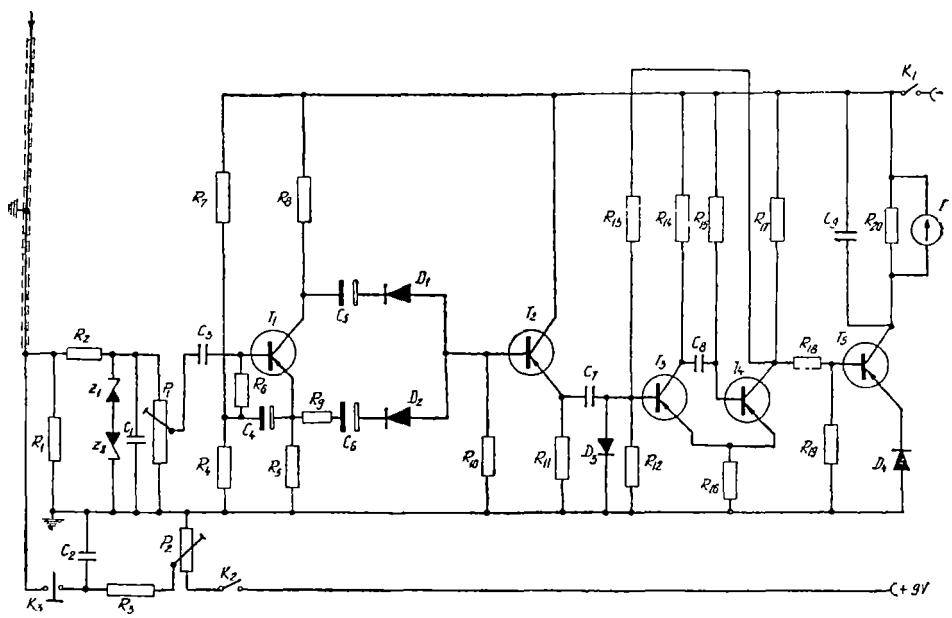

Fig 1 Le schéma électrique du compteur d'éclairs à transistors

* Institut pédagogique de Tîrgu-Mureş

potentiomètre P_1, à l'aide duquel on ajuste la sensibilité de l'appareil. L'étage d'amplification comprend le transistor T_1. Pour la protection du transistor T_1 des surtensions causées par les éventuels éclairs rapprochés, il y a deux diodes Zener Z_1 et Z_2 connectées par opposition de phase. Le signal amplifié est détecté par deux diodes D_1 et D_2. L'étage formé par le transistor T_2 aide le démarrage du circuit basculeur monostable connecté derrière celui-ci, sans celui-ci le démarrage étant incertain. Le circuit basculeur monostable comprend les transistors T_3 et T_4. Le blocage de l'étage est assuré par les impulsions négatives arrivées à la base de T_3. À la sortie du circuit basculeur monostable, on obtient des impulsions de la même amplitude, où le transistor T_4 joue aussi le rôle d'un discriminateur de l'amplitude. Pour réaliser la stabilité thermique, on utilise une diode au germanium D_3. Les signaux obtenus commandent le transistor T_5 et le circuit d'intégration du circuit du collecteur de T_5. L'enregistrement des signaux a lieu par l'enregistreur à papier I, la déviation de la plume étant proportionnelle au nombre d'impulsions par seconde. La portion P_2-C_2 sert au calibrage Après le chargement du condensateur C_2 d'une tension connue, il sera déchargé sur le côté d'entrée du filtre.

La gamme de fréquence de l'appareil est 3—15 kHz. Le seuil de sensibilité a été fixé à $0{,}4 \frac{V}{m}$. Le rayon de réception d'un compteur d'éclairs est à définir en termes statistiques [6] et dépend aussi de sa sensibilité [7]. Ayant en vue [6], [7], il résulte un rayon de réception d'environ 150 km.

3. **Les résultats expérimentaux.** L'appareil fonctionne depuis 1973, enregistrant les atmosphériques radiées par les éclairs. Les enregistrements effectués montrent la posibilité de la caractérisation des orages du point de vue de leur activité électrique. Par exemple, sur le diagramme de l'enregistrement des orages du 2 VIII 1974 et 3 VIII 1975, on observe que l'orage du 2 VIII 1974 (fig. 2) s'est caractérisé par une activité électrique plus intense que celui du 3 VIII 1975 (fig. 3), parce que la fréquence et le nombre des atmosphériques enregistrées a été plus grand dans le premier cas. Quand il fait beau temps, en absence des atmosphériques générées par les éclairs, la plumme de l'enregistrateur suit une ligne

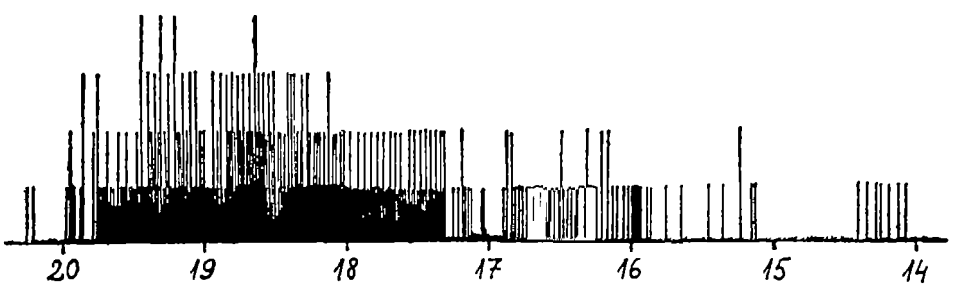

Fig 2 L'enregistrement de l'orage du 2 VIII 1974

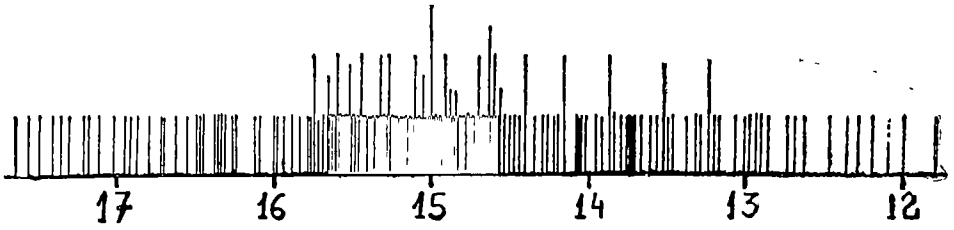

Fig 3 L'enregistrement de l'orage du 3 VIII 1975

droite. On peut déterminer le nombre des atmosphériques produites dans un seul orage. On peut utiliser cette valeur à la caractérisation de l'activité électrique des orages.

L'appareil signale l'arrivée des orages à quelques heures avant. Lors de l'orage du 2 VIII 1974, qui a eu lieu sur la ville vers les 19 heures, le compteur a signalé son arrivée dès les 14 heures (fig. 2). Lors de l'orage du 3 VIII 1975, qui a eu lieu sur la ville vers les 15 heures, le compteur a signalé son arrivée dès les 12 heures (fig 3)

L'analyse des enregistrements met en évidence aussi le fait que la fin des orages est relativement brusque en comparaison avec leur début.

En ce que concerne les fausses impulsions, la séparation de celles-ci des véritables impulsions est encore un problème qui n'est pas résolu du point de vue technique [8]. Premièrement les perturbations du réseau électrique peuvent être enregistrées à côté des perturbations atmosphériques. Dans ce sens, le filtre électronique conecté à l'entrée de l'appareil a le rôle d'éliminer en grande partie les perturbations que les différentes impulsions produiraient.

4. **Conclusions.** Les enregistrement obtenus de cet appareil offrent divers détails concernant la caractèrisation d'un orage et le mode de son déroulement. On peut déterminer la répartition en temps des nombres d'impulsions enregistrées pendant un orage, ou bien le nombre moyen d'impulsions enregistrées dans un intervalle établi (par exemple 5 minutes). De cette manière, on peut obtenir un indice objectif pour la classification des orages du point de vue de leur activité électrique.

Le compteur d'èclairs est utilisable dans la prévision des orages, en indiquant aussi le rapprochement de l'orage quelques heures avant, ce qui peut être utile pour prendre des mesures de protection.

(Manuscrit reçu le 29 janvier, 1977)

BIBLIOGRAPHIE

1. G Heydt, H Volland, Z angew Phys, **16**, 1, 701—704 (1963)
2 J Chapman, E T Pierce, L'onde éléctrique, **362**, 524—525 (1957)
3. R D Hill, J Geophys Res, **74**, 8, 1922—1929 (1969).

4. R. W. Chapman, R. C. V. Macario, Nature, **177**, 4516, 930—933 (1956).
5. K. Sao, H. Jindoh, J. Atm. Terr. Phys., **36**, 261—266 (1974).
6. F. Horner, Proc. I.E.E., **107** B, 321—323 (1960).
7. V. Gallo, M. Mezősi, Időjárás, **1**, 17—21 (1966)
8. E. Ventura, 1970: O.M.SZ. Beszàmolők, **35**, 22—29 (1968).

CONTOR DE FULGERE CU TRANZISTOARE

(Rezumat)

Lucrarea prezintă un contor de fulgere tranzistorizat (fig 1.) şi cîteva înregistrări efectuate (fig. 2 şi fig 3). Pragul de sensibilitate a fost fixat la 0,4 V/m, rezultînd o rază de acţiune în jur de 150 km. Contorul oferă detalii cu privire la caracterizarea unei furtuni şi modul ei de desfăşurare. Se poate determina repartiţia în timp a numărului de impulsuri înregistrate în timpul unei furtuni, sau numărul mediu de impulsuri înregistrate într-un anumit interval de timp. În felul acesta se poate obţine un criteriu obiectiv pentru clasificarea furtunilor din punctul de vedere al activităţii electrice.

CRONICĂ

Vizite din ţară şi străinătate

● Cu ocazia unei vizite făcută în ţara noastră, avînd ca scop un schimb de experienţă şi documentare, dr doc E I Riumţev de la Universitatea din Leningrad, catedra de fizica polimerilor, a prezentat la 3 februarie 1977, în cadrul facultăţii noastre, comunicarea *Proprietăţile fizice ale cristalelor lichide.*

● De asemeni, în ziua de 6 aprilie 1977, prof A. C Rose-Innes de la Universitatea din Manchester, Inst of Sci and Technology (Anglia), a expus comunicarea *Cristals of magnetic flux* (Cristale de flux magnetic).

● Prof dr C Beşliu de la Facultatea de fizică a Universităţii din Bucureşti, invitat de către conducerea facultăţii noastre, a prezentat în 8 aprilie 1977 comunicarea *Cercetări şi orientări noi în fizica particulelor elementare*

Cursuri litografiate

Lect. dr E Constantin, asist. O Cozar, *Fizica moleculei* — culegere de probleme, 1976.

Asist. O Cozar, lect A Farkaş, asist C Cosma, prof dr doc V Mercea, *Fizica moleculei* — lucrări de laborator, 1976

Lect dr. M. Crişan, *Fizica temperaturilor joase,* 1976

Lect. dr. Gh .Ilonca, asist. L. Cociu *Culegere de probleme de fizica semiconductorilor,* 1976.

Prof dr Al Nicula, *Fizica dielectricilor şi feroelectricilor,* 1976

Conf dr E Tătaru, *Bazele radiotehnicii,* 1976

Conf dr V Znamirovschi, asist. R. Câmpeanu, *Interacţiuni nucleare,* 1976.

Conf dr D Auslander, *Fizică generală şi nucleară,* I, 1977

Asist. V Crişan, asist. E Rus, *Raze X* — lucrări de laborator, 1977

Susţineri de teze de doctorat

În ziua de 11 decembrie 1976, Sorin Fărcaş de la Institutul de tehnologii izotopice şi moleculare, Cluj-Napoca, a susţinut în faţa comisiei teza intitulată *Studiul RES. al centrilor paramagnetici obţinuţi prin iradieri şi impurificare în cristale ionice* (conducător ştiinţific prof. dr. Al Nicula)

I P Cluj — Municipiul Cluj-Napoca 298/1977.

43 904

Abonamentele se fac la oficiile poştale, prin factorii poştali şi prin difuzorii de presă, iar pentru străinătate prin ILEXIM Departamentul Export-Import Presă, P O. Box 136—137, telex 11226 Bucureşti, str. 13 Decembrie nr. 3

Lei 10

În cel de al XXII-lea an (1977) *Studia Universitatis Babeş—Bolyai* apare semestrial în specialităţile:

matematică
fizică
chimie
geologie—geografie
biologie
filozofie
ştiinţe economice
ştiinţe juridice
istorie
filologie

На XXII году издания (1977) *Studia Universitatis Babes—Bolyai* выходит два раза в год со следующими специальностями:

математика
физика
химия
геология—география
биология
философия
экономические науки
юридические науки
история
филология

Dans sa XXII-e année (1977) *Studia Universitatis Babeş—Bolyai* paraît semestriellement dans les spécialités:

mathématiques
physique
chimie
géologie—géographie
biologie
philosophie
sciences économiques
sciences juridiques
histoire
philologie